

PRODUCTION OF AERATED ALKALI-ACTIVATED SLAG PASTES
AND MORTARS USING HYDROGEN PEROXIDE

A THESIS SUBMITTED TO
THE GRADUATE SCHOOL OF NATURAL AND APPLIED SCIENCES
OF
MIDDLE EAST TECHNICAL UNIVERSITY



BY

MURAT ŞAHİN

IN PARTIAL FULFILLMENT OF THE REQUIREMENTS
FOR
THE DEGREE OF DOCTOR OF PHILOSOPHY
IN
CIVIL ENGINEERING

SEPTEMBER 2017

Approval of the Thesis:

**PRODUCTION OF AERATED ALKALI-ACTIVATED SLAG PASTES
AND MORTARS USING HYDROGEN PEROXIDE**

submitted by **MURAT ŞAHİN** in partial fulfillment of the requirements for the degree of **Doctor of Philosophy in Civil Engineering Department, Middle East Technical University** by,

Prof. Dr. Gülbin Dural Ünver
Dean, Graduate School of **Natural and Applied Sciences** _____

Prof. Dr. İsmail Özgür Yaman
Head of Department, **Civil Engineering** _____

Assoc. Prof. Dr. Sinan Turhan Erdoğan
Supervisor, **Civil Engineering Dept., METU** _____

Asst. Prof. Dr. Özgür Bayer
Co-Supervisor, **Mechanical Engineering Dept., METU** _____

Examining Committee Members

Prof. Dr. Mustafa Tokyay
Civil Engineering Dept., METU _____

Assoc. Prof. Dr. Sinan Turhan Erdoğan
Civil Engineering Dept., METU _____

Assoc. Prof. Dr. Cemil Yamalı
Mechanical Engineering Dept., METU _____

Assoc. Prof. Dr. Berna Unutmaz
Civil Engineering Dept., Hacettepe University _____

Asst. Prof. Dr. Seda Yeşilmen
Civil Engineering Dept., Çankaya University _____

Date: September 8, 2017



I hereby declare that all information in this document has been obtained and presented in accordance with academic rules and ethical conduct. I also declare that, as required by these rules and conduct, I have fully cited and referenced all material and results that are not original to this work.

Name, Last name: Murat Şahin

Signature :

ABSTRACT

PRODUCTION OF AERATED ALKALI-ACTIVATED SLAG PASTES AND MORTARS USING HYDROGEN PEROXIDE

Şahin, Murat

Ph.D., Department of Civil Engineering

Supervisor: Assoc. Prof. Dr. Sinan Turhan Erdoğan

Co-Supervisor: Asst. Prof. Dr. Özgür Bayer

September 2017, 176 Pages

Utilization of ground granulated blast furnace slag (GGBFS) through alkali activation for the production of construction materials can provide economic and environmental advantages. In this study, cement-free lightweight composites based on the alkali activation of GGBFS were produced with the incorporation of hydrogen peroxide, and their physical, thermal, and mechanical properties were investigated, under different curing conditions. Various water-to-slag ratios (W/S), hydrogen peroxide contents, and sand-to-slag ratios (Sa/S) were used to explore the expansion mechanism of fresh mixtures and to investigate the apparent density of produced samples. The compressive and flexural strengths and water absorption of sealed-cured pastes and mortars were investigated at room temperature. In addition, the effect of ambient curing and humid-oven curing on the compressive strengths of selected series of pastes and mortars were investigated. Thermal conductivities of aerated pastes were measured. The size and amount of pores were assessed on selected series of aerated pastes and mortars. Aerated pastes and mortars were produced in the apparent density range of 516-1603 kg/m³ and with 0.5-30.0 MPa compressive strength. Thermal conductivities of aerated pastes varied from 0.117-

0.206 W/m.K in the dry density range of 480-1098 kg/m³. The use of hydrogen peroxide in the range of 0.25 %-0.75 % (by mass of slag) was sufficient to produce lightweight composites which can be used for insulation and semi-structural purposes in the construction industry.

Keywords: Aerated concrete, cellular concrete, alkali-activated slag, thermal conductivity, hydrogen peroxide.



ÖZ

HİDROJEN PEROKSİT KULLANARAK ALKALİLERLE AKTİVE EDİLMİŞ CÜRUF BAĞLAYICILI HAVA SÜRÜKLENMİŞ HAMUR VE HARÇLARIN ÜRETİMİ

ŞAHİN, Murat

Doktora, İnşaat Mühendisliği Bölümü

Tez Yöneticisi: Doç. Dr. Sinan Turhan ERDOĞAN

Ortak Tez Yöneticisi: Yrd. Doç. Dr. Özgür BAYER

Eylül 2017, 176 Sayfa

Yapı malzemelerinin üretimi için öğütülmüş yüksek fırın cürufunun (YFC) alkali aktivasyon yoluyla kullanılması çevresel ve ekonomik avantajlar sağlayabilir. Bu çalışmada, gaz üretici kimyasal olan hidrojen peroksit eklenerek alkali aktive YFC esaslı hafif kompozitler üretilmiş ve üretilen kompozitlerin fiziksel, termal ve mekanik özellikleri incelenmiştir. Karışımların genleşme sisteminin ve görünür yoğunluklarının araştırılması için çeşitli su/cüruf oranları (W/S), hidrojen peroksit miktarları ve kum/cüruf oranları (Sa/S) kullanılmıştır. Oda sıcaklığında kapalı kür edilen hamurların ve harçların basınç ve eğilme dayanımları, ve su emme miktarları incelenmiştir. Ayrıca, oda sıcaklığında açık kür ve 80 °C sıcaklıkta nemli fırında kür edilmiş seçilen hamur ve harç serilerinin basınç dayanımları incelenmiştir. Hava sürüklenmiş hamurların ısı iletkenlikleri belirlenmiştir. Seçilen hamur ve harç serilerinin hava boşluğu boyutu ve miktarı değerlendirilmiştir. Görünür yoğunlukları 516 kg/m³ ile 1603 kg/m³ aralığında ve basınç dayanımı 0.5 MPa ile 30.0 MPa arasında olan hava sürüklenmiş hamur ve harçlar üretilmiştir. Hava sürüklenmiş hamurların ısı iletkenlikleri 480 kg/m³ ile 1098 kg/m³ görünür

yoğunluk aralığında 0.117 W/m.K ile 0.206 W/m.K arasında değişmektedir. Yapı endüstrisinde yalıtım ve yarı yapısal amaçlı hafif kompozitler üretmek için cüruf ağırlığının %0.25'i ile %0.75'i arasında hidrojen peroksit kullanmanın yeterli olduğu görülmüştür.

Anahtar Kelimeler: Hava sürüklenmiş beton, gaz beton, alkalilerle aktive edilmiş cüruf, termal iletkenlik, hidrojen peroksit.





To My Family

ACKNOWLEDGEMENTS

First, I would like to express my deepest gratitude to my supervisor Assoc. Prof. Dr. Sinan Turhan Erdoğan, for his guidance, recommendations and endless support throughout the experimental and writing stages of the thesis. Without his support, this thesis would not have been completed. His support starting from my first day at METU will never be forgotten.

Secondly, I would like to thank my co-supervisor Asst. Prof. Dr. Özgür Bayer for his valuable suggestions and for his guidance during this research.

Thirdly, I would like to express my gratitude to my thesis progression committee members Prof. Dr. Mustafa Tokyay and Assoc. Prof. Dr. Cemil Yamalı for their support, comments, and directions. I would like to thank Prof. Dr. İsmail Özgür Yaman for his support and contributions throughout all my education at METU.

Special thanks go to my friends Hasan Eser, Kemal Ardoğa, Başak Varlı, and Serhat Keskin not only for their moral support during this research, but also for their endless friendship. I would like to thank my colleagues, and the staff of METU Materials of Construction Laboratory; Dr. Burhan Alam, Meltem Tangüler, Muhammet Atasever, Okan Koçkaya, Vesile Akansel, Mahdi Mahyar, and Cuma Yıldırım for their moral support during this research.

I would also like to thank KARÇİMSA Cement Production and Trade Company for providing the ground granulated blast furnace slag used in this research.

Finally, I am also grateful to my family for their invaluable support.

TABLE OF CONTENTS

ABSTRACT.....	v
ÖZ	vii
ACKNOWLEDGMENTS	x
TABLE OF CONTENTS	xi
LIST OF TABLES	xv
LIST OF FIGURES	xviii
LIST OF ABBREVIATIONS	xxvi
CHAPTERS	
1. INTRODUCTION	1
1.1 General.....	1
1.2 Objective and Scope	3
2. LITERATURE REVIEW	5
2.1 Introduction.....	5
2.2 Definitions	5
2.2.1 Pozzolanic Materials.....	5
2.2.2 Latent Cementitious Materials.....	6
2.2.3 Alkali Activation.....	6
2.2.3.1 The Need for Alkali Activation.....	7
2.2.3.2 Historical Background of Alkali-Activated Cement and Concrete	8
2.2.3.3 Classification of Alkali-Activated Cements.....	9
2.2.3.4 Alkali Activators	10
2.3 Ground Granulated Blast Furnace Slag	11
2.3.1 Alkali Activation of GGBFS	13
2.3.1.1 Reaction Mechanism.....	13
2.3.1.2 Hydration Products	14
2.3.2 Major Factors Affecting Activation of GGBFS.....	14
2.3.2.1 Chemical Composition of GGBFS	14
2.3.2.2 Type of Activators.....	15

2.3.2.3 Dosage of Activators.....	16
2.3.2.4 Curing Temperature	16
2.3.2.5 Fineness.....	16
2.3.3 Properties of Alkali-Activated Slag Concretes	17
2.3.3.1 Fresh Properties	17
2.3.3.1.1 Setting Time	17
2.3.3.1.2 Workability	19
2.3.3.2 Hardened Properties.....	19
2.3.3.2.1 Strength	19
2.3.3.2.2 Efflorescence.....	26
2.4 Lightweight Concrete	30
2.4.1 Aerated Concrete	31
2.4.1.1 Pore Formation Methods.....	32
2.4.1.1.1 Air-Entrainment Method.....	32
2.4.1.1.2 Foaming Method	35
2.4.1.2 Some Properties of Aerated Concretes	36
2.4.1.2.1 Density	36
2.4.1.2.2 Compressive Strength	36
2.4.1.2.3 Water Absorption	39
2.4.1.2.4 Thermal Conductivity	40
2.4.1.3 Alkali-Activated Aerated Concretes	43
2.5 Methods of Measuring Thermal Conductivity	50
2.5.1 Steady-State Methods	51
2.5.1.1 Guarded Hot Plate Apparatus	51
2.5.1.2 Unguarded Hot Plate Apparatus.....	52
2.5.1.3 Heat Flow Meter Method.....	52
2.5.2 Transient Methods	53
2.5.2.1 Hot-Wire Method.....	53
2.5.2.2 Transient Plane Source Method	54
3. EXPERIMENTAL STUDY	55
3.1 Materials	55
3.1.1 Ground Granulated Blast Furnace Slag	55
3.1.2 Water.....	56
3.1.3 Hydrogen Peroxide	56
3.1.4 Aggregates	57
3.1.5 Alkali Activators.....	57
3.2 Mixture Preparation	58
3.2.1 Mixing Procedure for Pastes.....	58
3.2.2 Mixing Procedure for Mortars	59

3.3 Identification of Samples	59
3.4 Mixture Proportions	60
3.5 Preparation of Test Samples	64
3.6 Curing	67
3.7 Tests Performed	67
3.7.1 Determination of Setting Time	67
3.7.2 Determination of Flow	68
3.7.3 Determination of Apparent Density	68
3.7.4 Determination of Porosity	69
3.7.5 Determination of Flexural and Compressive Strengths	69
3.7.6 Determination of Water Absorption	70
3.7.7 Scanning Electron Microscopy	71
3.7.8 Determination of Thermal Conductivity	72
3.7.8.1 Uncertainty Analysis of Thermal Conductivity Measurements	73
4. RESULTS AND DISCUSSION	77
4.1 Setting Time	77
4.2 Flow	78
4.3 Expansion Mechanism of Mixtures	80
4.4 Apparent Density	83
4.4.1 Influence of Hydrogen Peroxide and Water Content	84
4.4.2 Influence of Sand Addition on the Paste Phase	90
4.5 Porosity	93
4.6 Strength	94
4.6.1 Strength Development of Paste Samples	94
4.6.1.1 Influence of Sealed Curing	94
4.6.1.2 Strength Development of Sealed-Cured Pastes	104
4.6.1.3 Influence of Ambient Curing	105
4.6.1.4 Influence of Oven Curing	108
4.6.2 Strength Development of Mortar Samples	110
4.6.2.1 Influence of Sealed Curing	110
4.6.2.2 Influence of Oven Curing	114
4.7 Water Absorption	117
4.7.1 Water Absorption of Pastes	117
4.7.2 Water Absorption of Mortars	121
4.8 Pore Structure of Samples	122
4.9 SEM Analysis	129

4.10 Thermal Conductivity of Aerated Pastes.....	133
5. CONCLUSIONS AND RECOMMENDATIONS.....	137
5.1 Concluding Remarks	137
5.2 Recommendations for Future Work	141
REFERENCES	143
APPENDICES	161
A. TEST RESULTS	161
B. AERATED PASTE SAMPLES USED FOR THE THERMAL CONDUCTIVITY MEASUREMENTS	171
CURRICULUM VITAE	175



LIST OF TABLES

TABLES

Table 2.1 Classification of alkali activators (Glukhovsky, 1980).....	10
Table 2.2 Comparison of chemical compositions of various blast furnace slags and a Portland cement (Erdoğan, 1997).....	13
Table 2.3 Comparison of physical properties of hydrogen peroxide and water (Goor et al., 2000).....	34
Table 2.4 Physical properties of hydrogen peroxide solutions of different concentration (Goor et al., 2000).....	34
Table 3.1 Oxide composition and physical properties of the slag used.	55
Table 3.2 Summary of mixture proportions for pastes and mortars.....	60
Table 3.3 Mixture proportions for pastes.	61
Table 3.4 Mixture proportions for mortars with $S_a/S=1$	62
Table 3.5 Mixture proportions for mortars with $S_a/S=2$	63
Table 3.6 Uncertainty analysis for 40-0-25.....	75
Table 4.1 Pore size range of aerated pastes.....	125

Table 4.2 Pore size range of aerated mortars.	125
Table A.1 Initial and final setting times of non-aerated pastes.....	161
Table A.2 Effect of W/S on flow of non-aerated pastes.	161
Table A.3 Effect of W/S on flow of non-aerated mortars with Sa/S=1.	161
Table A.4 Apparent densities of pastes with different W/S and hydrogen peroxide contents.....	162
Table A.5 Apparent densities of mortars (Sa/S=1) with different W/S and hydrogen peroxide contents.....	162
Table A.6 Apparent densities of mortars (Sa/S=2) with different W/S and hydrogen peroxide contents.....	163
Table A.7 The calculated apparent densities (kg/m^3) of the paste phases of mortars (Sa/S=1) and pastes with different W/S and hydrogen peroxide contents.	163
Table A.8 Apparent density, powder density, and porosity of pastes with different W/S and hydrogen peroxide contents.....	164
Table A.9 Apparent density, flexural strength, and compressive strength of pastes with different W/S and hydrogen peroxide contents.....	165
Table A.10 Compressive strength development of sealed-cured pastes with W/S=0.45 and different hydrogen peroxide contents.....	166
Table A.11 Compressive strengths of ambient-cured pastes with W/S=0.45 and different hydrogen peroxide contents.....	167

Table A.12 Compressive strengths of oven-cured pastes with W/S=0.45 and different hydrogen peroxide contents.....	167
Table A.13 Effect of W/S and hydrogen peroxide content on the apparent density, flexural strength, and compressive strength of mortars (Sa/S=1).	168
Table A.14 Effect of oven curing on flexural and compressive strengths of mortars (Sa/S=1) with W/S=0.40 and 0.50, and different hydrogen peroxide contents... ..	168
Table A.15 Water absorption, apparent density, and oven-dry density of pastes with different W/S and hydrogen peroxide contents.	169
Table A.16 Water absorption, apparent density, and oven-dry density of mortars (Sa/S=1) with different W/S and hydrogen peroxide contents.....	170
Table A.17 Thermal conductivity of aerated pastes.....	170

LIST OF FIGURES

FIGURES

Figure 2.1 Ternary diagram of alkali-activated cements (Krivenko, 2010).....	9
Figure 2.2 Effect of activator type on 28-day strength of alkali-activated slag pastes (Bakharev et al., 1999a).	22
Figure 2.3 Effect of NaOH concentration on compressive strength of alkali-activated slag mortars (Altan and Erdoğan, 2012).....	23
Figure 2.4 Effect of sodium silicate concentration on compressive strength of alkali-activated slag mortars (Altan and Erdoğan, 2012).....	23
Figure 2.5 Effect of Na ₂ O concentration (n, by mass of slag) on early age compressive strength of alkali-activated slag concretes at different sodium silicate modulus: a) Ms=0.60, b) Ms=1.50 (Ravikumar and Neithalath, 2012).	24
Figure 2.6 Effect of W/S on compressive strength of alkali-activated slag mortars at room temperature (Altan and Erdoğan, 2012).....	25
Figure 2.7 Effect of W/S on compressive strength of alkali-activated slag mortars at 80 °C (Altan and Erdoğan, 2012).....	25
Figure 2.8 Efflorescence of AAFA sample after 50 days (Škvára et al., 2012)....	28

Figure 2.9 Types of lightweight concretes: a) No-fines concrete, b) Aerated concrete, and c) Lightweight aggregate concrete (adapted from Short and Kinniburgh, 1978)	31
Figure 2.10 Effect of aggregate size on compressive strength of aerated concretes (Nambiar and Ramamurthy, 2006).....	37
Figure 2.11 Effect of fly ash replacement on the compressive strength of aerated concretes (Nambiar and Ramamurthy, 2006).....	37
Figure 2.12 Strength gain of aerated concretes with various fillers (Jones et al., 2003).....	38
Figure 2.13 Effect of curing type on 28-day compressive strength of lime-cement based aerated concretes with percentage of sand replacement by fly ash (Ramamurthy and Narayanan, 2000).	39
Figure 2.14 Variation of thermal conductivity with oven-dry density for AAC (Aroni et al., 1993).	41
Figure 2.15 Effect of moisture content on the thermal conductivity of AAC (Millard, 1992).	42
Figure 2.16 Variation of apparent density and void fraction of aerated samples at different hydrogen peroxide amounts (Vaou and Panias, 2010).	45
Figure 2.17 Optical characterization of fly ash-metakaolin-based alkali-activated materials at different hydrogen peroxide contents and NaOH molarity (Novais et al., 2016).	49
Figure 2.18 Illustration of the guarded hot plate apparatus (ASTM C177, 2013).	51

Figure 2.19 Apparatus for heat flow meter method: a) One heat flux transducer and one specimen, b) One heat flux transducer and two specimens.....	53
Figure 2.20 Spiral plane probe as heating and temperature sensor (ISO 22007-2, 2008).	54
Figure 3.1 X-ray diffractogram of the slag used.	56
Figure 3.2 Grading of the sand used.	57
Figure 3.3 Identification of samples.....	60
Figure 3.4 Preparation of 40-0-25: a) Immediately after casting, b) 12 minutes after casting, and c) Surface cut ~2h after casting.....	65
Figure 3.5 Preparation of 40-0-75: a) Immediately after casting, b) 8 minutes after casting, c) 15 minutes after casting, and d) Surface cut ~2h after casting.	66
Figure 3.6 Sealed curing.....	67
Figure 3.7 Illustration of flow test (The scale bar shows cm units).	68
Figure 3.8 Unitherm 2022 thermal conductivity apparatus.....	72
Figure 4.1 Effect of W/S on the setting times of aerated pastes.	77
Figure 4.2 Effect of W/S on the flow of non-aerated pastes and mortars.	79
Figure 4.3 Effect of hydrogen peroxide content on the relative expansion of aerated pastes with different W/S (* no result).....	81

Figure 4.4 Effect of hydrogen peroxide content on expansion of pastes with identical mass (~240 g) and W/S=0.425 (from left to right, hydrogen peroxide contents 0 %, 0.25 %, 0.50 %, 0.75 %, 1.50 %, the scale bar shows cm units). ... 82

Figure 4.5 Effect of hydrogen peroxide content on the relative expansion of aerated mortars (Sa/S=1) with different W/S..... 83

Figure 4.6 Effect of hydrogen peroxide content on the apparent density of aerated pastes with different W/S. 84

Figure 4.7 Effect of W/S on the apparent density of aerated pastes with different hydrogen peroxide contents..... 85

Figure 4.8 Effect of hydrogen peroxide on the apparent density of mortars (Sa/S=1) with different hydrogen peroxide contents..... 87

Figure 4.9 Effect of W/S on of the apparent density of mortars (Sa/S=1) with different hydrogen peroxide contents..... 88

Figure 4.10 Effect of hydrogen peroxide on the apparent density of mortars (Sa/S=2) with different W/S..... 89

Figure 4.11 Comparison of the calculated density of the paste phases in paste and mortar (Sa/S=1) specimens with W/S=0.40 and different hydrogen peroxide contents..... 91

Figure 4.12 Comparison of the calculated of the paste phases of pastes in paste and mortar (Sa/S=1) specimens with W/S=0.45 and different hydrogen peroxide contents..... 91

Figure 4.13 Effect of mass ratio of sand in specimens on the apparent density of paste phase in specimens with W/S=0.50 and different hydrogen peroxide contents.	92
Figure 4.14 Porosity of pastes as a function of apparent density.	93
Figure 4.15 Relationship between the apparent densities of prism samples and cylindrical samples.	95
Figure 4.16 Effect of W/S ratio on the 28-day compressive and flexural strengths of sealed-cured non-aerated pastes.	96
Figure 4.17 Effect of hydrogen peroxide on the 28-day compressive strength of sealed-cured aerated samples with different W/S.	97
Figure 4.18 Variation of 28-day compressive strengths of sealed-cured prism samples with apparent density, at different hydrogen peroxide contents and W/S.	98
Figure 4.19 Comparison of compressive strengths of aerated pastes in the current study with aerated alkali-activated concretes produced using different types of gas-releasing agents from the existing literature.	100
Figure 4.20 Relationships between the 28-day flexural and compressive strengths of sealed-cured aerated pastes with different hydrogen peroxide contents and W/S.	101
Figure 4.21 Relationships between compressive strength ratio and apparent density ratio of pastes with different W/S and hydrogen peroxide contents.	102
Figure 4.22 Relationship between macro porosities and compressive strengths of aerated pastes with different W/S and hydrogen peroxide contents.	103

Figure 4.23 Strength development of pastes with W/S=0.45 and different hydrogen peroxide contents.....	104
Figure 4.24 Compressive strength of ambient-cured pastes with W/S=0.45 and different hydrogen peroxide contents.....	105
Figure 4.25 X-ray diffractogram of the leachate on samples.....	106
Figure 4.26 Visible changes during ambient curing for pastes with W/S=0.45 and different hydrogen peroxide contents: a) After demolding, b) After 2 days of curing, c) After 9 days of curing, and d) After 25 days of curing.	107
Figure 4.27 Effect of oven curing and duration on the compressive strengths of pastes with W/S=0.45 and different hydrogen peroxide contents.....	109
Figure 4.28 Relationship between apparent density of prism samples and cylindrical samples.....	110
Figure 4.29 Variation of 28-day compressive strengths with apparent densities for sealed-cured mortars containing different hydrogen peroxide contents with W/S=0.40 and 0.50.....	111
Figure 4.30 Relationship between 28-day flexural strengths and compressive strengths of sealed-cured mortars with W/S=0.40 and 0.50 and different hydrogen peroxide contents.....	112
Figure 4.31 Relationship between compressive strength ratios and density ratios for aerated mortars containing different hydrogen peroxide contents with W/S=0.40 and 0.50.	113

Figure 4.32 Effect of humid-oven curing at 80 °C and duration on the compressive strength of mortars ($S_a/S=1$) with $W/S=0.40$ and different hydrogen peroxide contents.....	115
Figure 4.33 Effect of humid-oven curing at 80 °C and duration on the compressive strength of mortars ($S_a/S=1$) with $W/S=0.50$ and different hydrogen peroxide contents.....	116
Figure 4.34 Effect of apparent density on water absorption (by volume) of pastes with different W/S and hydrogen peroxide contents.....	118
Figure 4.35 Effect of apparent density on water absorption (by volume) of pastes with $W/S=0.45$	119
Figure 4.36 Effect of apparent density on water absorption (by weight) of pastes with $W/S=0.45$	120
Figure 4.37 Effect of apparent density on water absorption (by volume) of mortars with $W/S=0.45$ and $S_a/S=1$	121
Figure 4.38 Effect of apparent density on water absorption (by weight) of mortars with $W/S=0.45$ and $S_a/S=1$	122
Figure 4.39 Cross sections of cylindrical samples: a) 40-0-50, b) 50-0-25, c) 375-1-50, d) 45-1-25, e) 60-2-50, and f) 50-2-25.....	124
Figure 4.40 Close-ups of cross sections of aerated pastes: a) 40-0-25, b) 40-0-50, c) 40-0-75, d) 50-0-25, e) 50-0-50, and f) 50-0-75 (images are 30 mm x 30 mm).	126
Figure 4.41 Close-ups of cross section of aerated mortars: a) 40-1-25, b) 40-1-50, c) 40-1-75, d) 50-1-25, e) 50-1-50, and f) 50-1-75 (images are 30 mm x 30 mm).	128

Figure 4.42 SEM images of pastes at 100x magnification: a) 45-0-0, b) 45-0-25, c) 45-0-50, and d) 45-0-100.....	130
Figure 4.43 SEM images of pastes at 1000x magnification: a) 45-0-0, b) 45-0-50, c) 45-0-75, and d) 45-0-125.	131
Figure 4.44 SEM images of aerated pastes at 500x magnification: a) 45-0-50 and b) 45-0-100.	132
Figure 4.45 SEM images of mortars at different magnifications: a) 40-1-0 and b) 40-1-75.	132
Figure 4.46 Variation of thermal conductivity with dry density for aerated pastes with different W/S and hydrogen peroxide contents.....	133
Figure 4.47 Comparison of thermal conductivities of aerated pastes to some of aerated concretes in literature.....	135
Figure B.1 Aerated Pastes: a) 45-0-100 and b) 45-0-125.....	171
Figure B.2 Aerated pastes: a) 40-0-25, b) 40-0-50, c) 40-0-75, d) 425-0-25, e) 25-0-50, and f) 425-0-75.....	172
Figure B.3 Aerated pastes: a) 45-0-25, b) 45-0-50, c) 45-0-75, d) 50-0-25, e) 50-0-50, and f) 50-0-75.....	173

LIST OF ABBREVIATIONS

AAAS	: Aerated alkali-activated slag.
AAS	: Alkali-activated slag.
AASC	: Alkali-activated slag cement.
ACI	: American Concrete Institute.
ASTM	: American Society for Testing and Materials.
CEMBUREAU	: The European Cement Association.
GGBFS	: Ground granulated blast furnace slag.
OPC	: Ordinary Portland cement.
Sa/S	: Sand-to-slag ratio.
W/S	: Water-to-slag ratio.

CHAPTER 1

INTRODUCTION

1.1 General

Aerated concrete, a cementitious material comprising more or less homogeneous macroscopic air voids formed by the addition of a prepared foam or by the generation of gas in the fresh state, is a lightweight construction material which has a history of more than 100 years. There exist several other names in the literature to describe similar materials including *cellular concrete*, *gas concrete*, and *foam concrete*. The most striking features of aerated concrete that distinguish it from ordinary concrete are its workability and low density. Workability allows for self-compactability, whereas low density allows for a significant reduction in structural weight, amounts of binder and fillers used, thermal conductivity, handling and transportation costs, and construction time. Aerated concrete can be produced in the density range of 200-1920 kg/m³ depending on the specific gravity of the constituent materials and air content. It can be classified into two categories according to its density range as insulating concrete or low-strength concrete which have densities lower than 800 kg/m³ and semi-structural concretes which have densities higher than 800 kg/m³ (Fouad, 2006). Aerated concrete has become a reliable and an attractive material for various applications including floor fills, roof deck fills, underground fills, and precast concrete blocks.

Portland cement-based concretes have become the most prevalent construction material all around the world over the past century and consume tremendous

amounts of resources. Typically, contemporary concrete contains about 16-20 % of cementitious material, 60-70 % of aggregate, 6-8 % of mixing water, and 2-3 % of admixtures by mass (Li, 2001). Judging by cement produced in 2015, it can be estimated that concrete consumes about 4.6 billion tons cement (CEMBUREAU, 2015), 16.5 billion tons of aggregate, 1.8 billion tons of mixing water, and 640 million tons of admixtures. The estimated concrete production is about 24 billion tons. Obtaining large amounts of aggregates and raw materials for cement production not only requires a significant amount of energy but also has a great environmental impact in terms of natural resource consumption and emission of greenhouse gases. It is already known that Portland-based cements have higher energy consumption and emission of greenhouse gases than other constituents of concrete. Therefore, reduction in the energy consumption and CO₂ emissions of concrete for the sustainability in the industry is directly related to the use of high amounts of Portland cement-based binders. As such alkali-activated binders, generally produced by using industrial by-products such as blast furnace slags and fly ashes or natural pozzolans with a small amount of alkali metals, are a promising alternative to Portland cement-based binders.

Ground granulated blast furnace slag (GGBFS) is a highly amorphous latent cementitious product, comprising essentially silicates and aluminosilicates of calcium. The activation of GGBFS with alkali metals has a history more than 100 years (Kühl, 1908). Owing to being a by-product of the iron industry and its ability to be activated with considerably lower amounts of alkalis, GGBFS has become one of the most-used cementitious materials for the production of alkali-activated composites all around the world. Furthermore, it is possible to achieve comparable strength and durability with alkali-activated GGBFS composites than those of Portland cement-based composites with a lower environmental footprint (Shi et al., 2006).

One way of producing aerated concrete is to mix a gas-releasing agent with cementitious pastes or mortars. The most commonly used gas-releasing agent is

aluminum powder, even though it is not only a high-cost material but also its production requires a significant amount of energy with high carbon dioxide emissions. Industrial pure aluminum powder is generally produced by atomizing molten aluminum (Davis, 1993). Hao et al. (2016) estimated the greenhouse gas emission of one ton aluminum ranging 8.2 t to 21.7 t CO₂ equivalent in China which is the leading country with about 55 % of the global aluminum production (USGS, 2015). Aluminum powder reacts with calcium hydroxide and alkalis, and forms hydrogen gas. Hydrogen peroxide is another type of gas-releasing agent which generates oxygen gas during its decomposition. It is generally available in liquid form at various concentration which makes it easier and practical to work with than aluminum powder. Production of one ton hydrogen peroxide by anthraquinone process emits about 3.7 t CO₂ equivalent (Ghanta and Subramaniam, 2017). Another advantage of hydrogen peroxide is being quite cheaper than aluminum powder (Abdollahnejad et al., 2017). Therefore, in this study, it was decided to use hydrogen peroxide as a gas-releasing agent for the motivation: to produce cement-free lightweight composites utilizing a by-product of iron industry, GGBFS, with alkali activation which can be used for insulation and semi-structural purposes in the construction industry.

1.2 Objective and Scope

The objective of the current study is to investigate the effect of hydrogen peroxide on physical, thermal, and mechanical properties of alkali-activated slag pastes and mortars under different curing regimes. Within in the scope of the thesis, experimental program was performed in two parts. In the first part, mixtures were prepared with various hydrogen peroxide, water-to-slag ratios (W/S) and sand-to-slag ratios (Sa/S) to explore the expansion mechanism and to investigate the apparent densities of produced samples. In the second part, pastes and mortars with Sa/S=1 containing hydrogen peroxide in the range of 0 to 1.25 % by mass of slag were prepared. For all the mixtures, the amount of alkali solution, a mixture of sodium hydroxide and sodium silicate, was kept constant. The sodium silicate

solution-to-slag ratio and sodium hydroxide solution-to-slag ratio were 0.25 and 0.11, respectively. Setting times of pastes without hydrogen peroxide were determined using a Vicat needle in accordance with ASTM C191-13 (2013). Flowability of pastes and mortars were determined using the standard flow cone. Compressive and flexural strength tests and water absorption tests were performed for mixtures cured in sealed condition to investigate the effect of W/S and hydrogen peroxide content. In addition, compressive strength of two base series (pastes containing hydrogen peroxide in the range of 0 to 1.25 % with W/S=0.45 and mortars containing hydrogen peroxide in the range of 0 to 0.75 % with W/S=0.40 and 0.50) were measured following ambient curing and humid-oven curing at a temperature of 80 °C. The effect of hydrogen peroxide content and W/S of mixtures on the size and amount of pores was visually assessed on images of smoothed cross sections of selected aerated pastes and mortars using optical microscopy. Furthermore, microstructures of selected samples were investigated using scanning electron microscopy. Thermal conductivities of aerated pastes were investigated in accordance with ASTM E1530 (2016).

This thesis is divided into five chapters, including the introduction. In Chapter 2, background information on alkali activation and properties of alkali-activated GGBFS are presented. Production methods and properties of aerated concrete are also given, along with a brief literature review of alkali-activated aerated concrete. In Chapter 3, properties and proportions of the materials used to prepare the mixtures, and details of performed experiments are given. In Chapter 4, the results of the tests performed are presented. Test results are interpreted and discussed in this chapter. Finally, the conclusions of the study and recommendations for future work are presented in Chapter 5.

CHAPTER 2

LITERATURE REVIEW

2.1 Introduction

Since alkali-activated materials are investigated in this study, background information on materials and methods used in such systems are provided in this section. Furthermore, background information on lightweight concretes, and production methods and properties of aerated concrete are also given, along with a brief literature review of alkali-activated aerated concrete.

2.2 Definitions

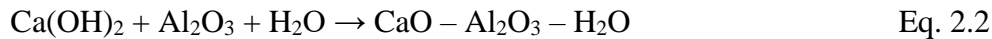
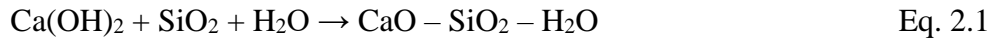
2.2.1 Pozzolanic Materials

ACI Committee 116 (2005) defines a pozzolan as;

“a siliceous or siliceous and aluminous material, which in itself possesses little or no cementitious value but will, in finely divided form and in the presence of moisture, chemically react with calcium hydroxide at ordinary temperatures to form compounds possessing cementitious properties.”

Pozzolans are divided into two forms: artificial, such as low-calcium fly ash, (LCFA) and silica fume (SF), and natural, such as volcanic tuffs or pumicites, opaline, cherts and shales, clays and diatomaceous earths (ACI 116, 2005).

“Pozzolanic reaction” is the reaction between the siliceous or aluminous pozzolans and calcium hydroxide, and it can be simply (in an unbalanced way) written as:



2.2.2 Latent Cementitious Materials

These materials can form cementitious products after reacting with water since they are generally highly amorphous and consist of CaO, SiO₂, and Al₂O₃. However, the reaction takes much longer than that of pozzolans. Calcium hydroxide, a small amount of Portland cement, calcium sulfate and alkali compounds can be used to shorten the reaction time (Purdon, 1940). High-calcium fly ashes (HCFA) or ground granulated blast furnace slags (GGBFS) are the best known of latent cementitious materials.

2.2.3 Alkali Activation

The term “*activation*” is used to describe the stimulation of the pozzolanic reaction in pozzolans or acceleration of reaction of latent cementitious materials with water (Jiang, 1997). According to Regourd (1980), three methods can be used for the activation of cementitious materials: i) mechanical, by means of grinding, ii) thermal, by means of elevated temperature curing, and iii) chemical, by means of adding alkali metal sources. Recently, there has been an increasing interest in the chemical activation of industrial by-products containing aluminosilicates.

Theoretically, all cementitious materials can be used for the production of alkali-activated binder by using an appropriate alkali metal source. Cementitious materials can be slags and high-calcium fly ashes that have significant amounts of calcium oxide or metakaolin, low calcium fly ash, perlite, red mud that have low calcium

oxide contents. Alkali hydroxides, silicates, carbonates, aluminates, sulfates etc. can be sources of alkali metals (Provis and van Deventer, 2012).

2.2.3.1 The Need for Alkali Activation

Portland-based cements have become the dominant binders used in the manufacture of concrete for construction purposes since the culmination of a Portland cement patent in 1824 by Joseph Aspdin (Juenger et al., 2011). Ordinary Portland cement (OPC) is produced by intergrinding a small amount of calcium sulfate and clinker obtained after cooling of raw materials, a mixture of limestone and clay or shale, burned at about 1500 °C. This process requires a significant amount of energy which leads to high carbon dioxide emissions (Erdoğan, 2014a). The manufacture of one ton Portland cement emits approximately 0.87 tons of CO₂ (Juenger et al., 2011). Thus, the cement industry is responsible for about 5-8 % of anthropogenic CO₂ emissions (Scrivener and Kirkpatrick, 2008) and 2-3 % of global energy consumption (Juenger et al., 2011). Therefore, there has been a growing search for low-CO₂ and low-energy binders in the construction industry. Since alkali-activated cements and concretes are produced using industrial by-products or wastes such as blast furnace slag or fly ashes, and natural pozzolans which do not require a burning and obtaining process, substantial amounts of energy and CO₂ savings can be achieved. However, the production processes of alkali activators have high CO₂ emissions (Erdoğan, 2014a). Duxson et al. (2007) estimated a greater than 80 % reduction in CO₂ emission for alkali-activated fly ash and/or metakaolin binders containing at most 10 % dissolved solids (Na₂O and SiO₂) content of the activating solution over Portland cement binder. Reduction in CO₂ emissions is generally evaluated under the environmental impact category of global warming potential. In addition there are other types of environmental impact categories such as abiotic depletion, ozone layer depletion, fresh and marine water ecotoxicity, human toxicity, eutrophication, acidification, and photochemical oxidation. It is important to take these impacts into the account for the evaluation of a construction material as an environmentally-friendly material (Erdoğan, 2014a). Habert et al. (2011)

compared the environmental impacts of producing fly ash-, metakaolin-, and GGBFS-based alkali-activated concretes with environmental impacts of 1 m³ of OPC concrete, and with 1 m³ of OPC concrete containing 30 % mineral admixture at identical 28-day strength. While fly ash-, and metakaolin-based alkali-activated concretes were reported to have much higher impacts than that of OPC concrete in the environmental impact categories other than global warming potential, GGBFS-based alkali-activated concretes were reported to have lower global warming, acidification and ozone layer depletion potential than that of OPC concrete.

2.2.3.2 Historical Background of Alkali-Activated Cement and Concrete

Alkali-activated materials have been developed since the beginning of the 20th century as an alternative to Portland cement-based materials. Kuhl (1908) patented the use of amorphous basic slag with alkali sulfate and carbonate to form a binder that had strength comparable to Portland cement-based materials. Reactivity of slags was investigated to use slag in the production of cement by Chassevent (1937) and Feret (1939). However, the first extensive study on the activation of slag using alkali compounds was performed by Purdon (1940). In the study, activation of 31 different Belgian slags was investigated using sodium hydroxide or a combination of sodium carbonate and lime. Later, Glukhovsky (1959) produced binders using low-calcium or calcium-free clays with alkali solutions and named them “*soil cements*”. Subsequently, Davidovits (1981) produced binders using kaolinite with alkali compounds and named them “*geopolymers*”. Since then, the term geopolymer has become popular and is often used to describe any and all alkali-activated cementitious materials, even though many believe the two do not signify the same thing (Erdoğan, 2014b). For a comprehensive historical background, the reader is referred to the book by Provis and van Deventer (2012).

2.2.3.3 Classification of Alkali-Activated Cements

Alkali-activated cements can be classified according to their hydration products and starting cementitious materials. Krivenko (2010) proposed a classification for alkali-activated cementitious materials according to composition of hydration products as: i) Alkaline hydro aluminosilicates ($R_2O - Al_2O_3 - SiO_2 - H_2O$) where low calcium materials such as metakaolin and fly ash can be used, and ii) Alkaline earth hydro silicates ($R_2O - CaO - Al_2O_3 - SiO_2 - H_2O$), where high calcium materials such as blast furnace slags can be used and R is an alkali cation such as Li, Na, or K. Krivenko (2010) classified alkali-activated cements into five categories according to their composition; i) Alkaline OPC cement (AOPC) which consists of OPC clinker and R_2O , ii) Blended alkaline OPC which consists of OPC clinker and additives (slag, ash, and basalt), iii) Slag alkali-activated cement (SAC) which consists of metallurgical slag and R_2O , iv) Fly ash alkali-activated cement (FAC) which consists of fly ash and R_2O , and v) Geocement (GC) which consists of clay and R_2O . Figure 2.1 illustrates the chemical composition of these cements using a $CaO - Al_2O_3 - SiO_2$ ternary diagram and compares them with OPC. An increase in the R_2O content can be seen with decreasing CaO content in the alkali-activated cements.

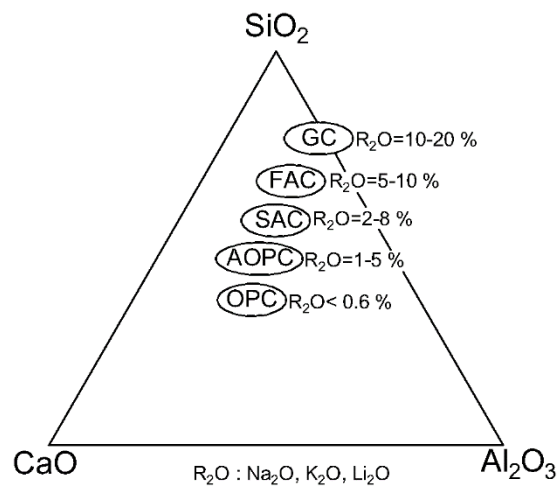


Figure 2.1 Ternary diagram of alkali-activated cements (Krivenko, 2010).

2.2.3.4 Alkali Activators

Various types of alkali activators have been used for the activation of cementitious materials and their physical and chemical properties directly influence the activation process. The choice of alkali activator depends not only on availability and cost of the alkali activators but also on the cementitious materials to be used. The selectivity of alkali activators is already known for the activation of cementitious materials (Shi and Day, 1996). Highly alkali activators are favorable for the activation of low-calcium materials i.e. fly ash and metakaolin. Moderate alkali activators are generally used for the activation of high-calcium materials (Pacheco-Torgal et al., 2013).

A classification of some alkali activators with respect to their chemical compositions is given in Table 2.1. Generally, potassium-based chemicals are more expensive and scarce in the market than sodium-based chemicals, which causes the high dominance of sodium-based activators for the activation of cementitious materials (Shi et al., 2006). Sodium hydroxide and sodium silicate are the most used activators.

Table 2.1 Classification of alkali activators (Glukhovsky, 1980).

Alkali Activator	Chemical Formula
Caustic alkalies	MOH
Non-silicate weak acid salts	M_2CO_3 , M_2SO_3 , M_3PO_4 , MF
Silicates	$M_2O \cdot nSiO_2$
Aluminates	$M_2O \cdot nAl_2O_3$
Aluminosilicates	$M_2O \cdot Al_2O_3 \cdot (2-6)SiO_2$
Non-silicate strong acid salts	M_2SO_4

M - Alkali metal

Sodium hydroxide, produced generally through the chlor-alkali process which has a considerable environmental footprint, has wide spread utilization for the activation of cementitious materials due to its availability, low cost and reasonable viscosity among the caustic alkalis. However, it has a corrosive nature which makes it difficult to produce and handle at high concentrations and large volumes. In addition, the use of high concentrations of sodium hydroxide in alkali-activated materials may lead to efflorescence through the reaction of excess alkali with CO₂ (Provis and Deventer, 2014).

Sodium silicates, commonly named waterglass, have been widely used for the activation of cementitious materials. Sodium silicate has the chemical formula Na₂O·nSiO₂ where n is the degree of polymerization. The mass ratio of SiO₂ to Na₂O is defined as the modulus of sodium silicate (M_b). The commercial liquid sodium silicates can be found with a modulus between 1.6 to 3.3 in the market. It is common practice to add sodium hydroxide to decrease the modulus of sodium silicate solutions as needed (Shi et al., 2006). Generally, the dosage of the sodium silicate solution for alkali-activated materials is indicated by Na₂O %, percentage of Na₂O in the alkali solution by mass of the slag.

2.3 Ground Granulated Blast Furnace Slag

Slag, a by-product of the metallurgical industry, is a non-metallic product which is comprised of silicates and aluminosilicates of calcium. Being a by-product, its chemical composition varies broadly according to types of raw materials used and the production process. Generally, the term “slag” is used to imply the by-product of the iron industry, known as “blast furnace slag” in cement and concrete terminology (Tokyay, 2016). In the current study unless stated otherwise, ground granulated blast furnace slag is meant by slag. Blast furnace slag has been used as a cementitious material in combination with slaked lime since 1774 in the cement and concrete industry (ACI 233, 2003).

Iron ores with an iron content of 50-70 % are generally used in the production of iron. These ores contain hematite (Fe_2O_3), magnetite (Fe_3O_4), limonite ($\text{Fe}_3\text{O}_4 \cdot n\text{H}_2\text{O}$) or siderite (FeCO_3) with impurities of silica and clay. It is essential to remove impurities from iron ore for the production of iron pig. For this purpose, a mixture of iron ore, coke (fuel and reduction agent) and limestone are subjected to air blowing at a high temperature and pressure in a blast furnace. Several chemical reactions take place during heating, and molten iron and liquid iron blast furnace slag are obtained. Owing to the density difference of these materials, they can be obtained separately (Erdoğan, 1997).

Temperature of liquid blast furnace slag is between 1,400 °C and 1,600 °C after discharging. Three types of solid slags can be produced with different cooling methods: i) air-cooled blast furnace slags, ii) expanded blast furnace slags, and iii) granulated blast furnace slags. Air-cooled blast furnace slags essentially consist of crystalline calcium silicates as a result of gradual cooling. Expanded blast furnace slags obtained by water or air cooling have hollow structure which makes them a suitable candidate for lightweight aggregate for concrete. Granulated blast furnace slag is generally obtained after rapid cooling in water. Among these, owing to their highly amorphous structure, granulated blast furnace slags show latent cementitious properties in ground form (Erdoğan, 1997).

GGBFS is mainly composed of CaO , SiO_2 , Al_2O_3 and MgO . A comparison of the chemical composition of blast furnace slags produced in different countries and that of Portland cement is given in Table 2.2 (Erdoğan, 1997).

Table 2.2 Comparison of chemical compositions of various blast furnace slags and a Portland cement (Erdoğan, 1997).

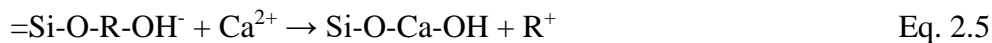
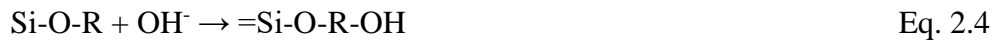
Oxide	US and Canada	South Africa	Australia	Turkey	Portland Cement
CaO	29-50	30-40	39-44	34-41	60-67
SiO ₂	30-40	30-36	33-37	34-36	17-25
Al ₂ O ₃	7-18	9-16	15-18	13-19	3-8
Fe ₂ O ₃	0.1-1.5	-	0-0.7	0.3-2.5	0.5-6
MgO	0-19	8-21	1-3.0	3.5-7	0.1-4
MnO	0.2-1.5	-	0.3-1.5	1-2.5	-
S	0-2	1.0-1.6	0.6-0.8	1-2	-
SO ₃	-	-	-	-	1-3

2.3.1 Alkali Activation of GGBFS

2.3.1.1 Reaction Mechanism

There have been several attempts to describe the reaction mechanism of the alkali activation of slag in the literature. As mentioned above, GGBFS is a latent cementitious material. After mixing slag with water alone, some portion of it dissolves. However, further reaction is restrained by a protective film deficient in Ca²⁺ that is formed readily. For the continuation of the reaction high pH is needed. At this point, Portland cement can be the pH supplier since its pore solution contains alkali hydroxides. However, the OH⁻ supply of Na⁺ and K⁺ ions is finite, and hydration products bind or use a certain extent of them. Besides all these, calcium hydroxide, one of the hydration products of Portland cements, provides needed OH⁻ up to a certain slag content. Therefore, hydration can be maintained by providing OH⁻ ions supplied from other sources. These sources may be calcium or sodium hydroxides, silicates or carbonates (Taylor, 1997). This process, the continuation of the hydration of slag with alkali compounds, can be called alkali activation.

Purdon (1940) evaluated alkalis as a catalyst in the activation process. The reaction process can be described in terms of three chemical reactions (Eqs. 2.3 - 2.5) where the alkali cations are replaced by Ca^{2+} (Glukhovsky, 1994; Krivenko, 1994);



where R is an alkali cation of Na, K, Li, Rb or Cs.

Krivenko (2010) also claimed that the role of alkali compounds in alkali-activated systems is twofold: to increase hydration of slag and to form the main zeolite-like hydration products.

2.3.1.2 Hydration Products

The hydration products of AAS essentially depend on the chemical composition of the slag and nature of the activator (Shi et al., 2006). Several researchers have reported calcium silicate hydrate as the primary hydration product of AAS pastes, but minor hydration products such as hydrotalcite, calcite, AFm etc. can also form depending on the activators used (Brough and Atkinson, 2002; Escalante-Garcia et al., 2003; Fernández-Jiménez and Puertas, 2003; Puertas et al., 2004; Shi and Day, 1996; Wang and Scrivener, 1995). The Ca/Si ratio of calcium silicate hydrate is much lower than that of Portland cement hydration.

2.3.2 Major Factors Affecting Activation of GGBFS

2.3.2.1 Chemical Composition of GGBFS

Chemical composition influences the structure and hydraulic properties of blast furnace slag. According to the oxides contained in the slag, hydraulic indices, are

defined for the evaluation of hydraulic reactivity of blast furnace slag for use as a replacement of Portland cement. A detailed summary of the hydraulic indices used in the literature is given in Shi et al. (2006).

Basicity coefficient ($K_b = [\text{CaO} + \text{MgO}] / [\text{SiO}_2 + \text{Al}_2\text{O}_3]$) and quality coefficient ($K_q = [\text{CaO} + \text{MgO} + \text{Al}_2\text{O}_3] / [\text{SiO}_2 + \text{TiO}_2]$) have been widely used to express the hydraulic activity of blast furnace slag. GGBFS are divided into three categories according to their basicity coefficients: basic slag ($M_b > 1$), neutral slag ($M_b \approx 1$), and acidic slag ($M_b < 1$). Generally, basic and neutral slags are favoured over acidic slags. The effect of type of slag on strength increases with decrease pH of the alkali activator (Wang et al., 1994). It was found that increase of MgO content of GGBFS from 8 % to 13 % for sodium hydroxide- or sodium silicate-activated slags increased the rate of reaction and compressive strength (Haha, 2011), and a decrease in the rate of the hydration for GGBFS activated by sodium hydroxide or sodium silicate was observed with the increase of Al_2O_3 content from 7 % to 17 % (Haha, 2012).

2.3.2.2 Type of Activators

According to Fernández-Jiménez and Puertas (2003), an appropriate activator to be used in the activation of slag should accelerate the solubility of slag in the activating solution, promote the formation of stable hydrates and form a network structure of hydrates. The dissolution of slag and further reactions are controlled by the pH of the activator since solubility of calcium, aluminum and silica depend on it. For a given alkali dosage, pH of sodium hydroxide is much higher than sodium silicate solutions, however the amount of reacted slag is similar and generally higher mechanical strengths are obtained for the sodium silicate-activated slag than that of sodium hydroxide-activated slag (Provis and Van Deventer, 2012). In the existing literature, the most commonly used activators of GGBFS are NaOH, Na_2SiO_3 , Na_2CO_3 and Na_2SO_4 .

2.3.2.3 Dosage of Activators

Generally, the strength of alkali-activated slag composites increases with the increase of dosage of the activators up to a certain point which depends on the type of the slag, activator and curing type (Al-Otaibi, 2002). Using higher dosages of alkalis in the activation process may lead to some problems such as rapid setting and efflorescence. There is no consensus on an optimum dosage of activator for activation of slag in the literature. Purdon (1940) suggested the use of 5-8 % of NaOH by mixing water for alkali-activated slag mortars and concretes. Wang et al. (1994) reported the optimum dosage as 3.0-5.5 % Na₂O of slag weight.

2.3.2.4 Curing Temperature

The effect of temperature on the hydration of alkali-activated slag is more explicit than that of Portland cement, due to the higher activation energy of slag (Shi and Day, 1996). The rate of hydration is a function of temperature and increases about two times with an increase in reaction temperature of 10 °C (Shi et al., 2006). Wang (1994) concluded that alkali-activated slag composites produced using low-quality slag with weak alkali or alkali by-products would be beneficial and feasible in practice by applying high-temperature curing.

2.3.2.5 Fineness

Fineness is an indicator of the average particle size of blast furnace slag and increase of fineness refers to smaller average particle size. Hydraulic reactivity of blast furnace slag generally increases with the increase of fineness. However, the ability of slag to be ground is lower than clinker (Öner, 2000), therefore it may not be economical to use slags with higher fineness. The chemical composition, type of activators and curing conditions influence the optimum fineness of slag. Wang et al. (1994) stated the optimum fineness to be between 450 m²/kg and 650 m²/kg for

acidic and neutral slags, and between 400 m²/kg and 550 m²/kg for basic slags by taking the strength of alkali-activated slag cements into account.

2.3.3 Properties of Alkali-Activated Slag Concretes

2.3.3.1 Fresh Properties

2.3.3.1.1 Setting Time

Previous studies on alkali-activated slag cements have shown that chemical composition and fineness of slag, type and dosage of activators, and additives directly influence setting time (Shi et al., 2006).

Purdon (1940) explored the effect of different activators and dosages on the setting times of various alkali-activated slag cements. It was found that the setting times of alkali-activated slag cements with a similar chemical composition varied for a given activator. Kovtun et al. (2015) investigated the setting times of AASCs activated by dry sodium carbonate. The initial setting times of AASCs did not exhibit a significant change with the increase of Blaine fineness from 390 m²/kg to 430 m²/kg, but final setting time decreased about 50 %.

Generally, increase of activator dosage decreases the setting times of AASCs for a given activator. The initial and final setting times of AASCs activated by 4 % sodium hydroxide solution were found to be 125 and 205 minutes, respectively, and increasing sodium hydroxide content to 8 % decreased initial and final setting times to 70 and 140 minutes, respectively (Purdon, 1940). Chang (2003) reported a decrease in the setting times of AASCs activated by sodium silicate solution with the increase of dosage of sodium silicate or sodium hydroxide. The fast reaction between Ca²⁺ and silicate ions of the sodium silicate solution was claimed to be the reason of decreased setting times (Fernández-Jiménez and Puertas, 2001).

Živica (2007) measured the setting times of AASCs activated by sodium hydroxide, sodium carbonate and sodium silicate with dosages of 3, 5 and 7 % by slag weight. Setting times did not change with the increase of sodium hydroxide dosage. Initial setting time of AASCs activated by 3 % and 5 % sodium carbonate were found to be the same, and with an increase of dosage to 7 % the initial setting time decreased from 60 minutes to 40 minutes, however no change was observed for the final setting time which was 140 minutes. Initial and final setting times of AASCs for the dosage of 3 % sodium silicate ($M_b=1.13$) were measured as 40 and 80 minutes, respectively. The increase of sodium silicate dosage from 3 % to 7 % decreased the initial and final setting times to 0 and 30 minutes. Fernández-Jiménez and Puertas (2003) investigated effect of different activators, namely Na_2SiO_3 , NaOH and Na_2CO_3 , and various combinations of these on the setting times of AASCs at 4 % Na_2O content. It was found that sodium silicate-activated slag exhibited the shortest setting times, and sodium carbonate-activated slag exhibited the longest setting times.

Setting times of AASCs can be controlled by using additives. Brough et al. (2000) investigated the effect of NaCl and malic acid on the setting times of AAS activated by sodium silicate ($M_s=1.5$). Initial and final setting times of AASC with solution-to-slag ratio of 0.50 were measured as 240 minutes and 300 minutes, respectively. Addition of 1 % and 4 % NaCl was found to be effective in reducing the setting times, but addition 8 % NaCl increased the setting times. Also, the initial and final setting times of AASC with the addition of 0.5% of malic acid were found to be 1200 and 1320 minutes, respectively. Chang (2003) found that setting times of sodium silicate-activated AASC is sensitive to phosphoric acid concentration.

2.3.3.1.2 Workability

Collins and Sanjayan (1999a) investigated the workability of alkali-activated slag concretes. It was found that the workability of alkali-activated slag concretes produced using powdered sodium silicate and lime slurry is higher than that of concrete produced using liquid sodium silicate and lime slurry or sodium hydroxide and sodium carbonate. Also, the slump loss in time of slag activated with dry sodium silicate and lime slurry was found to be negligible, while others exhibited significant loss. Bakharev et al. (1999a) suggested the use of a sodium silicate solution with a 4 % Na content and modulus of 0.75 by consideration of workability and strength of alkali-activated pastes, and reported a decrease in workability with the increase of sodium silicate modulus.

Workability of alkali-activated slag pastes activated by a combination of potassium hydroxide and sodium silicate as assessed by flow diameter was found to be mostly dependent on the alkali content (K_2O+Na_2O), silica (SiO_2) content and water content. Effect of increasing potassium hydroxide content at a given sodium silicate and W/S continuously increased the workability up to an alkali content of 12.1 %. Workability of pastes fluctuated with the increase of sodium silicate, whereas workability increased at silicate content of 4 % and 10 %, decreased at silicate content of 6 % and 8 %. Also, increase of water contents yielded a significant increase of workability in terms of flowability (Qureshi and Ghosh, 2013).

2.3.3.2 Hardened Properties

2.3.3.2.1 Strength

Several studies have been conducted on the strength gain characteristics of alkali-activated slag composites (Altan and Erdoğan, 2012; Atiş et al., 2009; Aydın and Baradan, 2012; Bakharev et al., 1999a, 1999b; Brough and Atkinson, 2002; Chi, 2012; Fernández-Jiménez et al., 1999; Fernández-Jiménez and Puertas, 2003;

Puertas et al., 2000; Purdon, 1940; Rashad et al., 2013; Ravikumar and Neithalath, 2012; Shi, 1996b; Wang et al., 1994; Yang et al., 2008). Major factors reported to influence the strength gain of alkali-activated composites are the nature and fineness of the slag, type and concentration of the activator, water content, curing type, and temperature.

Wang et al. (1994) investigated the effect of several activation parameters on the compressive strength of alkali-activated slag mortars. Six slags with different chemical compositions, two basic, two neutral, and two acidic slags, were used. The compressive strengths of mortars were found to vary with activator type and dosage. Among the activators used, sodium silicate resulted the highest strength.

Purdon (1940) found that an increase of the fineness of slag had a positive effect on the early strength of alkali-activated mortars and concretes, however it was observed that this effect decreased with age. Collins and Sanjayan (1999b) found that replacement of 10 % ultrafine slag with a Blaine fineness of 1496 m²/kg in alkali-activated slag concretes increased one-day strength. Bakharev et al. (2000) reported an increase in 28-day strength of sodium silicate-activated pastes with the addition of 5% ultrafine slag. In addition, water demand also increases with the increase of fineness. Thus, for a given workability increase of fineness leads to a decrease in strength at later ages (Fernández-Jiménez et al., 1999).

The nature of the activator used was found to be the most significant factor among activator dosage, fineness of slag and curing temperature on the mechanical strengths of alkali-activated slag mortars (Fernández-Jiménez et al., 1999). In the same study, among the activators used, a combination of NaOH and Na₂SiO₃, NaOH or NaCO₃, a combination of NaOH and Na₂SiO₃ gave the highest mechanical strengths for alkali-activated mortars regardless of the other factors. Alkali-activated slag mortars with 4 % Na₂O cured at 25 °C gave the highest compressive strength and flexural strength achieved, 100 MPa and 12 MPa, respectively. In addition, while fineness of slag was found to be the least

contributing factor, dosage of the activator was the second most significant factor on the mechanical strengths. Shi (1996) investigated the compressive strength gain of NaOH-, NaCO₃- and Na₂SiO₃.9H₂O-activated slag mortars with a dosage of 6 % Na₂O at a fixed water content and Na₂SiO₃ was found to be the most effective activator with 28-day strength of about 62 MPa.

Fernández-Jiménez and Puertas (2003) investigated the effect of different activators namely Na₂SiO₃, NaOH and Na₂CO₃, and various combinations of these on the compressive strength gain of alkali-activated slag pastes at 4 % Na₂O content. The highest early and later age strengths (~90 MPa at 28-days) were obtained for the samples activated by sodium silicate solutions. The reason for the high strength of pastes activated by sodium silicate was claimed to be the interaction of silicate anions with dissolved Ca²⁺ ions which forms calcium silicate hydrate.

Bakharev et al. (1999a) investigated the effect of activator type and dosage on the compressive strength of alkali-activated slag pastes produced using NaOH, Na₂SiO₃, Na₂CO₃, Na₃PO₄, and combinations of these. A neutral slag blended with 2 % gypsum was used. In the study, non-silicate salts of weak acids were not found to be suitable for the activation of neutral slags. Pastes activated using a combination of NaOH and Na₂SiO₃ solution gave the highest strengths among the activators used. Figure 2.2 shows the effect of activator type and dosage on the 28-day compressive strength of alkali-activated slag pastes.

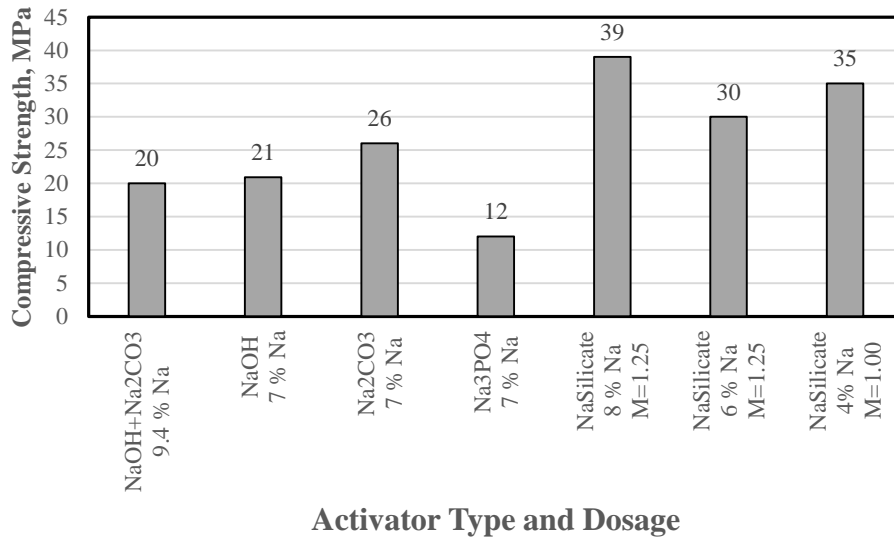


Figure 2.2 Effect of activator type on 28-day strength of alkali-activated slag pastes (Bakharev et al., 1999a).

Concentration of activators have a great influence on strength gain of alkali-activated composites. Altan and Erdoğan (2012) investigated the effect of several parameters such as activator type and concentration, curing type and duration, and water content on strength gain of alkali-activated slag mortars. It was found that in the case of room temperature curing increase of sodium hydroxide concentration increased the compressive strength of alkali-activated mortars produced using sodium hydroxide and sodium silicate blended activator solutions at a constant sodium silicate content of 25 % of mass of slag and W/S of about 0.42. Figure 2.3 shows the effect of NaOH concentration on the compressive strength of alkali-activated slag mortars. In addition, the compressive strength of alkali-activated mortars cured at 80 °C increased with the increase of sodium silicate content in mixtures containing similar water content. Figure 2.4 shows the effect of sodium silicate concentration on the compressive strength of alkali-activated slag mortars.

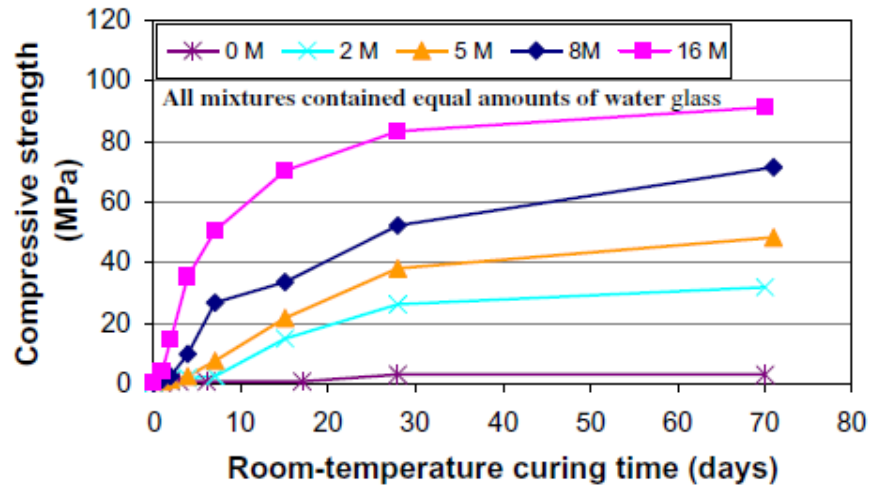


Figure 2.3 Effect of NaOH concentration on compressive strength of alkali-activated slag mortars (Altan and Erdoğan, 2012).

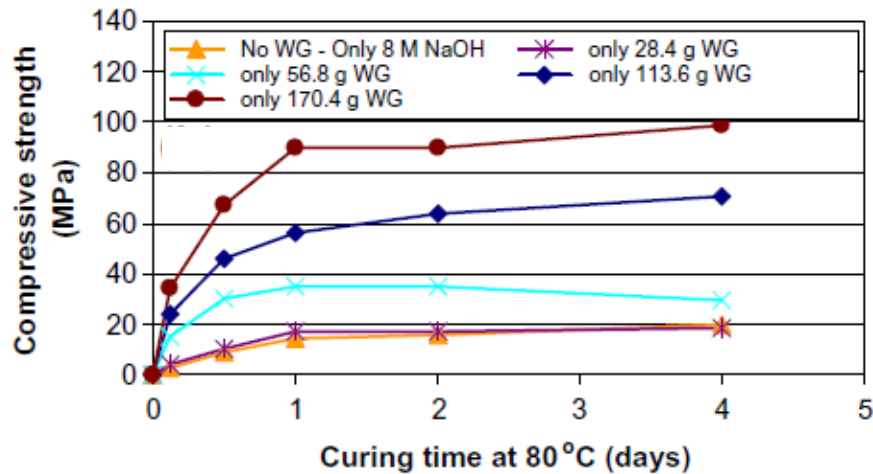


Figure 2.4 Effect of sodium silicate concentration on compressive strength of alkali-activated slag mortars (Altan and Erdoğan, 2012).

Early age compressive strengths of sodium silicate-activated slag composites depend on the Na_2O concentration and modulus of sodium silicate solution. Ravikumar and Neithalath (2012) found that the effect of Na_2O concentration on compressive strength was limited at the ages of 1 and 3 hours, but it was more obvious at 24 h for a given sodium silicate modulus at a constant water-to-powder

ratio. Figure 2.5 shows the effect of Na_2O concentration on early age compressive strength of alkali-activated concretes at different sodium silicate modulus.

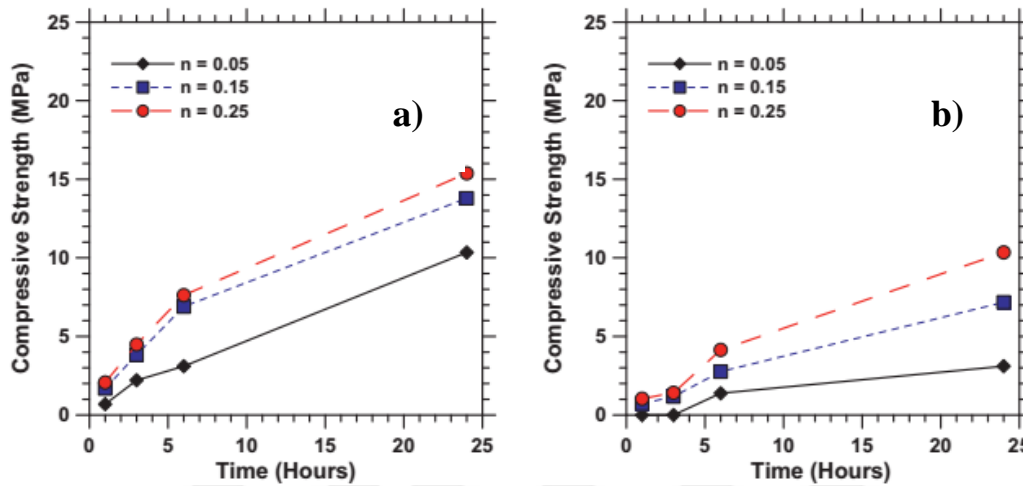


Figure 2.5 Effect of Na_2O concentration (n , by mass of slag) on early age compressive strength of alkali-activated slag concretes at different sodium silicate modulus: a) $M_s=0.60$, b) $M_s=1.50$ (Ravikumar and Neithalath, 2012).

The effect of water content on strength of alkali-activated slag composites are similar to the cement-based composites, where there is an inverse relationship between water content and strength. Besides, in alkali-activated materials increase of water content not only increases the porosity of the hardened material but also decreases the effectiveness of the activators by diluting them (Altan and Erdoğan, 2012). The effect of water content varies with the type of activators used (Shi et al., 2006). It was found that increase of water content had a significant effect on the compressive strength gain of alkali-activated mortars produced using sodium hydroxide- and sodium silicate-blended activator solutions regardless of curing temperature. Figure 2.6 and Figure 2.7 show the effect of W/S on compressive strength of alkali-activated slag mortars cured at room temperature and in a humid oven at $80\text{ }^\circ\text{C}$, respectively (Altan and Erdoğan, 2012).

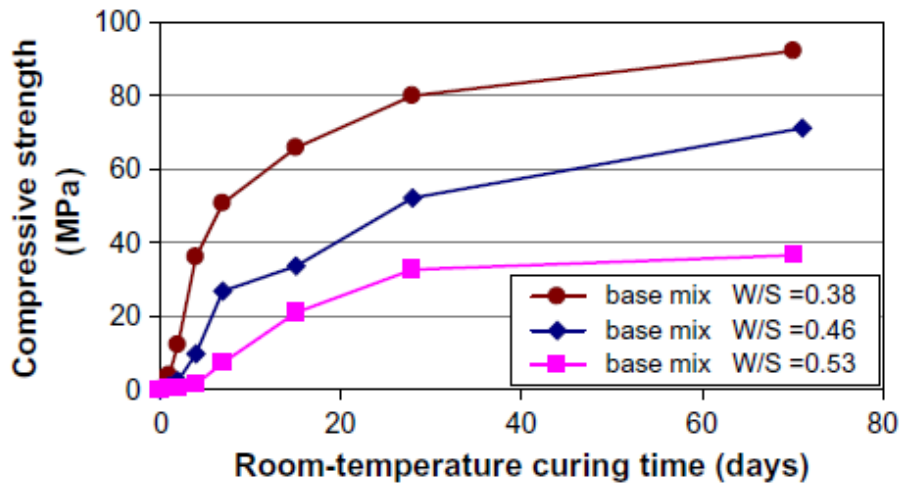


Figure 2.6 Effect of W/S on compressive strength of alkali-activated slag mortars at room temperature (Altan and Erdoğan, 2012).

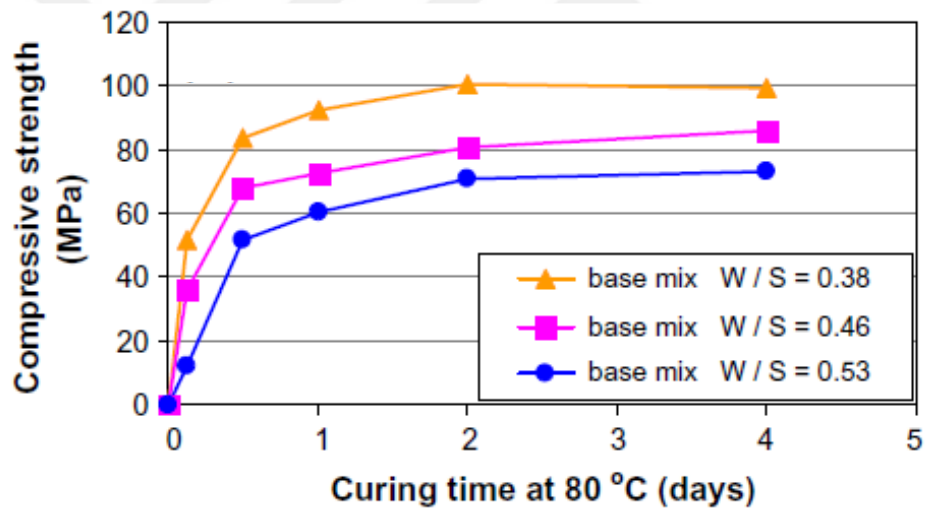


Figure 2.7 Effect of W/S on compressive strength of alkali-activated slag mortars at 80 °C (Altan and Erdoğan, 2012).

Curing type and temperature greatly influence the compressive strength of alkali-activated slag composites. Compressive strength of sodium silicate-activated slag concretes cured in saturated lime water at 23 °C were found to be considerably higher than those of sealed and exposed cured concretes at 23 °C (Collins and

Sanjayan, 2001). In another study, the compressive strength of sodium silicate-activated slag concretes cured at 60 °C and RH of 80 % were found to be significantly higher than those of cured in lime water and air (Chi, 2012). Altan and Erdoğan (2012) found that humid-oven curing at 80 °C exhibited better strength gain than that of dry oven cured at 80 °C for sodium silicate-activated slag mortars. Aydın and Baradan (2012) suggested that autoclave curing could be used instead of steam curing for high performance in sodium silicate-activated mortars containing activators with low Na₂O concentrations and high SiO₂/Na₂O ratios.

Effect of temperature on the strength gain of alkali-activated slag composites may vary for a given activator. Puertas et al. (2000) found that curing of NaOH-activated slag pastes at 65 °C had no positive effect on strength gain except one-day strength when compared to those cured at 25 °C. Altan and Erdoğan (2012) found that only sodium silicate was essential for the activation of slag at high temperature curing. Bakharev et al. (1999b) investigated the effect of heat treatment (pre-curing) on the compressive strength gain of sodium silicate-activated concrete. After exposing samples to heat treatment at 70 °C, compressive strength gain of samples were found to be higher than those of ambient-cured samples at early ages (i.e. 21 MPa vs 16 MPa at one-day), however further curing both at room temperature, compressive strengths of ambient-cured concretes were found to be higher at later ages. In addition, Altan and Erdoğan (2012) reported no significant effect of pre-curing at room temperature prior to oven curing at 80 °C on the compressive strength of sodium silicate-activated mortars.

2.3.3.2.2 Efflorescence

ACI 116 (2005) defines efflorescence as “*deposit of salts, usually white, formed on a surface, the substance having emerged in solution from within either concrete or masonry and subsequently been precipitated by reaction, such as carbonation, or evaporation*”. Generally, efflorescence is not harmful to cement-based materials, and considered as an aesthetic problem. The mechanism of formation for different

types of efflorescence is similar. The most common ones are the formation of calcium carbonate in Portland cement-based materials and sodium carbonate in alkali-activated materials (Allahverdi et al., 2013).

Dow and Glasser (2003) described the efflorescence formation of calcium carbonate in Portland cement-based materials through six coupled processes: dissolving of CO₂(g) in water, conversion of CO₂ to aqueous species, release of alkali(s), dissolution of calcium hydroxide, diffusion of reactants through the solution, and precipitation of calcium carbonate. The formation of calcium carbonate can be simply written as in Eq. 2.6 (Allahverdi et al., 2013).



Factors such as mix proportions, water content, and improper curing which affect the formation of efflorescence in Portland cement-based materials also have a similar effect in alkali-activated materials, however there are distinct differences in the type, nature, and characteristic of efflorescence that occurs in alkali-activated materials. The formation of efflorescence of sodium carbonate can be simply written as in Eq. 2.7 (Allahverdi et al., 2013).



Alkali-activated materials are sensitive to efflorescence formation of alkali carbonates. The influencing factors reported in literature on the formation of efflorescence in alkali-activated materials are the reactivity of raw materials (Škvára et al., 2012), type of alkalis (Zhang et al., 2014), dosage of alkali activators (Allahverdi et al., 2008) and curing duration (Yao et al., 2016) and temperature (Kani et al., 2012).

Škvára et al. (2012) investigated effect of leaching of Na and K alkali-activated fly ash (AAFA) and metakaolin (AAMK) on compressive strength. AAFA and AAMK particles with a size of 0.5 mm were immersed in distilled water to leach alkalis where the leached solution was changed regularly. It was found that at least 94 % of the alkalis were leached in 150 days. It was concluded that Na and K are weakly bonded in (N, K)-A-S-H gel which is the reason for being vulnerable to efflorescence. It was claimed that leaching of all Na would not lead a strength loss in AAM. Figure 2.8 shows the formation of efflorescence of AAFA sample which was partially immersed in water for 50 days.

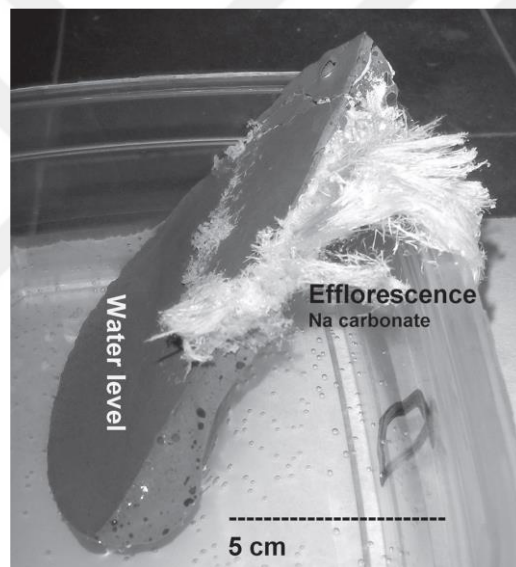


Figure 2.8 Efflorescence of AAFA sample after 50 days (Škvára et al., 2012).

Temuujin and van Riessen (2009) investigated properties of geopolymers produced using raw and fly ashes calcined at a temperature of 500 °C or 800 °C with sodium hydroxide and sodium silicate. They reported different amounts of efflorescence on the samples produced, as a result of using excess alkali compound. While there was no efflorescence observed on raw fly ash-based geopolymer, efflorescence was visible on the surface of 800 °C calcined fly ash-based geopolymer, and it was

possible to observe the efflorescence in 500 °C calcined fly ash-based geopolymer by conducting scanning electron microscopy.

Kani et al. (2012) attempted to reduce efflorescence by using Al-bearing mineral additives and hydrothermal curing in alkali-activated natural pozzolans. Samples were produced with various SiO₂/Na₂O molar ratios using sodium hydroxide and sodium silicate combinations and different Na/Al ratios to explore the efflorescence behavior. For the assessment of efflorescence severity on samples, 2 cm cube paste samples cured at ambient temperature and 95 % relative humidity for 28 days were immersed in 40 mL of water and kept in open-air at room temperature until the complete evaporation of water. After visual inspection of samples, it was seen that efflorescence increased with the increase of Na₂O content. Further, influence of hydrothermal curing between 45 °C and 125 °C, and pozzolan replacement with slag, metakaolin, or calcium aluminate cement between 2 % and 8 % were separately investigated for two different samples with highest strength and lowest efflorescence extent. It was concluded that hydrothermal curing higher than 65 °C and using calcium aluminate cements were beneficial for the decrease of efflorescence.

Zhang et al. (2014) investigated the efflorescence in fly ash-based, and fly ash and slag blended precursors activated by sodium hydroxide, sodium silicate or a combination of both. Alkali-activated binders were cured at ambient temperature and at 80 °C. In addition, effect of efflorescence on the pore structure was investigated on foamed alkali-activated binders. The formation and rate of efflorescence of sodium hydroxide-activated binders was found to be less than that of sodium silicate-activated binders cured at ambient temperature for a given alkali content. Replacement of 20 % of fly ash with slag was found to be effective to reduce formation of efflorescence. Incorporation of foam in fly ash and slag blended binders were seen to have lower impact of efflorescence formation in visual inspections.

Yao et al. (2016) investigated the effect of efflorescence on the compressive strength of alkali-activated fly ash and slag blends. A combination of sodium hydroxide and sodium silicate at a $\text{SiO}_2/\text{Na}_2\text{O}$ molar ratio of 1.4 was used for the activation. Samples cured at room temperature were exposed to different conditions: bottom-contact with water, fully immersed in water and in air, at various ages to evaluate the effect of efflorescence. Increasing initial curing duration decreased the formation of efflorescence. The efflorescence severity of samples in bottom contact with water was found to be higher than that of samples exposed to other conditions. It was reported that increase of slag content higher than 50 % in precursors increased the rate of formation of efflorescence.

2.4 Lightweight Concrete

As evident from its name, lightweight concrete, a special type of concrete, is lighter than conventional concrete. It is not a new construction material. It has a history of more than 2000 years (ACI 213, 2003) and has been used for several civil and military applications (Rudnai, 1963). Today, it is widely used worldwide as a result of its several advantages. Being lighter than conventional concrete is one of its remarkable advantages in the production and operation stages. Reduction of dead load in commercial and residential buildings, increase in construction rate, lower transportation costs, increased thermal comfort and opportunities in waste management can be considered some of them (Short and Kinniburgh, 1978)

The most practical way of producing lightweight concrete is to incorporate air into the concrete. Air can be introduced into the concrete in three different ways: i) eliminating the finer sizes from the aggregate grading (no-fines concrete), ii) replacement of aggregate with porous aggregates (lightweight aggregate concrete), iii) inclusion of gas bubbles in cement paste (aerated, foam, or cellular concrete). Lightweight concrete can also be produced using a combination of these methods (Short and Kinniburgh, 1978; Newman and Choo, 2003). Figure 2.9 describes the types of lightweight concretes.

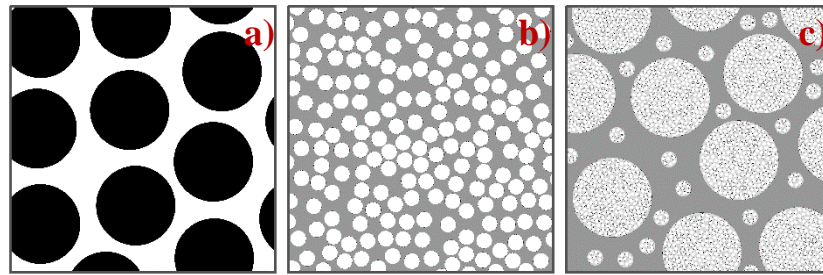


Figure 2.9 Types of lightweight concretes: a) No-fines concrete, b) Aerated concrete, and c) Lightweight aggregate concrete (adapted from Short and Kinniburgh, 1978)

2.4.1 Aerated Concrete

“Concretes having oven-dry density less than 800 kg/m^3 , which are commonly referred to as cellular or aerated concrete, may be defined as lightweight products consisting of Portland cement and/or lime with siliceous fine material, such as sand, slag, mixed with water to form a paste that has a homogeneous void or cell structure. The cellular structure is attained essentially by the inclusion of macroscopic voids resulting from a gas-releasing chemical reaction or the mechanical incorporation of air or other gases” (ACI 523, 1996).

Rudnai (1963) classified cellular concretes according to the structure and formation of pores as aerated concrete and microporites. The materials used for the production of these concretes are similar except in microporites neither gas-releasing agents nor foams are used. Microporites are produced using an excessive amount water. Evaporation of this water after hardening forms a porous material with a homogeneous structure. Rudnai (1963) classified aerated concretes according to pore forming method as foamed, air-entrained, or a combination of these. Short and Kinniburgh (1963) divided aerated concrete into two forms according to the production method as in-situ type to which air curing at ambient temperature applied and precast products to which autoclave curing applied. Also moist curing can be used for the production of aerated concrete (Valore, 1961).

As expected, aerated concrete weighs considerably less than normal-weight concrete. It has a density between 200 and 1920 kg/m³. It can be classified into two categories according to its density range as insulating concrete or low-strength concrete which have densities lower than 800 kg/m³ and semi-structural concretes which have densities between 800 and 1920 kg/m³ (Fouad, 2006). Even though aerated concrete is a special type of concrete, it cannot be considered concrete since it contains no coarse aggregate. Therefore, the term “concrete” is not appropriate for aerated concrete, it can be named “aerated mortar”. However, it has been described as “aerated concrete” or “gas concrete” or “foam concrete” in common use (Short and Kinniburgh, 1978; Neville, 2003).

2.4.1.1 Pore Formation Methods

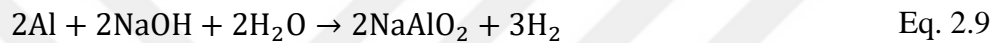
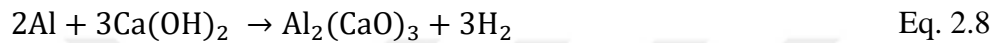
There are essentially two common methods for the formation of pores in aerated concrete. These are the air-entraining method and foaming method. In addition to these, a combination of these methods can be used.

2.4.1.1.1 Air-Entrainment Method

In this method, carbon dioxide-, hydrogen-, or oxygen-releasing agents/chemicals are used. After mixing of gas-releasing agents into the cementitious paste or mortar, the gas is released and air bubbles are formed. These air bubbles are entrapped in the cementitious matrix while still in the fresh state and the bulk volume of the paste increases. Since, it is the paste that entraps the air bubbles, its consistency has great importance (Rudnai, 1963).

Aluminum powder has been a widely used gas-releasing agent for producing aerated concrete since the beginning of the twentieth century. The first use of aluminum powder for the production of porous materials was patented by Aylsworth and Dyer (1914). The chemical literature involves a large number of reactions involving aluminum powder. In an alkali environment, such as when in

the presence of calcium hydroxide or sodium hydroxide, aluminum powder reacts with these alkalis and generates hydrogen gas. The reactions of aluminum powder with calcium hydroxide and sodium hydroxide are given in Eq. 2.8 and Eq. 2.9 (Valore, 1957). The efficiency of aluminum powder essentially depends on its fineness, freshness, purity and pH of cementitious matrix. The given reactions are also influenced by the ambient temperature and that of the cementitious matrix during production (Rudnai, 1963), therefore, it is important to control the temperature (Valore, 1957).



Beside aluminum powder, hydrogen peroxide is another type of popular gas-releasing agent for producing aerated concrete. Hydrogen peroxide, a chemical compound with the formula H_2O_2 , is generally found in liquid form, clear, colorless, and soluble in water. A comparison of some important properties of H_2O and H_2O_2 is given in Table 2.3 (Goor et al., 2000). Various aqueous hydrogen peroxide solutions with different concentrations are available. Table 2.4 compares some physical properties of different aqueous hydrogen peroxide solutions (Goor et al., 2000).

Table 2.3 Comparison of physical properties of hydrogen peroxide and water (Goor et al., 2000).

Property	Value	
	H ₂ O ₂	H ₂ O
Freezing point, °C	-0.43	0
Boiling point (101.3 kPa), °C	150.2	100.0
Heat of fusion, J/g	368	334
Heat of vaporization, J/(g.K)		
At 25 °C	1519	2443
At boiling point	1387	2258
Specific heat, (J/(g.K))		
Liquid (25 °C)	2.629	4.182
Gas (25 °C)	1.269	1.865
Relative density, g/cm ³		
0 °C	1.47	0.9998
20 °C	1.45	0.9980
Viscosity, mPa.s		
0 °C	1.819	1.792
20 °C	1.249	1.002
Critical temperature, °C	457.0	374.2
Critical pressure, MPa	20.99	21.44

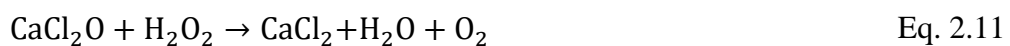
Table 2.4 Physical properties of hydrogen peroxide solutions of different concentration (Goor et al., 2000).

Property	H ₂ O ₂ concentration, wt %			
	35	50	70	90
Relative density, g/cm ³				
0 °C	1.1441	1.2110	1.3071	1.4136
20 °C	1.1312	1.1953	1.2886	1.3920
25 °C	1.1282	1.1914	1.2839	1.3867
Viscosity, mPa.s				
0 °C	1.82	1.87	1.93	1.88
20 °C	1.11	1.17	1.23	1.26
Melting point, °C	-33.0	-52.2	-40.3	-11.9
Boiling point (101.3 kPa), °C	107.9	113.8	125.5	141.3

Decomposition of hydrogen peroxide is an exothermic reaction which forms water and oxygen as given in Eq. 2.10. Hydrogen peroxide is considered a non-stable chemical product by some researchers, however it is a stable product in the absence of catalysts (Schumb et al., 1955). The rate of decomposition of hydrogen peroxide depends on its concentration, temperature, pH, existence of impurities and stabilizers and the physical and chemical properties of storage conditions as well as the duration of storage (Schumb et al., 1955). It is reported that each 10°C rise in temperature increases the rate of decomposition approximately 2.2 times over the range of 20-100 °C (Goor, 1992).



In the literature, hydrogen peroxide has been used with several catalysts to increase the rate of decomposition. The use of hydrogen peroxide with catalyst such as calcium or sodium hypochlorite for the production of porous building materials was first patented by Adolph and Pohl (1935). The main advantage of calcium or sodium hypochlorite is the acceleration of hydration of Portland cement, however it may be harmful for the steel reinforcement. The reaction between calcium hypochlorite and hydrogen peroxide is given in Eq. 2.11.



2.4.1.1.2 Foaming Method

Pore formation is achieved by introducing foam into the matrix using either the pre-formed method or mixed foaming method. In the former, foam is prepared separately by mixing foaming agents with water and then mixed with the other ingredients of the concrete. In the latter, foaming agents are directly added to the mixture in the mixed foaming method (Ramamurthy et al., 2009).

2.4.1.2 Some Properties of Aerated Concretes

2.4.1.2.1 Density

Density is the major property that governs the physical, mechanical and thermal properties of aerated concretes, and depends on their porosity, specific gravity of binders and the aggregates used (Rudnai, 1963). Hence, evaluation of aerated concrete using density is common practice. Density also significantly varies with moisture content, therefore indication of moisture content, whether it is in oven or air dry condition, is necessary (Narayanan and Ramamurthy, 2000).

2.4.1.2.2 Compressive Strength

Compressive strength of aerated concrete decreases dramatically with the decrease of density. Parameters reported affecting the compressive strength of aerated concrete are specimen size and shape, age, water content, method of curing, direction of loading and characteristics of ingredients (Narayanan and Ramamurthy, 2000).

Compressive strength of aerated concrete increases with the increase of fine particles. Nambiar and Ramamurthy (2006) found that mixtures containing fine sand exhibited higher strengths than mixtures with coarse sand where the strength differences increased with the increase of density. The variation of compressive strength with density for different size of aggregates is given in Figure 2.10. In addition, replacement of fine sand with fly ash increased the compressive strength for a given density. The effect of fly ash replacement on the compressive strength of aerated concretes are given in Figure 2.11.

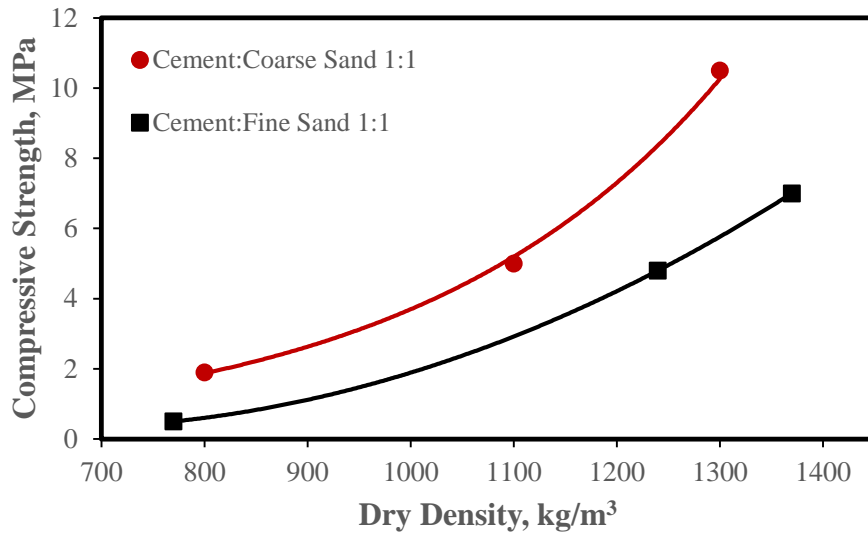


Figure 2.10 Effect of aggregate size on compressive strength of aerated concretes (Nambiar and Ramamurthy, 2006).

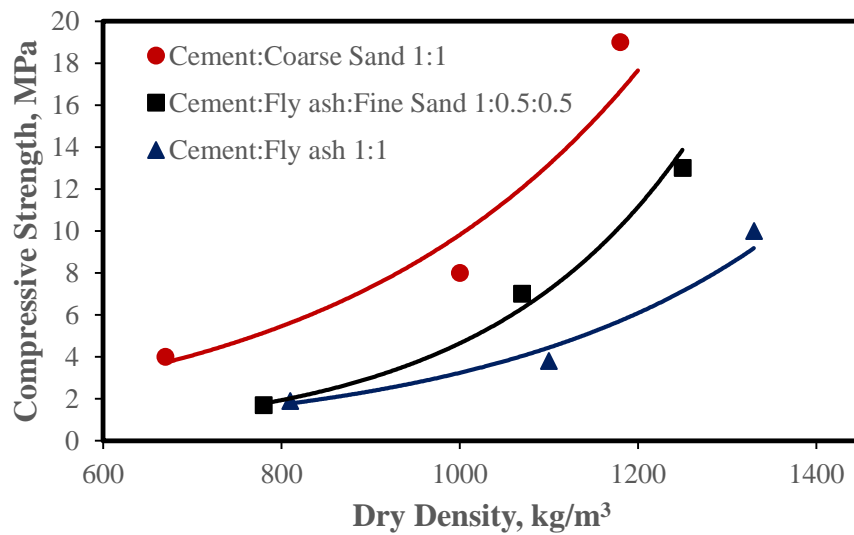


Figure 2.11 Effect of fly ash replacement on the compressive strength of aerated concretes (Nambiar and Ramamurthy, 2006).

Compressive strength of aerated concrete increases with the age of concrete for a given density. Figure 2.12 shows strength gain of sealed-cured aerated concretes at a density of 1000 kg/cm³ with various fillers (Jones et al., 2003).

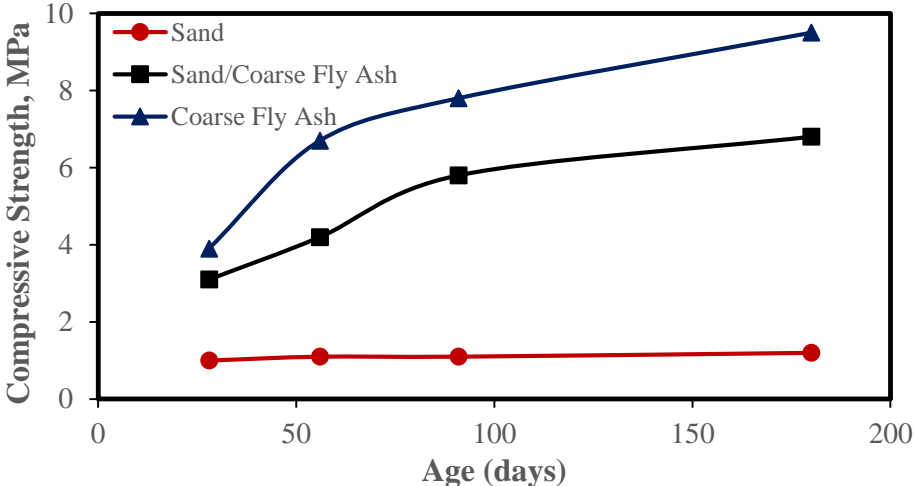


Figure 2.12 Strength gain of aerated concretes with various fillers (Jones et al., 2003).

Autoclave curing is more beneficial than other types of curing with the consideration of strength of aerated concrete. For a given mix design, the compressive strength of autoclaved lime-cement based aerated concrete produced using aluminum powder was found to be higher than that of moist cured (Ramamurthy and Narayanan, 2000). Figure 2.13 shows the effect of curing type on the 28-day compressive strength of lime-cement based aerated concretes with the percentage of sand replacement with fly ash.

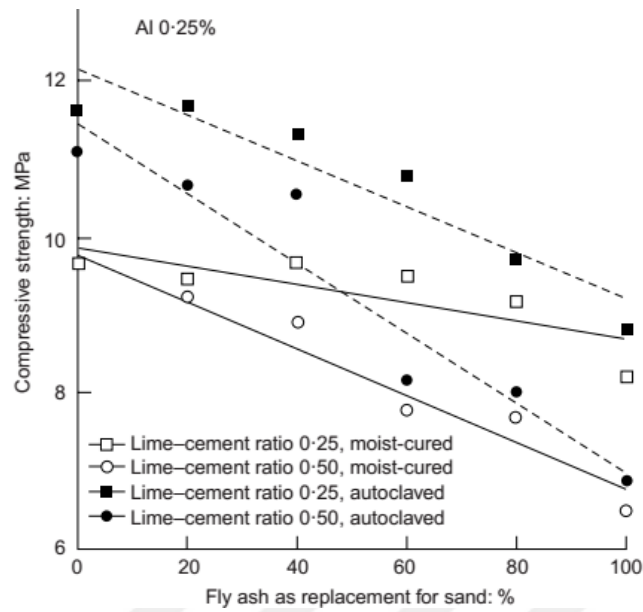


Figure 2.13 Effect of curing type on 28-day compressive strength of lime-cement based aerated concretes with percentage of sand replacement by fly ash (Ramamurthy and Narayanan, 2000).

2.4.1.2.3 Water Absorption

Water absorption measurements are performed for the determination of the volume of permeable pores in the concrete. For the measurement of absorption, test samples are oven-dried and immersed in water. The increase in the mass of the test sample as a percentage of the oven-dry mass is expressed as water absorption. There exist several different procedures for the measurement of water absorption: i) immersing non-oven dried test samples in water 24 h, designed to determine the water absorption for cellular concretes (ASTM C796, 2012), ii) immersing oven-dried test samples until constant mass (ASTM C642, 2013), and iii) adopting a vacuum saturation method on oven-dried samples (Kearsley and Wainwright, 2001). As expected, water absorption results widely vary among these tests. One of the reasons for the variation of water absorption may be incomplete drying at ordinary temperatures or loss of combined water at high temperatures (Kearsley and

Wainwright, 2001). In addition, oven drying may lead to excessive cracking in aerated concrete, which may increase water absorption (Brady et al., 2001).

Water absorption is governed by the capillary pores, and is expected to be lower for aerated concrete than normal weight concrete as a result of the decrease in the paste content (Nambiar and Ramamurthy, 2007; Rudnai, 1963). However, it is generally higher for aerated concrete than normal weight concrete as a result of its lower density. Density, mix proportions and the quality of ingredients are the most influential factors on water absorption (Fouad, 2006).

2.4.1.2.4 Thermal Conductivity

Thermal conductivity of aerated concrete depends on its density, moisture content, temperature, size and shape of its pores, and thermal conductivities of its components (Rudnai, 1963). Since thermal conductivity is essentially governed by density and moisture content in aerated concrete, method of curing is generally not significant (Narayanan and Ramamurthy, 2000).

Among the thermal conductivity measurement methods, the guarded hot plate method is used as a reference method for the testing of autoclaved aerated concrete (AAC) across Europe. However, there are differences in performing this test such specimen size, moisture content, and mean temperature ranges. Detailed information about performing test across Europe can be found in Millard (1992). Millard (1992) compared thermal conductivities of more than 100 samples of AAC from different manufactures across Europe which were produced using different raw materials, but conditioned similarly and tested in the same way. A linear relationship with a high correlation was found between thermal conductivity and dry density. Figure 2.14 shows the variation of thermal conductivity of AAC with oven-dry density (Aroni et al., 1993).

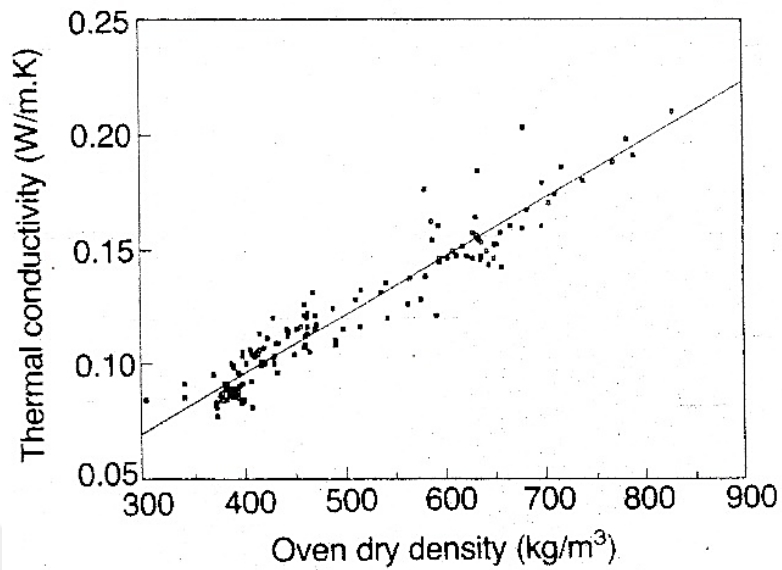


Figure 2.14 Variation of thermal conductivity with oven-dry density for AAC (Aroni et al., 1993).

The thermal conductivity of water ($k_w=0.63$ W/m.K) is about 25 times higher than that of air ($k_a=0.024$ W/m.K) (Exerowa and Kruglyakov, 1997). As a result, increasing water content in the pores of aerated concrete increases its thermal conductivity. Even though the effect of moisture content (by mass) changes with oven dry density of AAC, Millard (1992) reported a linear relationship between thermal conductivity and moisture content in which increasing moisture content by % 1 approximately increases thermal conductivity by 4 %, as given in Figure 2.15.

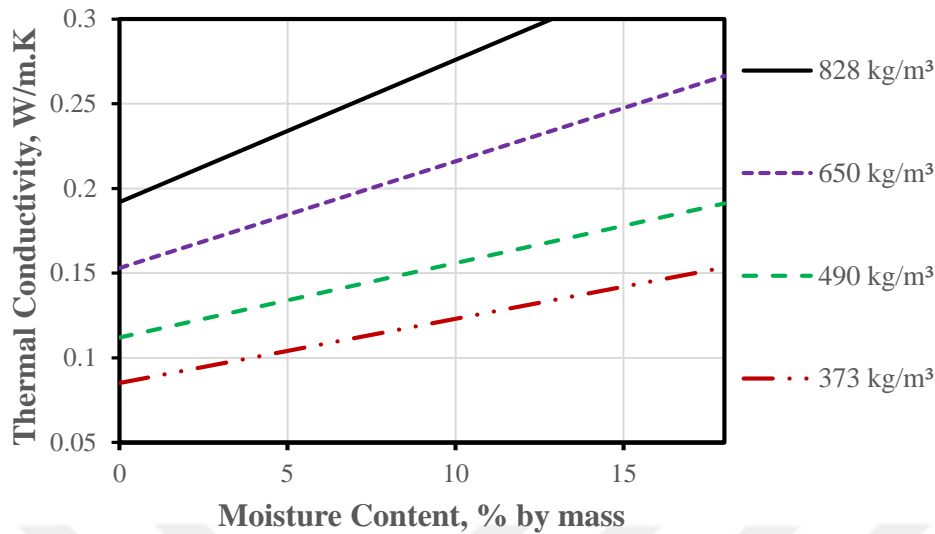


Figure 2.15 Effect of moisture content on the thermal conductivity of AAC (Millard, 1992).

Thermal conductivity of aerated concrete also increases with increasing temperature (Ramamurthy et al., 2009). Othuman and Wang (2011) investigated thermal conductivity of aerated concrete having densities 650 kg/m^3 , 1000 kg/m^3 , and 1850 kg/m^3 up to $250 \text{ }^\circ\text{C}$. It was reported that while thermal conductivity increased with increasing temperature up to $170 \text{ }^\circ\text{C}$, it decreased with increasing temperature beyond $170 \text{ }^\circ\text{C}$. Richard et al. (1975) investigated thermal and mechanical properties of aerated concretes with densities of 705 kg/m^3 and 1230 kg/m^3 at temperatures of $22 \text{ }^\circ\text{C}$ and $-196 \text{ }^\circ\text{C}$. It was found that when temperature was decreased from $22 \text{ }^\circ\text{C}$ to $-196 \text{ }^\circ\text{C}$, thermal conductivity of specimens with densities of 705 kg/m^3 and 1230 kg/m^3 decreased about 26 % and 34 %, respectively.

Size and distribution of pores in aerated concrete influences thermal conductivity of aerated concrete because of different heat transfer modes in pores, namely: conduction, convection, and radiation. Wei et al. (2013) reported that heat transfer due to convection is negligible when pores have diameter less than 4 mm. Besides

increase of pore size increases thermal conductivity at high temperatures due to the radiation effect in pores (Francl and Kingery, 1954). Distribution and size of pores may also affect the thermal conductivity of porous materials. Francl and Kingery (1954) reported a substantial decrease in thermal conductivity by changing heat flow from parallel to perpendicular to pores.

Factors affecting thermal conductivity of aerated concrete produced using Portland cement-based binders are also effective on the thermal conductivity of alkali-activated aerated concretes. However, differences in the microstructure may lead to differences in thermal conductivity. Zhang et al. (2014) investigated thermal conductivity of alkali-activated fly ash and GGBFS-blended aerated concrete. Thermal conductivity measurements were performed with a commercial transient plate source (TPS) apparatus at room temperature. Thermal conductivity of samples were found to be in the range of 0.15-0.48 W/m.K for dry density range of 585-1370 kg/m³. Thermal conductivity of alkali-activated aerated concrete with a density of 1000 kg/m³ were reported as 0.24 W/m.K which is lower than for Portland cement-based aerated concretes (0.3-0.5 W/m.K). It was claimed that the low level of chemically-bound water in alkali-activated materials provides a discontinuous gel structure leading to lower thermal conductivity than in Portland cement-based aerated concretes.

2.4.1.3 Alkali-Activated Aerated Concretes

Bean and Malone (1997) patented the production of aerated concrete using blast furnace slag, sodium peroxide and water. Activation of slag was achieved by decomposition of sodium peroxide to water and sodium hydroxide. They also claimed that the use of sodium hydroxide and potassium hydroxide can reduce the amount of sodium peroxide needed in the mixtures. There was no detailed information about the properties of the produced aerated concrete.

Vlcek et al. (2009) investigated the relation between sodium silicate content and aluminum powder contents in lightweight composites produced using blast furnace slag. Densities of the samples were found to be 534 kg/m³ to 1030 kg/m³ and their compressive strengths 1.8 MPa to 5.1 MPa. It was found that mixtures containing sodium silicate with 3.5 % to 4.0 % Na₂O or 0.26 % and 0.30 % aluminum powder are not suitable for the production of aerated composites as a result of formation of large pores.

Aguilar et al. (2010) synthesized aerated sodium silicate-activated composites using metakaolin and metakaolin-fly ash blends. Aerated pastes and mortars containing blast furnace slag aggregate were produced using aluminum powder as a gas-releasing agent. The amount of aluminum powder was calculated to achieve densities of 600 kg/m³, 900 kg/m³ and 1200 kg/m³. The 28-day compressive strengths of produced samples were found to be between 1.4 MPa and 14.3 MPa. Replacement of metakaolin with 25 % fly ash was found to increase the compressive strength of produced samples. Also, slag aggregates were found to have a positive effect on the strengths of samples with a density of 1200 kg/m³.

Vaou and Panias (2010) produced aerated alkali-activated materials using perlite, sodium hydroxide and hydrogen peroxide. A 30 % w/w hydrogen peroxide solution was used for aeration with a solution-to-paste mass ratio between 0.7 and 3.2 %. The solid-to-liquid ratio and concentration of sodium hydroxide were kept constant as 1.2 g/mL and 8 M, respectively. Apparent density and porosity of produced samples were found to be between 290 kg/m³ and 665 kg/m³ and between 74% and 89%, respectively. Figure 2.16 shows apparent density and void fraction of the samples produced as a function of hydrogen peroxide content. Two distinct regions were obtained for the apparent density and cell volume of materials. In the first region, a sharp linear decrease was observed in the apparent density up to a hydrogen peroxide content of 2 %. In the second region, a limited density reduction was observed above 2 % hydrogen peroxide as a consequence of coalescence of air bubbles and extreme expansion. Closed spherical pores were reported for low

hydrogen peroxide contents. As the hydrogen peroxide content increased, the shape of the pores was found to change to oval as a consequence of aggregation of the air bubbles. The compressive strength of produced samples was found to be between 0.25 and 0.78 MPa. Samples with the highest densities were found to have the lowest strength, the reason claimed to be incomplete geopolymerization due to the effect of closed small pores produced with low contents of hydrogen peroxide that limits the vaporization of water during curing.

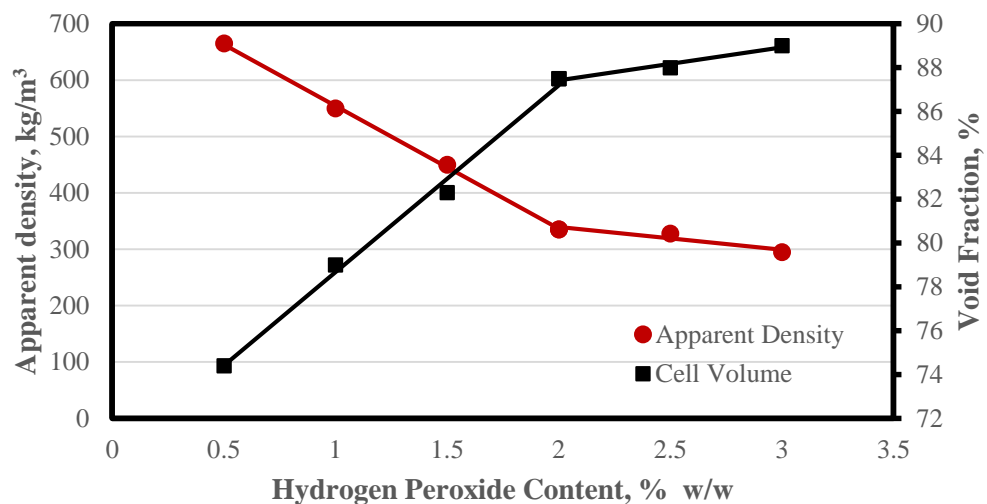


Figure 2.16 Variation of apparent density and void fraction of aerated samples at different hydrogen peroxide amounts (Vaou and Panias, 2010).

Bell and Kriven (2009) proposed to introduce micropores into the paste using hydrogen peroxide or aluminum powder as a foaming chemical to limit diffusion distance of water through the paste. Paste composition was selected as $K_2O \cdot Al_2O_3 \cdot 4SiO_3 \cdot 11H_2O$ to form refractory leucite ($KAlSi_2O_6$) after heating to above 1200 °C. To obtain cured pastes without cracks at a curing temperature of 200 °C; different mixtures were prepared using 0.5, 1.0 and 1.5 % hydrogen peroxide and different amounts of Al powders. Mixtures were cast in pressure-sealed molds. Since the free water contents were changing in the pastes, the pressure

applied to their surfaces was also changed. Apparent densities of samples produced using hydrogen peroxide were found to be between 2197 kg/m³ and 2214 kg/m³ with a maximum pore size range of 20-80 μm. Strength of samples with 0.5 and 1.5 % were found to be 77.3±7.9 MPa and 49.5±4.5 MPa, respectively. The control and 1.0 % H₂O₂ samples could not be produced without cracks. Spherical pores were reported for samples produced using hydrogen peroxide. Also, after heating to 1200 °C, no crack-free leucite had been obtained. On the other hand, fast geopolymerization and rapid setting were reported due to partial consumption of Al powder. The density of samples produced Al powder was found to be 2291 kg/m³, and they were successfully converted to crack-free leucite.

In another study, both Al powder and hydrogen peroxide were used to reduce the diffusion distance of water in fly ash based alkali-activated materials. A mixture of 12 M sodium hydroxide and sodium silicate with a modulus of ~3.2 was used for the activation of fly ash with 3 different Na₂SiO₃-to-NaOH ratios of 2.5, 3.0 and 3.5. Specimens were prepared with a powder-to-alkali solution ratio of 2.5, 3.0 and 3.5. After curing for one day in a 60 °C dry oven, compressive strengths of the specimens were found to be in the range of 12.1-22.0 MPa. The amount of Al powder and hydrogen peroxide was not given in the study, a heterogeneous matrix with open pores were reported (Al Bakri Abdullah et al., 2012).

Esmaily and Nuranian (2012) produced aerated alkali-activated slag materials using a combined pore formation method. Air entraining and foaming agents were used together in different proportions. Sodium silicate was used for the activation of slag. After performing a comparative analysis on the pore structure and density of samples produced with a combination of aluminum powder and one of three different bubble stabilizing agents (alkyl ether sulfate, oleic acid and sodium lauryl sulfate) at similar consistency, sodium lauryl sulfate (SLS) was found to be an effective stabilizer to form homogeneous, fine, and separated pores. Then, the effect of various aluminum powder and SLS contents were investigated on density, strength, and pore structure of aerated pastes. Samples were cured at 87 °C. The

wet densities of produced samples were found to be between 681 kg/m³ and 1127 kg/m³ with a compressive strength range of 1.0 MPa to 15.0 MPa.

Masi et al. (2014) compared the physical and mechanical properties of alkali-activated concretes based on fly ash binders aerated with aluminum powder, hydrogen peroxide, and a commercial surfactant. Also, a combination of gas-releasing agents and surfactant were used in different proportions. Strength and density of the non-aerated alkali-activated pastes were found to be 21 MPa and 1720 kg/m³, respectively. After addition of surfactant into mixture at 1 % and 5 % of the slurry mass, samples produced were found to be in the density range of 1280-1320 kg/m³ and in the compressive strength range of 3.6-7.2 MPa, with a maximum pore size range of 30-60 µm. The density, strength and maximum pore size ranges of samples produced using aluminum powder were found to be 800-920 kg/m³ and 1.7-2.4 MPa, 500-3500 µm, respectively. Coarse and non-homogeneous pores were reported for all samples produced using aluminum powder. Addition of 1 % surfactant into the mixtures containing aluminum powder was found to improve homogeneity of the pore distribution. Samples produced using hydrogen peroxide content of 0.1 %, 0.2 % and 0.3 % by the slurry mass. The density, strength and maximum pore size ranges of samples produced using hydrogen peroxide were found to be 910-1120 kg/m³ and 2.9-4.7 MPa, 200-3000 µm, respectively. Pore distribution of produced samples having hydrogen peroxide content of 0.1 % and 0.2 % was found to be homogeneous. Using surfactant and hydrogen peroxide together was found to decrease maximum pore size and improve homogeneity of pores.

Hlaváček et al. (2015) produced aerated alkali-activated fly ash using aluminum powder. The densities of samples were found to be 400-800 kg/m³. The mechanical, thermal and chemical resistance of samples with a density of 671 kg/m³ were evaluated and found to be similar to those of autoclaved aerated concrete at similar densities.

Sanjayan et al. (2015) also produced aerated alkali-activated materials through the replacement of fly ash with aluminum powder. Samples were prepared using different sodium silicate-to-sodium hydroxide weight ratios of 1.0 and 2.0, and alkali activator-to-fly ash weight ratios of 0.25, 0.30 and 0.35. Samples having bulk densities between 403 kg/m^3 and 1309 kg/m^3 were produced in a compressive strength range of 0.9 to 4.35 MPa by replacement of 1.5, 3.0, and 5.0 wt.% of fly ash with aluminum powder. It was observed experimentally that the amount of liquid activator used is the most influential factor for obtaining low density materials. Also, plenty of unreacted fly ash particles were discovered after microstructure analysis of produced samples. The reason of this was stated to be the rapid reaction between alkali activator and aluminum powder which hinders the geopolymerization process.

Abdollahnejad (2015) investigated the physical, thermal and mechanical properties of fly ash-based aerated alkali-activated materials using two different gas-releasing agents, namely hydrogen peroxide and sodium perborate, at identical amounts. It was found that aerated concretes with lower thermal conductivity produced using sodium perborate than using hydrogen peroxide.

Ducman and Korat (2016) compared the efficiencies of hydrogen peroxide and aluminum powder on mechanical and physical properties of fly ash-based aerated concretes. Aluminum powder was used in the range of 0.07 % to 0.2 % of the slurry mass. The densities of samples were found to be between 640 kg/m^3 and 740 kg/m^3 . A 30 % w/w hydrogen peroxide solution was used in the range of 0.5 % to 2.0 % of the slurry mass. The densities of samples were found to be 610 kg/cm^3 and 1000 kg/m^3 . Compressive strengths of samples were found to be between 2.9 MPa and 9.3 MPa. It was concluded that the strength is a function of density regardless of the type of gas-releasing agent (Ducman and Korat, 2016).

Novais et al. (2016) investigated the effect of NaOH concentration, water content and hydrogen peroxide content on fresh and hardened properties of fly ash- and

metakaolin-based alkali-activated materials with a mass ratio of 2:1. Three different NaOH hydroxide solutions (8, 10, and 12 M) were used. Lightweight alkali-activated materials with densities between 990 kg/m³ and 1170 kg/m³ were produced without hydrogen peroxide by using excessive water in the mixtures. Apparent densities of the samples produced with hydrogen peroxide were found to be between 440 kg/m³ and 910 kg/m³. Compressive strengths of samples were found to be between 0.26 and 14.5 MPa. Figure 2.17 shows the optical characterization of produced samples. A decrease in the concentration of sodium hydroxide and an increase in the hydrogen peroxide content resulted in an increase of both porosity and pore size. It was concluded that NaOH concentration and hydrogen peroxide content govern the expansion of mixtures.

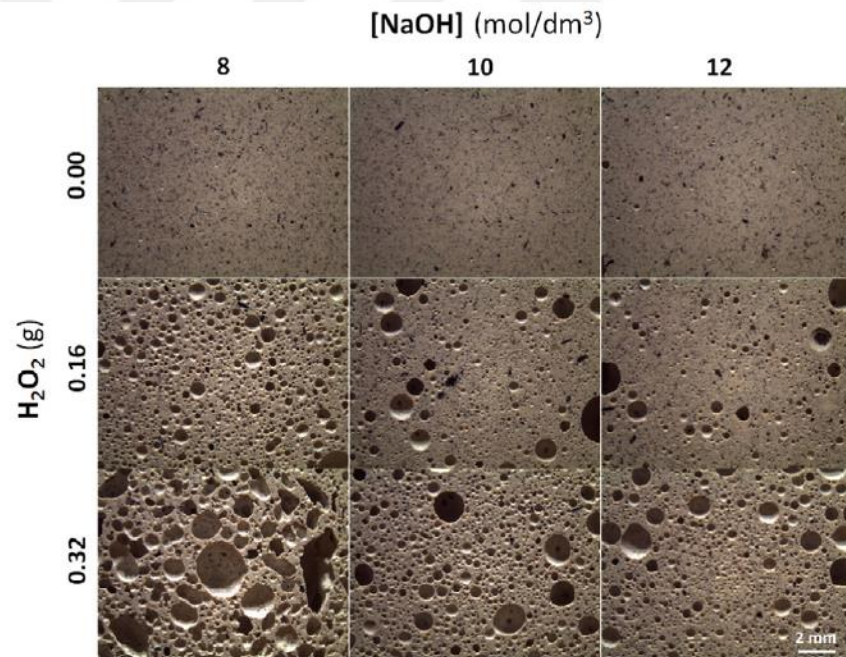


Figure 2.17 Optical characterization of fly ash-metakaolin-based alkali-activated materials at different hydrogen peroxide contents and NaOH molarity (Novais et al., 2016).

2.5 Methods of Measuring Thermal Conductivity

Thermal conductivity, k , is a measure of the ability of a material to conduct heat which is defined as the ratio of heat flow to temperature gradient as given Eq. 2.12.

$$Q = -k \cdot \frac{\partial T}{\partial x} \quad \text{Eq. 2.12}$$

where Q (heat flux) is the heat transfer per unit area (W/m^2), $\frac{\partial T}{\partial x}$ is the temperature gradient through the specimen (K/m), and k is the thermal conductivity ($\text{W}/\text{m}\cdot\text{K}$) (Bergman et al., 2011). Thermal conductivity measurements are divided into two groups: steady state and transient methods. The classification depends on whether temperature distribution in the sample is time dependent or not. In steady-state methods, a constant temperature is reached at each point in the sample, and it does not change with time, in other words it is not a function of time. On the other hand, transient tests are performed while heating or cooling a test sample, so the temperature distribution in the sample is a function of time. The nature and physical condition of the material, the magnitude of the thermal conductivity of the material, available sample size, duration of test, accuracy of results, and test temperature range are crucial and main considerations for selecting suitable method for measurement of thermal conductivity (Touloukian et al., 1970). It is noteworthy that thermal conductivity of a given material can be measured to be different even though the applied measurement methods have good reproducibility (Kingery and McQuarrie, 1954).

2.5.1 Steady-State Methods

2.5.1.1 Guarded Hot Plate Apparatus

The guarded hot plate apparatus is generally used on specimens with a relatively low thermal conductivity, especially on non-metals such as ceramics, glass, polymers, and insulation materials. For the determination of thermal conductivity, two-identical test specimens or a single test specimen with circular or square shape can be used, depending on the apparatus. It is preferable to use samples whose diameter, or edge length is an order of magnitude larger than the thickness of the specimen (Flynn, 1999) to assure the heat flow is one-dimensional. Measurement of thermal conductivity using the guarded hot plate apparatus on two identical specimens and a single specimen are described in ASTM C177 (2013) and ASTM C1044 (2016), respectively. Figure 2.18 shows the test set-up for the measurement of thermal conductivity using two identical specimens. The guarded hot plate apparatus consists of a hot plate (heater) with surrounded guard heaters, two cold plates, and edge insulators. For the single specimen measurements, a low thermal conductance material with similar dimensions is used instead of second specimen.

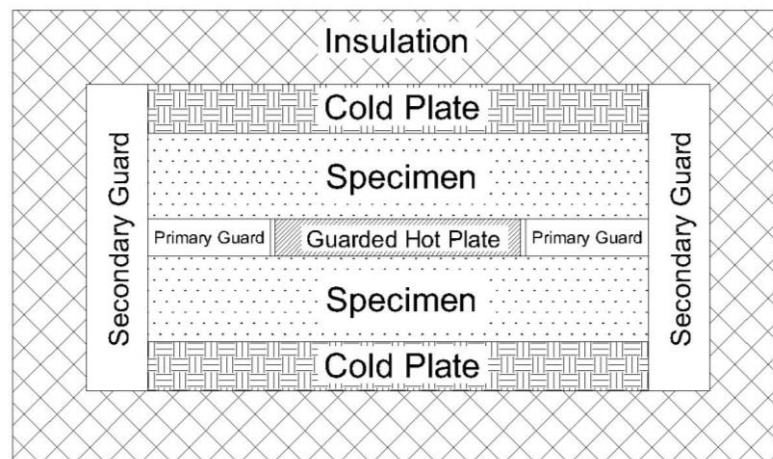


Figure 2.18 Illustration of the guarded hot plate apparatus (ASTM C177, 2013).

Temperature measurements are taken over the section of the heater at steady state. The guard heaters are used to maintain one-dimensional heat flow through specimen without any heat loss by supplying no temperature difference around the heater and specimens. Thus, the uncertainty of measurements can be reduced to about 2 % (Buck and Rudtsch, 2006). Thermal conductivity measurements can be made in the temperature range of about -190 °C to 650 °C. Even though achieving equilibrium temperature (steady state condition) requires a very long time, steady state measurement enables the determination of thermal conductivity without occurrence of possible chemical reactions during measurements (Flynn, 1999).

2.5.1.2 Unguarded Hot Plate Apparatus

As evident from its name, unguarded hot plate apparatus is similar to the guarded hot plate apparatus. The main difference is in the heater used, which is quite thin. Thus, heat loss around the heater becomes very low. In other words being quite thin, the heater enables for being self-guarded, and no additional guard heater is required. In addition, using a thin heater increases the thermal response of the heater and provides shorter durations for achieving thermal equilibrium. Detailed information related to the design and test procedure can be found in ASTM C1114 (2003). It is also noteworthy that the set-up and operation of unguarded hot plate apparatus are much easier than the guarded hot plate apparatus (Flynn, 1999).

2.5.1.3 Heat Flow Meter Method

The heat flow meter method is a comparative method for the determination of thermal conductivity of a wide range of materials. A calibration is required using reference specimens with known thermal transmission properties prior to the determination of the thermal conductivity of the unknown sample. Figure 2.19 shows two different apparatus set-ups for the heat flow meter method. Heat flux transmitter produces electric input which is a function of the heat flux. Depending on the type of the apparatus, a single or two specimens can be used. ASTM C518

(2017) and ASTM E1530 (2016) provide the detailed information about the design and test procedure.

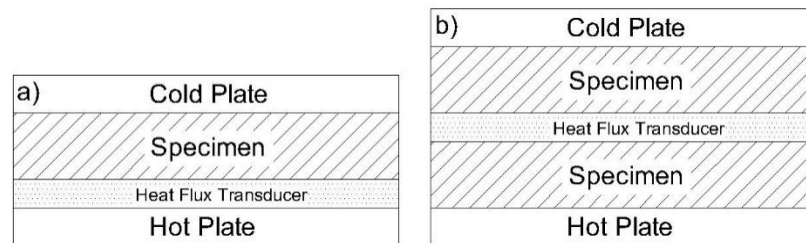


Figure 2.19 Apparatus for heat flow meter method: a) One heat flux transducer and one specimen, b) One heat flux transducer and two specimens.

2.5.2 Transient Methods

2.5.2.1 Hot-Wire Method

The hot-wire method, a transient method, which is also called the line-heat source method was originally proposed by Carslaw and Jaeger (1959), and is commonly used for determination of thermal conductivity of liquids, loose-fill, and blanket-type insulation materials (Flynn, 1999). A linear heat source (hot wire) with an infinite length and infinitesimal diameter is attached between two identical specimens or embedded into a single specimen. Generally, platinum wires are used. They have two functions: as a heater and a temperature sensor. A constant electric current supplied by a power supply is given to the hot wire, and the temperature of the hot-wire increases as well as those of test samples. Then, thermal conductivity is determined through the slope of the temperature increase as a function of time taken from measurements (Franco, 2007). Detailed information about the design and test procedure can be found in ASTM C1113 (2013).

2.5.2.2 Transient Plane Source Method

Gustafsson et al. (1979) developed the transient plane source method for the measurement of thermal conductivity of liquids and solids. A spiral thin plane sensor that is electrically insulated is used as a heat source and a temperature sensor, as given in Figure 2.20. Depending on the available specimen size, sensor diameters (D) from 4 mm to 100 mm can be used. Thermal conductivity measurement is performed by placing the plane between two specimens. It is crucial that test specimens have flat and smooth surfaces. Similar to the hot-wire method, a constant electric current is supplied using a power supply, and the increase of resistance as a function of time is recorded. Thermal conductivity of the test specimen is determined by using the measured data (ISO 22007-2, 2008).

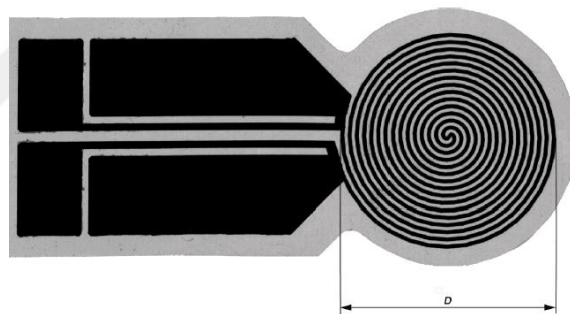


Figure 2.20 Spiral plane probe as heating and temperature sensor (ISO 22007-2, 2008).

CHAPTER 3

EXPERIMENTAL STUDY

3.1 Materials

3.1.1 Ground Granulated Blast Furnace Slag

In the current study, ground granulated blast furnace slag, received from Kardemir Iron and Steel Plant was used. The oxide composition of the slag determined using X-ray fluorescence (XRF) spectroscopy and its physical properties are given in Table 3.1. Based on the basicity coefficient, $K_b = (\text{CaO} + \text{MgO}) / (\text{SiO}_2 + \text{Al}_2\text{O}_3)$, the slag is determined to be an acidic slag.

Table 3.1 Oxide composition and physical properties of the slag used.

Oxide	w/w (%)
SiO ₂	38.20
Al ₂ O ₃	10.00
Fe ₂ O ₃	1.16
CaO	36.70
MgO	6.09
SO ₃	1.46
Na ₂ O	0.25
K ₂ O	1.10
Blaine fineness (cm ² /g)	4140
Specific gravity	2.95

Figure 3.1 shows the x-ray diffractogram of the slag used. It can be seen in the diffraction pattern that it is mostly amorphous with a characteristic hump at about $30^\circ 2\theta$.

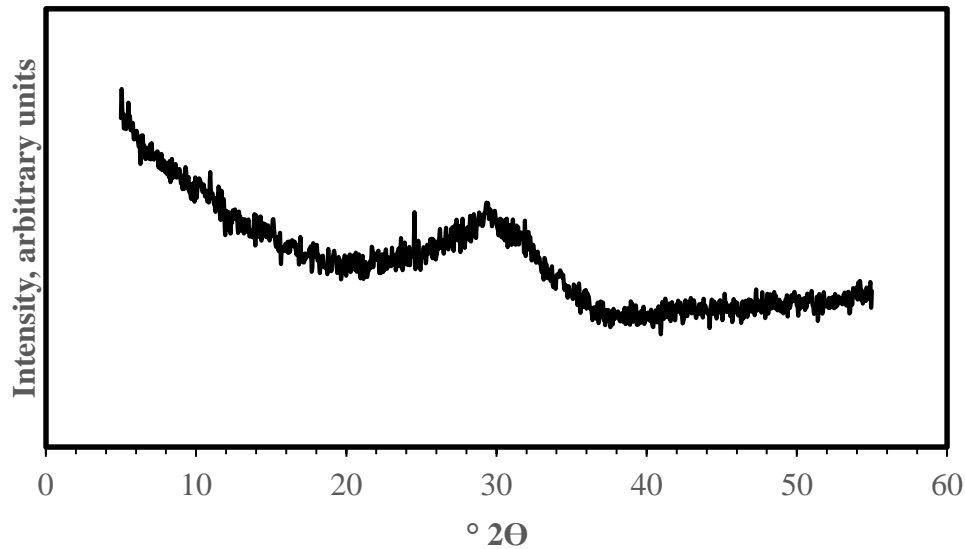


Figure 3.1 X-ray diffractogram of the slag used.

3.1.2 Water

Distilled water, at a temperature of $21 \pm 1^\circ\text{C}$, was used in preparing the pastes and mortars.

3.1.3 Hydrogen Peroxide

A 35 % w/w hydrogen peroxide solution was used in preparing the pastes and mortars. The producer (Merck Chemicals) reported the density of hydrogen peroxide 1.13 g/cm^3 at 20°C .

3.1.4 Aggregates

Silica sand with a specific gravity of 2.65 was used in preparing mortars. The sand was obtained from Şile, İstanbul. The absorption capacity of the sand used was determined as 0.6 %. The grading of sand used is given in Figure 3.2. It can be seen that its grading is quite close to that of “Graded Sand” defined in ASTM C778 (2017) which has particles mostly between the 600- μm sieve and 150- μm sieve.

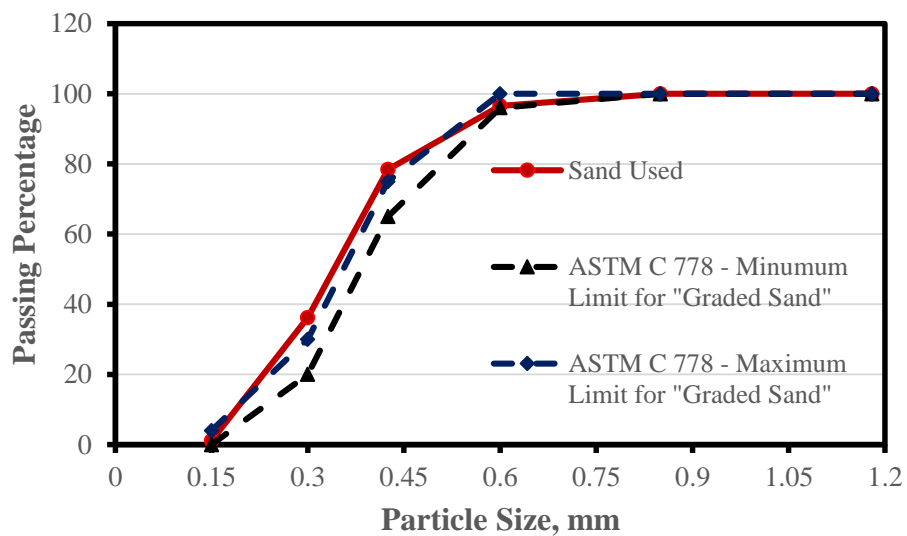


Figure 3.2 Grading of the sand used.

3.1.5 Alkali Activators

A combination of sodium hydroxide solution and sodium silicate solution was used as the alkali activator. The sodium hydroxide used was in the form of laboratory grade flakes with >99 % purity. A commercially available sodium silicate solution, 40-42° Baume solution, with a chemical composition of Na_2O =8.9 %, SiO_2 =28.6 % and H_2O =62.5 % (thus $\text{SiO}_2/\text{Na}_2\text{O}$ ratio of 3.2) was used.

First, sodium hydroxide flakes were dissolved in distilled water using a magnetic stirrer to obtain a concentration of 8M. The beaker in which the sodium hydroxide solution was prepared was sealed with clear plastic wrap and cooled in a climate-controlled room to a temperature of 21 ± 1 °C. The sodium hydroxide solution and the sodium silicate solution were always kept separate in the climate-controlled room at a temperature of 21 ± 1 °C until needed. The solutions were mixed 24 ± 0.5 h prior to mixing with slag at moderate speed using a magnetic stirrer for 2 minutes at room temperature. The beaker in which the combined solution was prepared was sealed with clear plastic wrap and kept in a climate-controlled room at a temperature of 21 ± 1 °C until mixing.

The sodium hydroxide-to-sodium silicate ratio was based on a study by Altan and Erdoğan (2012). Sodium silicate solution-to-slag ratio and sodium hydroxide solution-to-slag ratio were kept at 0.25 and 0.11, respectively. Thus, the Na₂O wt % was 4.46 by mass of the slag for all pastes and mortars.

3.2 Mixture Preparation

Two different types of samples were prepared to be used in the various tests conducted in this study; pastes and mortars.

3.2.1 Mixing Procedure for Pastes

A high-speed blender was used for the production of pastes. The duration of mixing was 180 s for all pastes. Immediately after pouring water on the alkali solution in the blenders jug, slag was added and mixed for 60 s. Then, the chosen amount of hydrogen peroxide was added, while mixing at slow speed. After mixing for 120 s, the paste was cast in molds without any compaction.

3.2.2 Mixing Procedure for Mortars

A 5 L-capacity planetary mixer was used for the production of mortars. The duration of mixing was around 6.5 minutes. The mixing procedure applied for all the mortars was as follows:

- The alkali solution and slag were mixed at low speed for 60s.
- The paste on the insides of the bowl was scraped down for 30 s.
- Water was added to the bowl.
- Sand was slowly poured in over a 30 s period, while mixing at medium speed.
- The mortar collected on the sides of the bowl was scraped down in the following 30 s.
- The mortar was mixed for 60 s more at moderate speed (For mortars without hydrogen peroxide, this was the final stage i.e. the duration of mixing was 180 s).
- The chosen amount of hydrogen peroxide was added to the bowl.
- Finally, the mortar was mixed for another 120 s at moderate speed.
- Mortars were cast in molds without compaction.

3.3 Identification of Samples

In the current study, water-to-slag ratio, sand-to-slag ratio, and hydrogen peroxide content of the mixtures produced are indicated by the name of the samples, as illustrated in Figure 3.3. For instance, 40-0-25 indicates the samples were cast from a mixture with $W/S=0.40$, $Sa/S=0$, and hydrogen peroxide content of 0.25 % by mass of the slag.

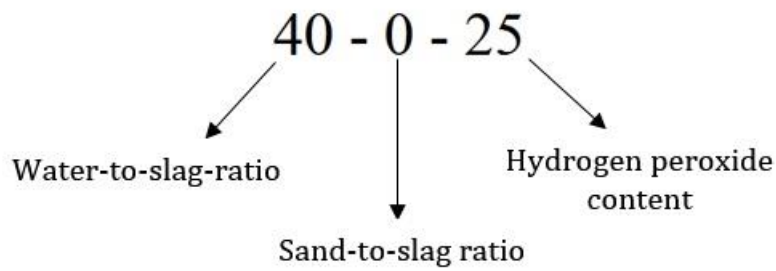


Figure 3.3 Identification of samples.

3.4 Mixture Proportions

Mixture proportions were selected through a trial and error process in which the effect of hydrogen peroxide content, W/S, SA/S, sand type and fineness, and alkali solution type were investigated on the apparent density in the first part of the study. Samples were produced using plastic beakers, and some of the results and observations are presented in Chapter 4, in the section on apparent density. Table 3.2 presents a summary of the mixture proportions for pastes and mortars. Tables 3.3-3.5 present the mixture proportions of pastes and mortars.

Table 3.2 Summary of mixture proportions for pastes and mortars.

Summary of mixture proportions	
Slag content (kg/m ³)	~350 - 1250
Water-to-slag ratio	0.35 - 0.65
Sand-to-slag ratio	0, 1, 2
Hydrogen peroxide, % by mass of slag	0 - 2.25
Concentration of NaOH solution	8 M
Sodium silicate-to-slag ratio	0.25
NaOH solution-to-slag ratio	0.11

Table 3.3 Mixture proportions for pastes.

Code	Sa/S	W/S	H₂O₂ (%) by mass of slag	Slag (g)	Sodium Silicate (g)	8M Sodium Hydroxide Solution (g)	Water (g)	H₂O₂ (g)	Sand (g)
40-0-0			0				73.0	0	
40-0-25			0.25				70.9	3.2	
40-0-50	0	0.4	0.50	450	112.5	49.7	68.8	6.4	-
40-0-75			0.75				66.7	9.6	
40-0-100			1.00				64.6	12.8	
40-0-150			1.50				60.5	19.2	
425-0-25			0				84.2	0	
425-0-25			0.25				82.2	3.2	
425-0-50	0	0.425	0.50	450	112.5	49.7	80.1	6.4	-
425-0-75			0.75				78.0	9.6	
425-0-100			1.00				75.9	12.8	
425-0-150			1.50				71.7	19.2	
45-0-25			0				95.5	0	
45-0-25			0.25				93.4	3.2	
45-0-50			0.50				91.3	6.4	
45-0-75	0	0.45	0.75	450	112.5	49.7	89.2	9.6	-
45-0-100			1.00				87.1	12.8	
45-0-125			1.25				85.0	16.1	
45-0-150			1.50				83.0	19.2	
50-0-25			0				118.0	0	
50-0-25			0.25				115.9	3.2	
50-0-50	0	0.50	0.50	450	112.5	49.7	113.8	6.4	-
50-0-75			0.75				111.7	9.6	
50-0-100			1.00				109.6	12.8	
50-0-150			1.50				105.5	19.2	

Table 3.4 Mixture proportions for mortars with Sa/S=1.

Code	Sa/S	W/S	H ₂ O ₂ (%) by mass of slag	Slag (g)	Sodium Silicate (g)	8M Sodium Hydroxide Solution (g)	Water (g)	H ₂ O ₂ (g)	Sand (g)
35-1-0			0				50.5	0	
35-1-25			0.25				48.4	3.2	
35-1-50	1	0.35	0.50	450	112.5	49.7	46.3	6.4	450
35-1-75			0.75				44.2	9.6	
35-1-100			1.00				42.1	12.8	
35-1-150			1.50				38.0	19.2	
375-1-0			0				61.7	0	
375-1-25			0.25				59.7	3.2	
375-1-50	1	0.375	0.50	450	112.5	49.7	57.6	6.4	450
375-1-75			0.75				55.5	9.6	
375-1-100			1.00				53.4	12.8	
375-1-150			1.50				49.2	19.2	
40-1-0			0				73.0	0	
40-1-25			0.25				70.9	3.2	
40-1-50	1	0.40	0.50	450	112.5	49.7	68.8	6.4	450
40-1-75			0.75				66.7	9.6	
40-1-100			1.00				64.6	12.8	
40-1-150			1.50				60.5	19.2	
45-1-0			0				95.5	0	
45-1-25			0.25				93.4	3.2	
45-1-50	1	0.45	0.50	450	112.5	49.7	91.3	6.4	450
45-1-75			0.75				89.2	9.6	
45-1-100			1.00				87.1	12.8	
45-1-150			1.50				83.0	19.2	
50-1-0			0				118.0	0	
50-1-25			0.25				115.9	3.2	
50-1-50	1	0.50	0.50	450	112.5	49.7	113.8	6.4	450
50-1-75			0.75				111.7	9.6	
50-1-100			1.00				109.6	12.8	
50-1-150			1.50				105.5	19.2	

Table 3.5 Mixture proportions for mortars with Sa/S=2.

Code	Sa/S	W/S	H ₂ O ₂ (%) by mass of slag	Slag (g)	Sodium Silicate (g)	8M Sodium Hydroxide Solution (g)	Water (g)	H ₂ O ₂ (g)	Sand (g)
50-2-0			0				118.0	0	
50-2-25			0.25				115.9	3.2	
50-2-50	2	0.50	0.50	450	112.5	49.7	113.8	6.4	900
50-2-75			0.75				111.7	9.6	
50-2-100			1.00				109.6	12.8	
50-2-225			2.25				99.2	28.8	
55-2-0			0				140.5	0	
55-2-25			0.25				138.4	3.2	
55-2-50	2	0.55	0.50	450	112.5	49.7	136.3	6.4	900
55-2-75			0.75				134.2	9.6	
55-2-100			1.00				132.1	12.8	
55-2-225			2.25				121.7	28.8	
60-2-0			0				163.0	0	
60-2-25			0.25				160.9	3.2	
60-2-50	2	0.60	0.50	450	112.5	49.7	158.8	6.4	900
60-2-75			0.75				156.7	9.6	
60-2-100			1.00				154.6	12.8	
60-2-225			2.25				144.2	28.8	
65-2-0			0				185.5	0	
65-2-25			0.25				183.4	3.2	
65-2-50	2	0.65	0.50	450	112.5	49.7	181.3	6.4	900
65-2-75			0.75				179.2	9.6	
65-2-100			1.00				177.1	12.2	
65-2-225			2.25				166.7	28.8	

In light of the experience gained from the initial tests, pastes and mortars with $S_a/S=1$ at different water-to-slag-ratios and hydrogen peroxide contents were selected for the investigation of their physical and mechanical properties. 18 different mixture proportions were used for the pastes. These were 4 mixes without hydrogen peroxide at $W/S=0.40, 0.425, 0.45,$ and $0.50,$ and 12 mixes containing 0.25 %, 0.50 %, 0.75 % hydrogen peroxide at $W/S=0.40, 0.425, 0.45,$ and $0.50,$ and another 2 mixes containing 1.00 % and 1.25 % hydrogen peroxide at $W/S=0.45.$ 8 different mixture proportions were used for the mortars. 2 of these mixtures did not contain hydrogen peroxide and had $W/S=0.40$ and $0.50,$ and 6 mixes contained hydrogen peroxide of 0.25 %, 0.50 %, 0.75 % of hydrogen peroxide at $W/S=0.40$ and $0.50.$

Pastes containing hydrogen peroxide in the range of 0-1.25 % with $W/S=0.45$ were selected as the base series for pastes. Similarly, mortars containing hydrogen peroxide in the range of 0-0.75 % at $W/S=0.40$ and 0.50 were selected as base series for mortars. While the motivation for selecting the base series for pastes with $W/S=0.45$ is their production in a wider apparent density range, it is the investigation of effect of large variation in water content for mortars. Their physical and mechanical properties were investigated under different curing conditions.

3.5 Preparation of Test Samples

Samples were cast into 1 L-capacity transparent polypropylene beakers with a diameter of 10 cm in the initial tests. The motivation for using the plastic beakers is to be able to observe the expansion of mixtures, to prevent sticking of the produced mixtures to the walls of the mold, and to demold easily after casting. Almost all of the samples were taken from the molds after one day. Apparent density was measured on three samples per mixture and averaged.

For the determination of flexural and compressive strength, and water absorption of samples, prism samples with dimensions of 40x40x160 mm were used. Steel

molds were used and the inside surfaces of the molds were covered with duct tape to prevent sticking. After casting the mixtures in prism molds, expansion of pastes started and volume of the samples increased. The increase in the volume essentially depends on the amount of hydrogen peroxide, W/S, and ingredients in the mixture. Although, the reproducibility of the expansion of the mixtures was high, it was not possible to obtain test samples with the exact dimension of 40x40x160 mm. As such, samples were allowed to expand freely and then their top surfaces were cut using a spatula. This process is given in Figure 3.4 and Figure 3.5 for mixtures with a W/S=0.40 and hydrogen peroxide contents of 0.25 % and 0.75 %.

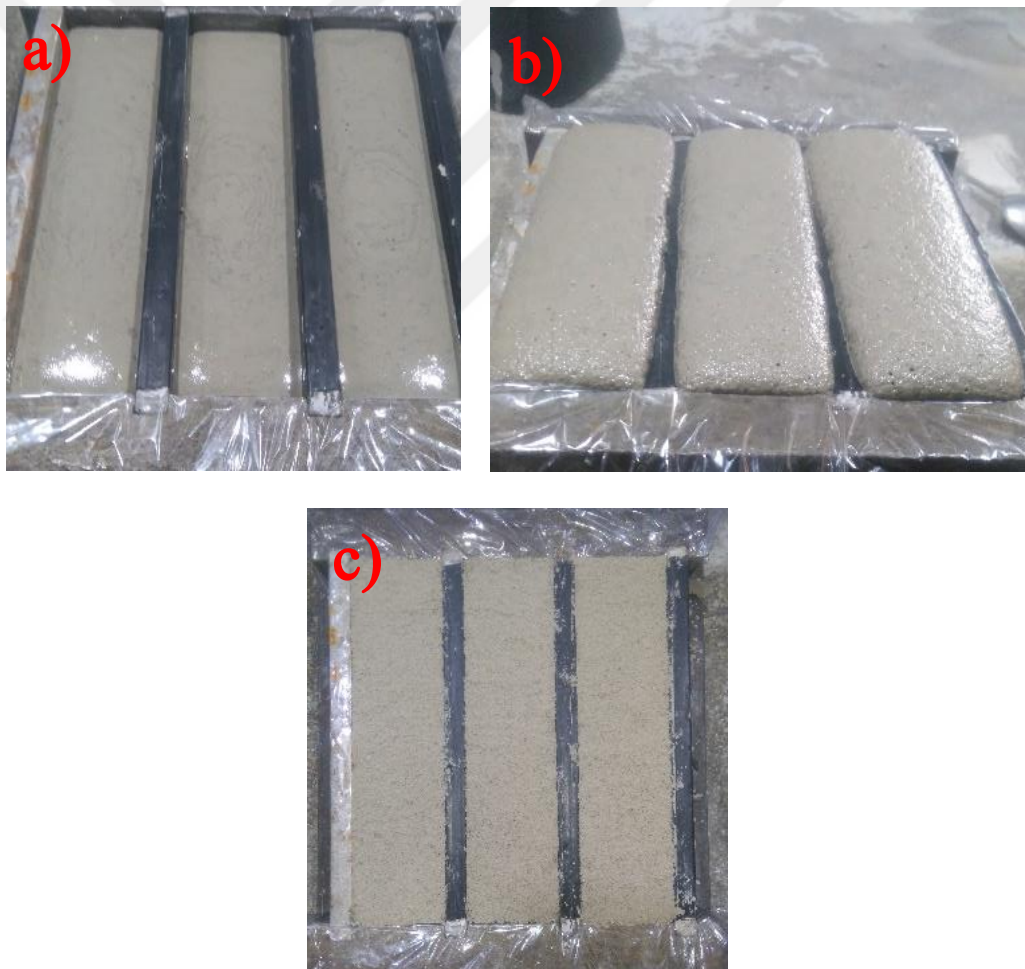


Figure 3.4 Preparation of 40-0-25: a) Immediately after casting, b) 12 minutes after casting, and c) Surface cut ~2h after casting.

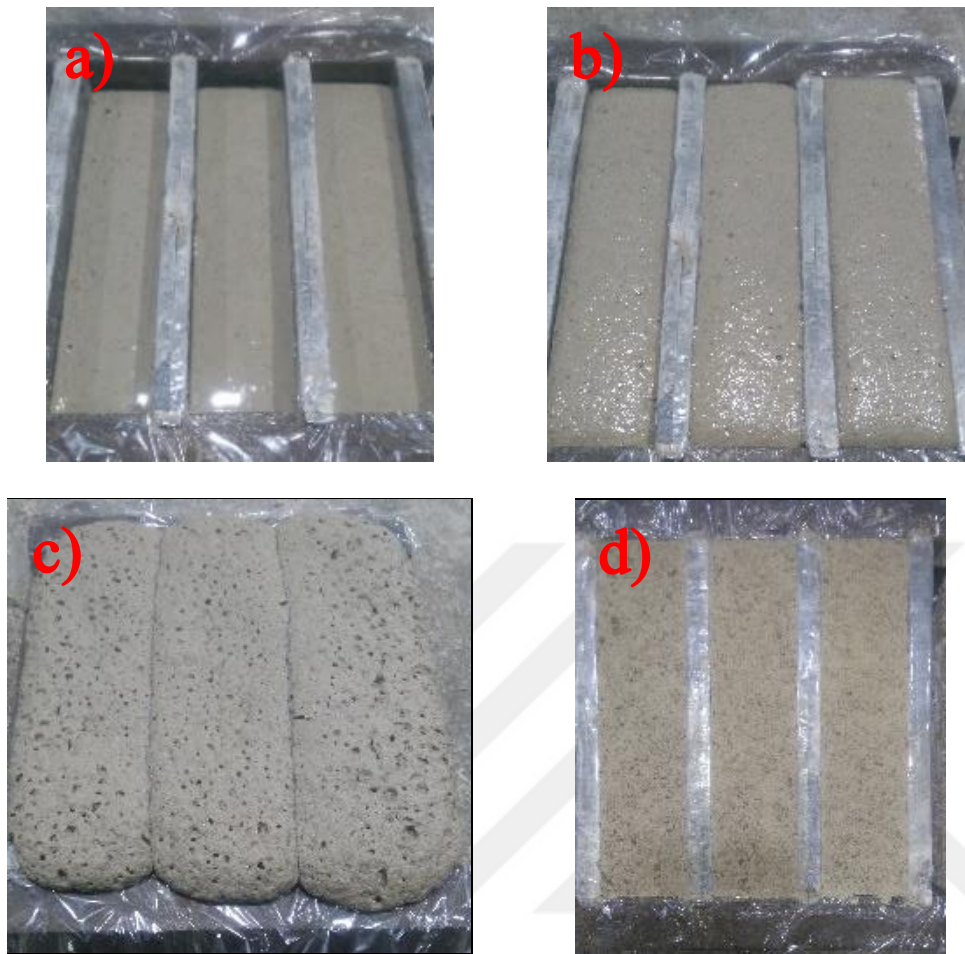


Figure 3.5 Preparation of 40-0-75: a) Immediately after casting, b) 8 minutes after casting, c) 15 minutes after casting, and d) Surface cut ~2h after casting.

As clearly seen from the figures, the increase in hydrogen peroxide content not only increased the expansion amount but also increased the rate of expansion. However, with the increase of W/S to 0.50, this behavior was reversed, and expansion of mixtures was much slower. This is most probably due to the low consistency and low pH of the mixtures. The timing of the cut is also of great importance. If it is too early, the pores break down where as if it is too late, cutting becomes difficult. Thus, the cut was made at a time when the sample was still in a semi-plastic state, which depended on with the amount of water in the mixtures. Then, the molds were sealed with clear plastic wrap until demolding. Demolding was done 3 days later.

3.6 Curing

In the current study, three curing methods were applied; sealed curing at room temperature, ambient curing at room temperature, and humid-oven curing at 80 °C. In sealed curing, after demolding each sample was sealed with clear wrap and placed into a clear plastic bag (Figure 3.6) until the desired test age, as given in Figure 3.6. The motivation for sealed curing is to prevent leaching of excess Na. Ambient and humid-oven curing at 80 °C were performed on the samples after demolding.



Figure 3.6 Sealed curing.

3.7 Tests Performed

3.7.1 Determination of Setting Time

The initial and final setting times of non-aerated pastes were determined using a Vicat needle in accordance with ASTM C191 (2013) but at W/S=0.40, 0.425, 0.45 and 0.50, instead of at normal consistency.

3.7.2 Determination of Flow

A standard flow cone, described in ASTM C230 (2014), was used for the assessment of flowability of the mixtures. After mixing, the cone was immediately filled with the mixture and pulled up. Unlike in the standard, tests were performed without raising and dropping the flow table (Nambiar and Ramamurthy, 2006; Yang et al., 2014). Since some of the mixtures had a flow value greater than the diameter of the flow table, a wider platform was placed on the flow table and the tests were performed on it (Figure 3.7). The flow tests were completed within approximately 30 s of mixing.

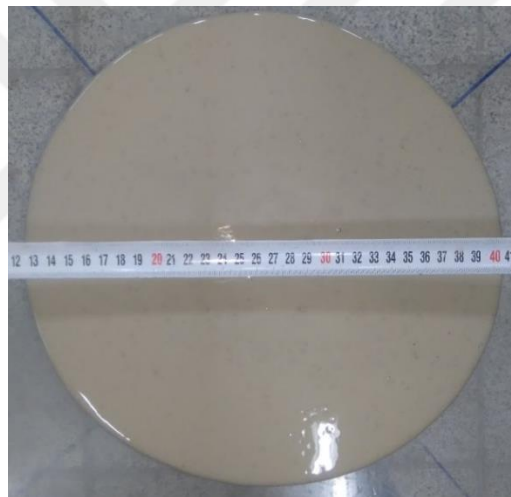


Figure 3.7 Illustration of flow test (The scale bar shows cm units).

3.7.3 Determination of Apparent Density

The mass of samples per unit volume was taken as apparent density. The volumes of samples were calculated by measuring their edge lengths using a digital caliper. The apparent densities of samples were determined: i) immediately after demolding, ii) after the applied curing method, and iii) after drying in the oven. Three samples were measured for each mixture, and their average calculated.

3.7.4 Determination of Porosity

Similar to conventional cement paste, there are three types of pores in AAAS pastes: gel pores, capillary pores and air voids. While pores larger than 50 nm are generally accepted as *macropores*, voids smaller than 50 nm are generally accepted as *micropores* (Mehta and Monteiro, 2006). Porosity is the fraction of the volume of all pores over total volume. In the current study, macro porosity, the fraction of volume of air voids over the total volume, is used as porosity. After compressive strength tests, the crushed samples were ground in a steel mortar to pass a 150 μm sieve to determine the density of the ground sample. Then, their densities were determined in accordance with ASTM C188 (2016). Two measurements were averaged for each sample. Porosity, ρ , is calculated as:

$$\rho = 1 - \frac{\gamma_a}{\gamma_d} \cdot 100 \quad \text{Eq. 3.1}$$

where γ_a is apparent density (kg/m^3), γ_d is density of the ground sample (kg/m^3).

3.7.5 Determination of Flexural and Compressive Strengths

There exists no standard test method for the determination of mechanical properties of aerated alkali-activated materials. RILEM Technical Committees 78-MCA and 51-ALC have recommended two distinct methods of compressive strength measurements for autoclaved aerated concrete. In the first one, compressive strength tests are performed at a moisture content of 15 to 25 %. In the second, oven-dried samples are used. In both tests, the desired moisture content is achieved by heating the sample at temperatures lower than 70 °C (Aroni et al., 1993). ASTM C495 (2012) and ASTM C513 (2011) dictate 3 days of air-drying before compressive strength tests for Portland cement- or lime-based cellular materials at 28 days.

In the current study, three different curing methods were applied. Mechanical tests were performed without pre-conditioning for the room temperature-cured samples to investigate the influence of W/S on mechanical properties. In addition, compressive strength of specimens having W/S=0.45 at different hydrogen peroxide amounts were investigated after curing in humid oven at a temperature of 80 °C. Oven cured samples were pre-conditioned at room temperature for 3 days, and then mechanical tests were performed.

A manually-controlled universal testing machine with an adjustable loading capacity of 100 kN was used for compressive and flexural strength testing of the aerated samples. Tests were performed on prism samples with dimensions of 40x40x160 mm. Flexural strength tests were performed mostly in accordance with ASTM C348 (2014), but at a slightly lower rate of loading than in this standard. Three samples were used. Compressive strength tests were performed on the six half samples remaining after the flexural strength tests. The averages of three and six measurements are presented as the compressive and flexural strengths. Necessary care was taken to prevent shock loading by adjusting the rate of loading at the beginning of tests. Failure loads were reached in not less than 20 s, as stated in ASTM C513 (2011).

For non-aerated samples, compressive strength tests were performed using a 250 kN-capacity automatic universal testing machine. The applied loading rate was 1.5 kN/s. For flexural strength tests, a manually-controlled universal testing machine with an adjustable loading capacity of 100 KN was used.

3.7.6 Determination of Water Absorption

Water absorption of samples was determined in accordance with ASTM C796 (2012) with the minor modification of exposing the samples to air drying from day 25 to day 28 and using cylindrical samples. The test was performed in a climatic chamber at 22 ± 1 °C. After 28 days of sealed curing, prism samples with

dimensions of 40x40x160 mm were directly immersed in 23 °C water for 24 h. Then, the samples were taken out, allowed to release excess water for 30 s, and the wet mass of samples was measured. The difference between the wet and initial mass of sample gives the amount of absorbed water in 24 h. The water absorption as a percentage of total volume was expressed as:

$$\text{Absorption, \% by volume} = 100 \cdot \frac{V_w}{V_s} \quad \text{Eq. 3.2}$$

$$V_w = \frac{W_{w,a} - W_{w,c}}{\gamma_w} \quad \text{Eq. 3.3}$$

where, V_w is the volume of water absorbed in 24 h, V_s is the sample volume, $W_{w,a}$ is weight of water absorbed sample, $W_{w,c}$ is the weight of sample after curing, and γ_w is the unit weight of water. Water absorption as a percentage of total weight was also calculated using the obtained data:

$$\text{Absorption, \% by weight} = 100 \cdot \frac{W_{w,a} - W_{w,c}}{W_{w,c}} \quad \text{Eq. 3.4}$$

After the determination of absorption, samples were exposed to a temperature of 40 °C for 3 days, and then to a temperature of 105 °C to achieve oven-dry condition for the purpose of determination of oven-dry unit weight.

3.7.7 Scanning Electron Microscopy

After the determination of compressive strength of sealed-cured samples at 28 days age, a piece of the sample about 1 cm wide and long was taken from the inner parts of the selected samples. Then samples were kept in acetone for one week to stop hydration. Prior to scanning electron microscopy (SEM) examination, samples

were oven dried at 40 °C for 24 hours and coated with gold-palladium in a high-pressure vacuum. SEM examination was performed at METU Central Laboratory.

3.7.8 Determination of Thermal Conductivity

Thermal conductivities of aerated pastes were determined in accordance with ASTM E1530 (2016) using a commercial device, Anter Unitherm 2022, at General Directorate of Mineral Research and Exploration (MTA). The measurement of thermal conductivity is based on the Fourier's law at steady-state condition. A sample with a diameter of 5 cm is sandwiched between two heat sources, cold plate and hot plate. There is a device that measures the heat flux between hot plate and sample. During the test a reproducible load is applied on the samples to increase the contact between plates and sample. Thermal conductivity measurements were performed on cylindrical samples with a diameter of 5 cm and thickness of about 1 cm taken from cylindrical samples with diameter of 10 cm at the age of about 270 days. Prior to the testing samples were oven dried. Tests were performed at a mean temperature of about 30 °C, and temperature difference between hot and cold plates was about 25 °C. Figure 3.8 shows the thermal conductivity apparatus used. Thermal conductivity of 16 samples were determined. The images of the samples used in the measurement of thermal conductivity are given in Appendix B.



Figure 3.8 Unitherm 2022 thermal conductivity apparatus.

3.7.8.1 Uncertainty Analysis of Thermal Conductivity Measurements

For the determination of thermal conductivity of a sample, several parameters such as thickness, temperature, heat flux, etc. are measured at the steady state. Even though these measurements are taken automatically by the apparatus, there exist some error in the measurement instruments due to the nature of the measurement. It was decided to perform an uncertainty analysis to observe effect of uncertainties of measured parameters on the thermal conductivity. For this purpose, propagation of error method was used. The propagation of error formula for $A=f(B, C)$, a function of two variables with measurements (B, C) that are uncorrelated gives the following estimate for uncertainty of A as:

$$s_A = \sqrt{\left[\left(\frac{dA}{dB} \right)^2 \cdot s_B^2 + \left(\frac{dA}{dC} \right)^2 \cdot s_C^2 \right]} \quad \text{Eq. 3.5}$$

where: s_A , s_B , and s_C are uncertainties in A, B and C, respectively, and dA/dB and dA/dC are the partial derivatives of the function A with respect to B and C, respectively.

According to ASTM E1530 (2016), first thermal resistance of sample is calculated using Eq. 3.6, then thermal conductivity of the sample is calculated using Eq. 3.7.

$$R_s = \frac{N \cdot (T_1 - T_2)}{Q} - R_o \quad \text{Eq. 3.6}$$

$$k = \frac{h}{R_s} \quad \text{Eq. 3.7}$$

where: k is thermal conductivity of sample (W/m.K), h is thickness of sample (mm), R_s is thermal resistance of sample (W/m².K), N is heat flux transducer calibration constant (W/m².mV), T_1 and T_2 are temperature of the surfaces of the sample (K),

Q is heat flow (W), R_o is the contact resistance between sample and plate surfaces (W/m.K).

First uncertainty in thermal resistance of sample was found. For this purpose, the propagation of error formula given in Eq. 3.5 is adapted to the Eq. 3.6. Thus, the uncertainty in thermal resistance of sample is:

$$s_{R_s} = \sqrt{\left[\left(\frac{dR_s}{dQ} \right)^2 \cdot s_Q^2 + \left(\frac{dR_s}{dN} \right)^2 \cdot s_N^2 + \left(\frac{dR_s}{dT_1} \right)^2 \cdot s_{T_1}^2 + \left(\frac{dR_s}{dT_2} \right)^2 \cdot s_{T_2}^2 + \left(\frac{dR_s}{dR_o} \right)^2 \cdot s_{R_o}^2 \right]} \quad \text{Eq. 3.8}$$

Similarly, the uncertainty in thermal conductivity is;

$$s_k = \sqrt{\left[\left(\frac{dk}{dh} \right)^2 \cdot s_h^2 + \left(\frac{dk}{dR_s} \right)^2 \cdot s_{R_s}^2 \right]} \quad \text{Eq. 3.9}$$

where s indicates the uncertainty of the parameter.

Manufacturer of the test apparatus used reported the accuracy of the apparatus between 3 %-8 % depending on the thickness of the test sample. There was no information given by the manufacturer of the apparatus about the uncertainty of the parameters that measured for the determination of thermal conductivity. Therefore, uncertainties of the parameters were taken from ASTM C518 (2015) which gives a comprehensive information related to the heat flow apparatus design. It is noteworthy to remind that test method in ASTM E1530 is similar in concept to test method ASTM C518, but the former was modified to test quite smaller samples. For the calculation of uncertainties of the thermal conductivity of the samples, the uncertainties of the parameters used are listed below.

s_h : ± 0.1 mm

s_Q : ± 0.5 % of value

s_N : ± 0.1 % of value

s_{T_1} : ± 0.5 % of value

s_{T_2} : ± 0.5 % of value

s_{R_0} : ± 1.0 % of value (There is no such a parameter, R_o , in ASTM C518, and there is no value for the uncertainty of this parameter in ASTM E1530. Thus, it was taken 1.0 % which can be considered quite high.)

Table 3.2 shows the measured parameters during the thermal conductivity test with their uncertainties for 40-0-25, and uncertainty in thermal of conductivity of 40-0-25 was calculated using Eq. 3.8 and 3.9. The calculated uncertainties in the thermal conductivity of aerated pastes are given in Table A.17 in Appendix A.

Table 3.6 Uncertainty analysis for 40-0-25.

	Measured Value	Uncertainty	Unit
Thermal Conductivity (k)	0.206	± 0.014	W/m.K
Thickness of sample (h)	9.09	± 0.10	mm
Thermal resistance of sample (R_s)	0.0441	± 0.003	$m^2.K/W$
Heat flux transducer calibration constant (N)	0.33951	± 0.0003	$W/m^2.mV$
Heat flow (Q)	36.68	± 0.18	W
Hot plate temperature (T_1)	43.19	± 0.22	$^{\circ}C$
Cold plate temperature (T_2)	19.94	± 0.10	$^{\circ}C$
Contact resistance (R_0)	0.1711	± 0.0017	$m^2.K/W$



CHAPTER 4

RESULTS AND DISCUSSION

4.1 Setting Time

The relation between setting time and duration of gas evolution has great importance in the production of aerated concretes produced using air-entraining agents. Setting time controls the duration of expansion in aerated concretes. If the formation of gas continues after setting, cracks may develop in the material (Rudnai, 1963). Figure 4.1 shows the effect of W/S on setting time of the non-aerated pastes.

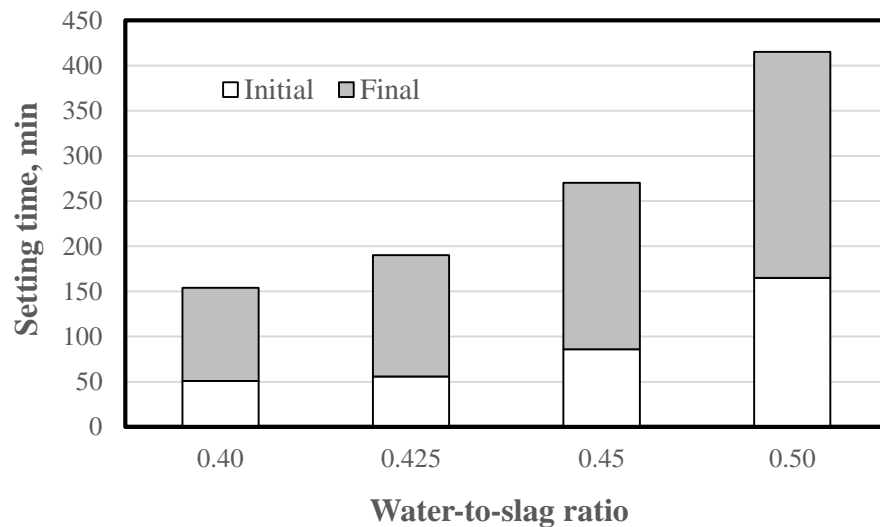


Figure 4.1 Effect of W/S on the setting times of aerated pastes.

Initial and final setting times of alkali-activated pastes increase considerably with the increase of water content. As a result of increasing water content, concentration of the activating solution decreases, leading to a decrease in rate of reaction and volume of hydration products. Due to the heterogeneous structure and difficulties to obtain test samples of the aerated pastes, their setting times could not be determined. However, a similar relation with water content and similar setting times may be expected for the aerated pastes produced using hydrogen peroxide.

4.2 Flow

The consistencies of the mixtures were assessed using flow which is commonly used as an indication of the viscosity of aerated concrete (Esmaily and Nuranian, 2010). The consistency of a mixture is important for the production of aerated concrete using air-entraining agents. A certain consistency is needed for the production of aerated concrete (Just and Middendorf, 2009). There is a direct relationship between consistency and viscosity of homogeneous and non-segregated alkali-activated pastes and mortars.

In the determination of compressive strength of hydraulic cements, mortars with a consistency of 110 ± 5 %, measured after 25 drops of the flow table are used (ASTM C109, 2016). In the current study, flow tests were performed without dropping the flow table. It can be observed that the flow of non-aerated pastes and mortars are considerably higher than that used in compressive strength measurement of cement mortars. Actually, the mixtures were in slurry form. Figure 4.2 shows the effect of W/S on the flow of non-aerated pastes and mortars.

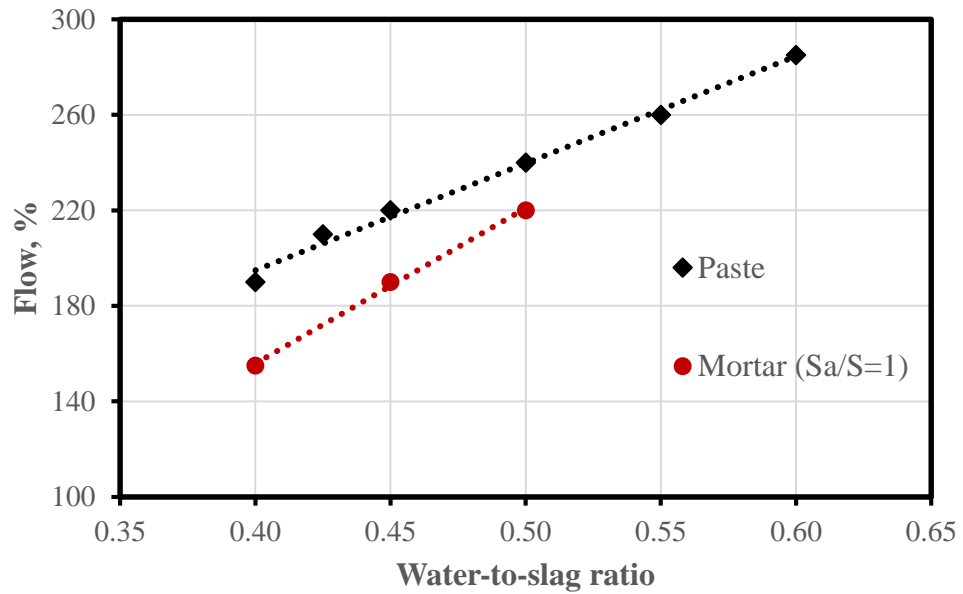


Figure 4.2 Effect of W/S on the flow of non-aerated pastes and mortars.

The consistencies of the non-aerated pastes and mortars both increased with the increase of water content. In addition, incorporation of sand into the pastes increased the consistency at identical water content, which was expected, since addition of solid particles increases viscosity of the mixtures. Some of the flow values of the pastes and mortars were found to be close, however this does not mean that their viscosities are identical. It is noteworthy that the mixers used for the production of pastes and mortars were different. A high-speed mixer was used for the production of pastes. Straub et al. (2014) reported an increase in flow with high-energy mixing compared to normal mixing for autoclaved aerated concretes. Flow tests were also performed on pastes and mortars containing hydrogen peroxide. There was no measurable change in the flow of pastes after incorporation of hydrogen peroxide in the range of 0.25 % to 1.25 % at a W/S=0.45. However, incorporation of 1.50 % hydrogen peroxide in pastes with W/S=0.45 yielded dramatic decomposition of hydrogen peroxide, and the test could not be performed as a result of fast expansion of mixtures. Similarly, no measurable change was obtained for mortars with W/S=0.40 and 0.50 after incorporation of 0.25 to 0.75 %

hydrogen peroxide. It is also noteworthy to mention that there was a sensible change in the temperature of the mixtures with the use of hydrogen peroxide beyond 0.75 %. W/S and hydrogen peroxide content affect the temperature change in the mixtures.

4.3 Expansion Mechanism of Mixtures

Decomposition of hydrogen peroxide starts immediately after its incorporation into alkali-activated slag pastes or mortars, and continues during mixing. Oxygen produced during mixing can partly escape and is released to the atmosphere. After casting the mix, unless all the hydrogen peroxide has reacted, tiny air bubbles form inside the non-Newtonian plastic paste. Further liberation of oxygen due to the decomposition exerts pressure on the walls of the air bubbles which acts as a shear stress on the paste. In time, the air bubbles expand and the volume of the paste increases. However, the pressure applied on the walls of bubbles decreases with the expansion of air bubbles, and expansion of the bubbles ceases after a while (Vaou and Panyas, 2010). On the other hand, the shear stress applied on the walls of air bubbles which is a function of hydrogen peroxide content, and the stress encountered which is a function of viscosity/consistency of the paste must match, otherwise efficient aeration and volume increase cannot be achieved. When the shear stress applied to the walls of the air bubbles is higher, air bubbles either escape from the paste or collapse due to the over expansion. When the stress encountered is higher, either air bubbles remain small or they collapse.

Figure 4.3 shows the relative expansion of aerated pastes produced using cylindrical molds after the addition of different hydrogen peroxide contents.

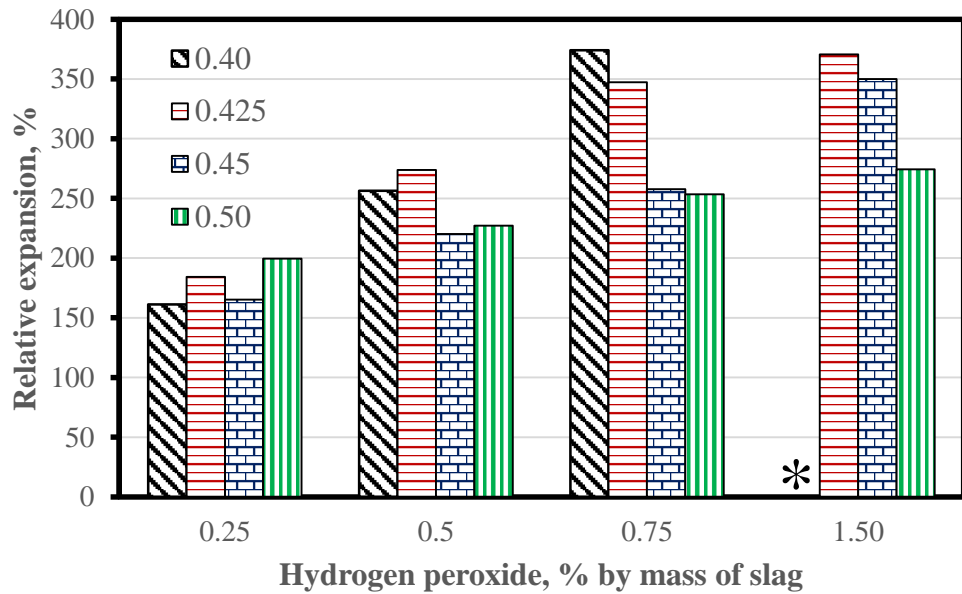


Figure 4.3 Effect of hydrogen peroxide content on the relative expansion of aerated pastes with different W/S (* no result).

An increase in the hydrogen peroxide content increased the expansion in aerated pastes regardless of the W/S. Theoretically when the hydrogen peroxide content doubles, the amount of oxygen produced also doubles. However, the amount of expansion is not proportional to the hydrogen peroxide content. This result suggests that not all the oxygen produced was entrapped in the pastes, and/or some of the air bubbles collapsed and/or not all the hydrogen peroxide decomposed. In addition, changes in the W/S of mixtures yielded readily observable differences in expansion at identical hydrogen contents. The relationship between W/S and expansion is more complex due to the several changes in properties of the mixture. It is well known that large variations in the water content of a mixture directly influences initial setting time, viscosity/consistency, pH, and heat of hydration. Decomposition rate hydrogen peroxide decreases with decreasing pH and temperature, viscosity/consistency of mixtures controls the formation of pores, and initial setting time affects the duration of expansion. Therefore, it can be concluded that expansion and aeration essentially depend on water content and hydrogen

peroxide content for aerated alkali-activated pastes. Figure 4.4 compares the paste samples with identical initial mass, and identical $W/S=0.425$, but containing different hydrogen peroxide contents.



Figure 4.4 Effect of hydrogen peroxide content on expansion of pastes with identical mass (~240 g) and $W/S=0.425$ (from left to right, hydrogen peroxide contents 0 %, 0.25 %, 0.50 %, 0.75 %, 1.50 %, the scale bar shows cm units).

The increase in the expansion of pastes with increasing hydrogen peroxide content can be seen clearly. In addition, increasing hydrogen peroxide increased the size and amount of pores on the exterior faces of the samples. Figure 4.5 shows the relative expansion of aerated mortars with $S_a/S=1$ and containing different hydrogen peroxide contents produced using cylindrical molds.

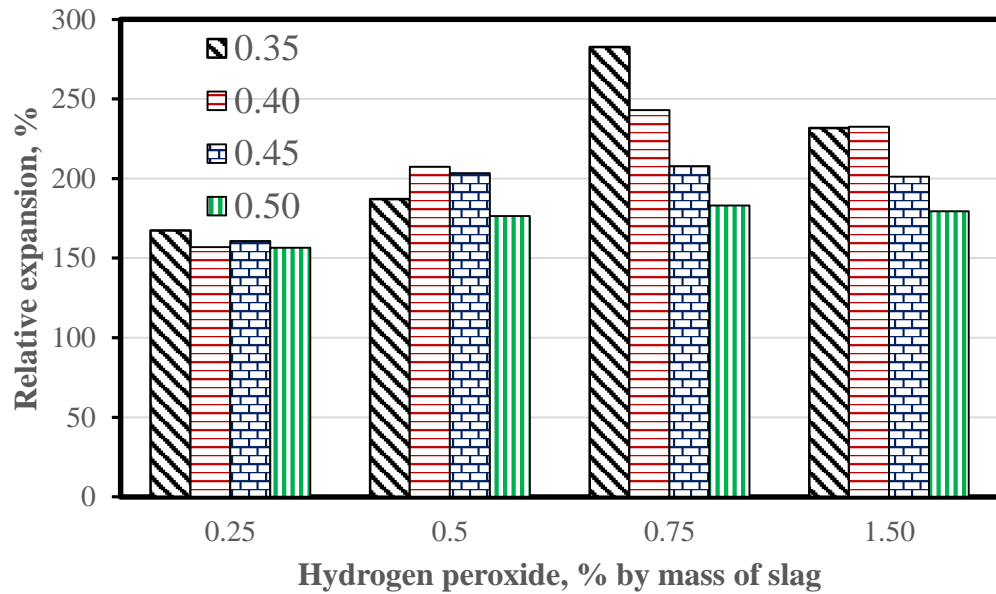


Figure 4.5 Effect of hydrogen peroxide content on the relative expansion of aerated mortars ($S_a/S=1$) with different W/S.

Similar to the results obtained on aerated pastes, increasing hydrogen peroxide 0.25 % to 0.75 % increased expansion of mixtures regardless of W/S for aerated mortars with $S_a/S=1$. However, further increase of hydrogen peroxide (to 1.50 %) decreased the expansion. As a result of increase of hydrogen peroxide content, the amount of oxygen produced and decomposition rate increases, thus air bubbles collapse or leave the mixture easily. In comparison, the relative expansions of aerated pastes were much higher than those of aerated mortars for a given W/S and hydrogen peroxide content, because of the increase in viscosity and increase in the unit weight with the incorporation of sand.

4.4 Apparent Density

The apparent densities of pastes, mortars with a $S_a/S=1$, and mortars with a $S_a/S=2$ were investigated. Samples were produced using plastic beakers with a diameter of about 100 mm. Apparent densities of samples were determined after demolding and

the average of three measurements is presented for each mixture. These results are given in Tables A.4 to A.5 in Appendix A.

4.4.1 Influence of Hydrogen Peroxide and Water Content

When selecting the W/S of pastes, the lowest W/S of mixtures, 0.40, was chosen according to the mixing capability of the high-speed mixer. Since a 35 % w/w hydrogen peroxide solution was used and added to the mixtures as the final ingredient. Increasing hydrogen peroxide for a given W/S decreased the amount of mixing water. Therefore, some of the mixtures could not be prepared such as those with W/S=0.40 containing hydrogen peroxide more than 0.75 % by mass of slag. Figure 4.6 shows the effect of hydrogen peroxide content on the apparent density of aerated pastes with different W/S. For a given W/S, data points are connected only to make the changes in apparent density easier to follow.

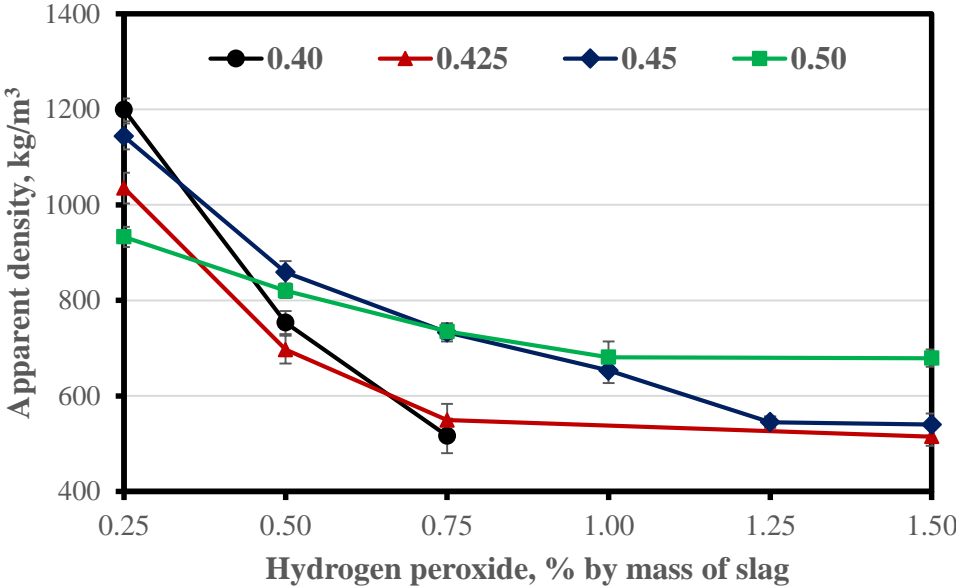


Figure 4.6 Effect of hydrogen peroxide content on the apparent density of aerated pastes with different W/S.

Apparent densities of aerated pastes decreased with increasing hydrogen peroxide content regardless of the W/S. However, there is no significant change in the apparent densities beyond a certain hydrogen peroxide content for the mixtures with a W/S=0.425, 0.45, and 0.50. This may be attributed to the high decomposition rate of hydrogen peroxide at excessive contents, the low consistency of the pastes which cannot prevent the escape of oxygen, and the collapse of the pastes due to the merging of air bubbles. It is also seen that the relation between apparent density and hydrogen peroxide amount appears to be strong at lower hydrogen peroxide contents. There is a linear relationship between apparent density and hydrogen peroxide content for pastes with W/S=0.50 in the hydrogen peroxide range of 0.25 to 1.00 %. Figure 4.7 shows the effect of W/S on the apparent density of aerated pastes prepared with different hydrogen peroxide contents.

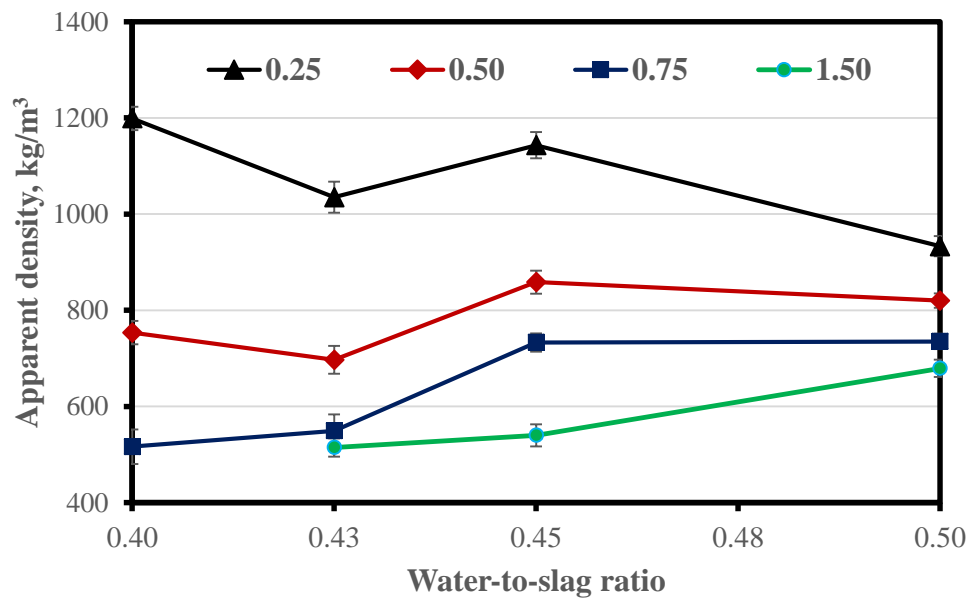


Figure 4.7 Effect of W/S on the apparent density of aerated pastes with different hydrogen peroxide contents.

The relation between W/S and apparent density is not as strong as the relation between hydrogen peroxide amount and apparent density. For the samples produced

using 0.25 % hydrogen peroxide, an increase of water content yielded a decrease in apparent density, except at $W/S=0.45$. This can be explained as follows. Decomposition of hydrogen peroxide is high at low W/S , due to the high pH and heat evolution of the pastes. This leads to the escape of a considerable amount of oxygen during mixing. Therefore, the remaining amount of hydrogen peroxide hardly expands the pastes at low consistency. However, pH and heat evolution of the pastes decrease, and the consistency of the mixture decreases with increasing water content. Therefore, much expansion was observed with 0.25 % hydrogen peroxide. In addition, the difference between initial setting times of mixtures due to change in the water content might have played a role, since expansion of pastes continues up to initial setting. Furthermore, it can be observed from Figure 4.6 that the apparent densities of samples containing 0.50 %, 0.75 %, and 1.50 % hydrogen peroxide obviously increase with increasing water content. However, there are some exceptional data points where apparent density increases: samples containing 0.50 % hydrogen peroxide at $W/S=0.425$ and samples containing 0.75 % hydrogen peroxide at $W/S=0.50$. There can be several explanations for this exceptional behavior: i) fast interaction between alkali solution and high contents of hydrogen peroxide, ii) exponential increase in the setting times of pastes due to the increase of water content, iii) differences in evolved heat during decomposition of hydrogen peroxide, iv) collapse of air bubbles due to the merging, and v) Reduced air entrapment capacity of pastes with the decrease of viscosity.

Figure 4.8 shows the effect of hydrogen peroxide content on the apparent density of mortars ($S_a/S=1$) with different hydrogen peroxide contents. Again, in this figure and several of the following figures, data points are connected by straight lines only to make changes in the apparent densities for a given W/S easier to follow.

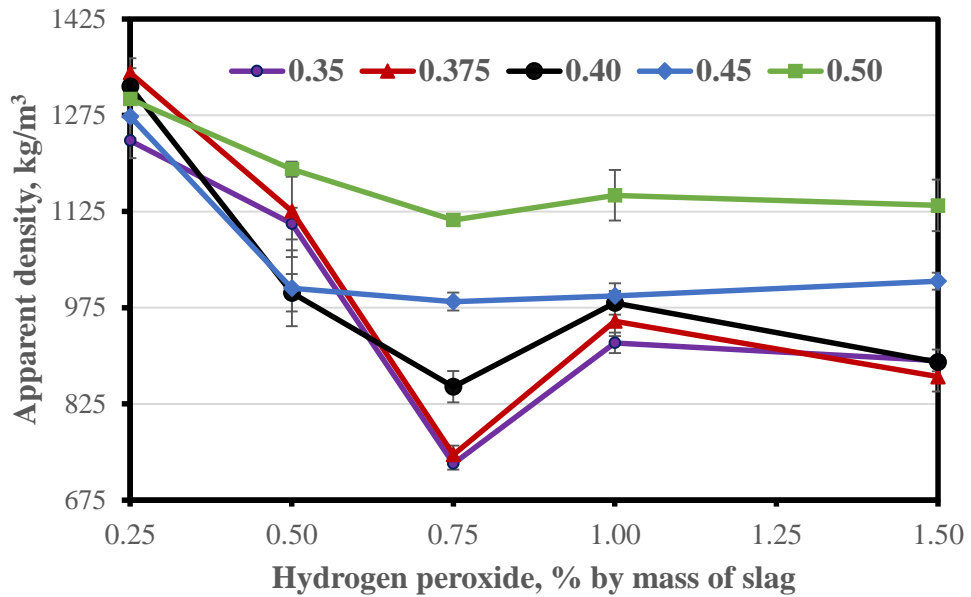


Figure 4.8 Effect of hydrogen peroxide on the apparent density of mortars (Sa/S=1) with different hydrogen peroxide contents.

Apparent densities of samples noticeably decreased with the increase of hydrogen peroxide compared to the samples containing 0.25 % hydrogen peroxide, for all W/S. The samples can be grouped two according to their apparent density curves as; Group I (samples with W/S=0.35, 0.375 and 0.40) and Group II (samples with W/S=0.45 and 0.50). Apparent densities decreased with increasing hydrogen peroxide up to 0.75 %, increased at 1.0 % hydrogen peroxide, and then decreased at 1.50 % hydrogen peroxide in Group I. The reason for these fluctuations is not clear, but can be explained by one or a combination of observations presented above for the pastes. In addition, sand in the mixtures may have altered the expansion mechanism. Addition of sand increases the pressure on the air bubbles due to its higher specific gravity, and a porous interfacial zone between sand particles, and paste is formed. Therefore, at high hydrogen peroxide contents air bubbles may leave the paste or collapse easily. It can be deduced that the maximum useful amount of hydrogen peroxide to achieve low-density samples is between 0.75 % and 1.0 % by mass of the slag for Group I. In Group II, fluctuations in apparent

density are limited. There is no significant change in the apparent densities of samples with W/S=0.45 beyond a hydrogen peroxide amount higher than 0.50. For the samples with W/S=0.50, the change in apparent density becomes negligible beyond 0.75 % hydrogen peroxide. The reason for this is the reduction in air entrapment capacity due to the decrease of viscosity. Use of hydrogen peroxide was found to be inefficient beyond these limits. Figure 4.9 shows the effect of W/S on of apparent density of mortars (Sa/S=1) with different hydrogen peroxide contents.

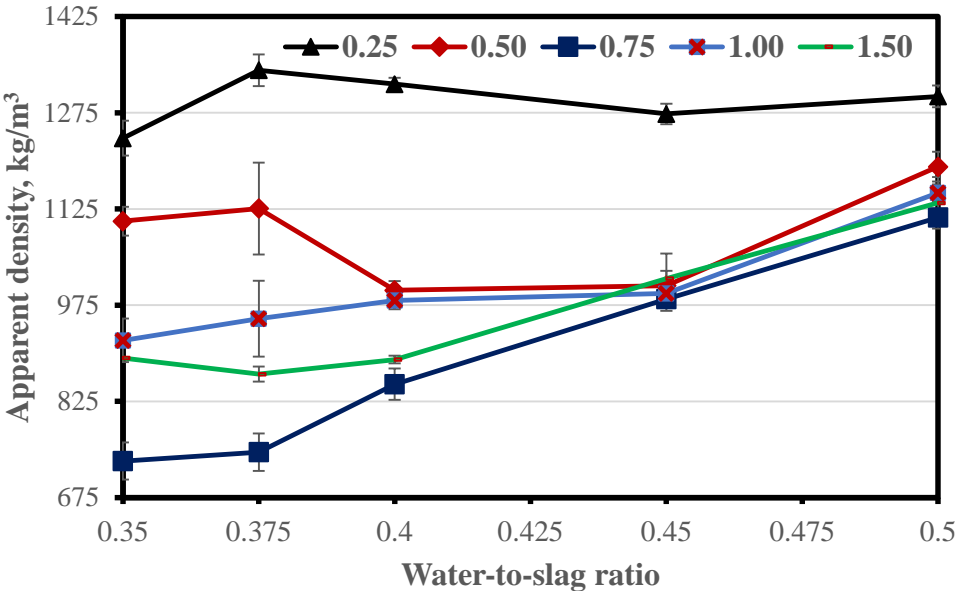


Figure 4.9 Effect of W/S on of the apparent density of mortars (Sa/S=1) with different hydrogen peroxide contents.

The apparent densities of mortars noticeably increased with the increase of water content compared to the apparent densities of samples containing 0.25 % hydrogen peroxide, except for samples with 0.50 % hydrogen peroxide content at W/S=0.40 and 0.45. The reason for this density increase could be directly the increase of water content which decreases pH and viscosity, and increases setting time. As a result, not only the decomposition rate of hydrogen peroxide decreases but also air bubbles

escape easily. Figure 4.10 shows the effect of hydrogen peroxide content on apparent density of mortars ($S_a/S=2$) with different W/S.

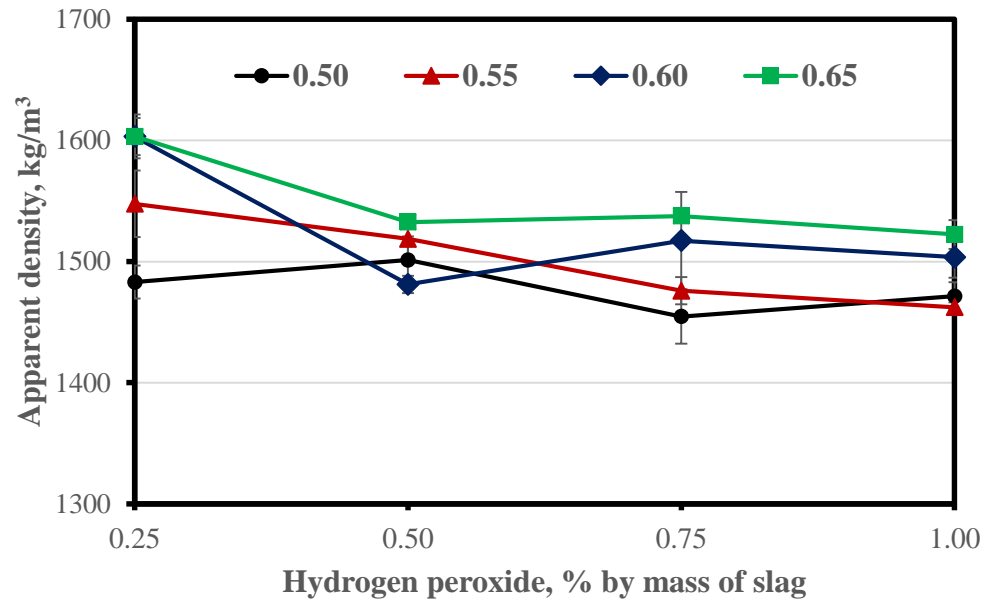


Figure 4.10 Effect of hydrogen peroxide on the apparent density of mortars ($S_a/S=2$) with different W/S.

Changes in the apparent densities of the samples with the increase of hydrogen peroxide were found to be limited regardless of the W/S of the mixtures. The main reasons for this could be: i) the decrease of free paste volume in the matrix, since the amount of paste that covers the surface of the sand increases, collapse or escape of air bubbles taking place easily, ii) the increase of matrix weight, since the specific gravity of the sand is higher than that of the paste and expansion becoming difficult, and iii) extension in the setting times of the mixtures, due to the high water contents.

4.4.2 Influence of Sand Addition on the Paste Phase

Addition of sand to the pastes yielded an increase in the apparent densities for a given hydrogen peroxide content and W/S. Since the density of a system depends on the constituent materials, this is an expected result. It is also noteworthy that mixtures with a Sa/S=3 could not be prepared due to the segregation of sand particles in these high consistency mixtures. Apparent density is not only a function of sand content but also apparent density of paste for aerated concretes. As is known, oxygen produced by the decomposition of hydrogen peroxide is trapped in the matrix and air bubbles are always generated in the paste phase. Therefore, apparent density of the paste phase can be estimated with the knowledge of the density of sand and the apparent density of the produced specimen. The apparent density of paste phase can be calculated as follows;

$$AD_{\text{paste}} = \frac{M_p}{V_p} = \frac{D_f \cdot (1 - M_{\%})}{1 - \frac{D_f \cdot M_{\%}}{\rho_s}} \quad \text{Eq. 4.1}$$

where, AD_{paste} is apparent density of the specimen, M_p is mass of paste phase, V_p is volume of the paste phase, D_f is apparent density of the mortar, $M_{\%}$ is mass % of sand in mixtures, ρ_s is density of sand (2.65 kg/m^3). The apparent densities of the paste phases of mortars with a Sa/S=1 were calculated and compared to those of pastes with identical W/S and hydrogen peroxide contents. These results are given in Table A.7 in Appendix A. Figure 4.11 shows the calculated apparent density of the paste phase in paste and mortar (Sa/S=1) specimens with W/S=0.40 and different hydrogen peroxide contents.

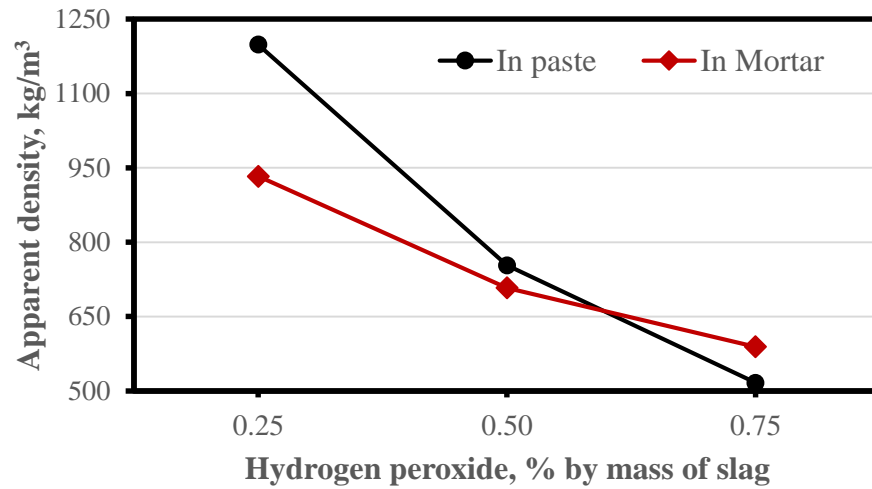


Figure 4.11 Comparison of the calculated density of the paste phases in paste and mortar ($S_a/S=1$) specimens with $W/S=0.40$ and different hydrogen peroxide contents.

Figure 4.12 shows the calculated apparent density of paste phases in paste and mortar ($S_a/S=1$) specimens with $W/S=0.45$ and different hydrogen peroxide contents.

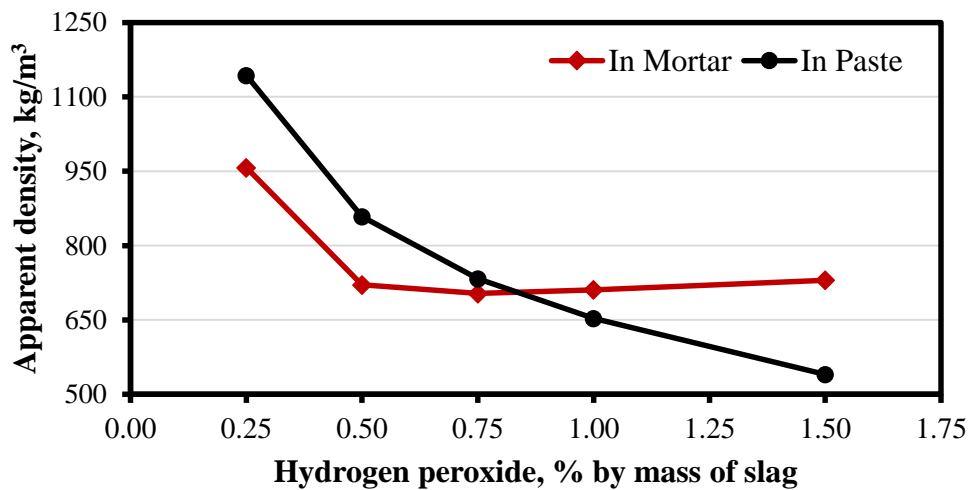


Figure 4.12 Comparison of the calculated of the paste phases of pastes in paste and mortar ($S_a/S=1$) specimens with $W/S=0.45$ and different hydrogen peroxide contents.

The apparent densities of the paste phase in mortar specimens were lower than those in paste specimens except in the samples with 0.75 % hydrogen peroxide content at W/S=0.40 and 1.00 % and 1.50 % hydrogen peroxide content at W/S=0.45. This can be attributed to the increased viscosity due to the addition of sand resulting in an increase for oxygen entrapped in the mixtures. Thus, it could be deduced that by using aggregates lighter than the sand used in the current study, it may be possible to produce aerated mortars lighter than aerated pastes. Therefore, the obtained mortars can be less expensive and have better physical and thermal properties. Figure 4.13 shows the effect of mass ratio of sand in specimens on the apparent density of paste phase in samples with W/S=0.50 and different hydrogen peroxide contents.

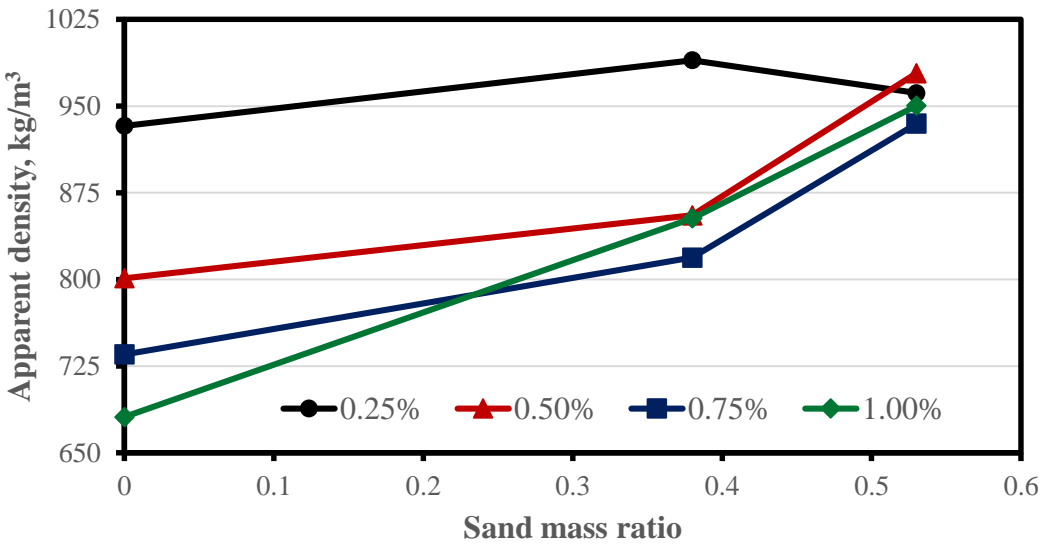


Figure 4.13 Effect of mass ratio of sand in specimens on the apparent density of paste phase in specimens with W/S=0.50 and different hydrogen peroxide contents.

The apparent densities of the paste phase increased with increasing sand content in mixes, except for samples with 0.25 % hydrogen peroxide at a 0.53 mass ratio of sand. This may be attributed to the change in consistency with the addition of sand to the mixtures. At a 0.38 mass ratio of sand, the consistency of the mixture was

much lower than that of 0.53. Therefore, the amount of entrapped oxygen in the system was lower, and as a result these samples had a higher density. In other words, increasing sand content increased the total mass of mixture and increased the consistency at 0.53 mass ratio of sand, however 0.25 % of hydrogen peroxide was able to expand the volume without collapse of air bubbles.

4.5 Porosity

The porosities of pastes varied between 6.5 % (for non-aerated paste with W/S=0.40) and 70.9 % (for paste with W/S=0.45 and 1.25 % hydrogen peroxide). Porosity of samples increases with increasing hydrogen peroxide as a result of increasing amount of pores. In addition, the distance between pores decreases, and the average size of pores increases with increasing porosity for the aerated pastes. This can be clearly seen on the images of aerated pastes given in Section 4.8, on pore structure of samples. The change in the porosity of pastes with apparent density is given in Figure 4.14.

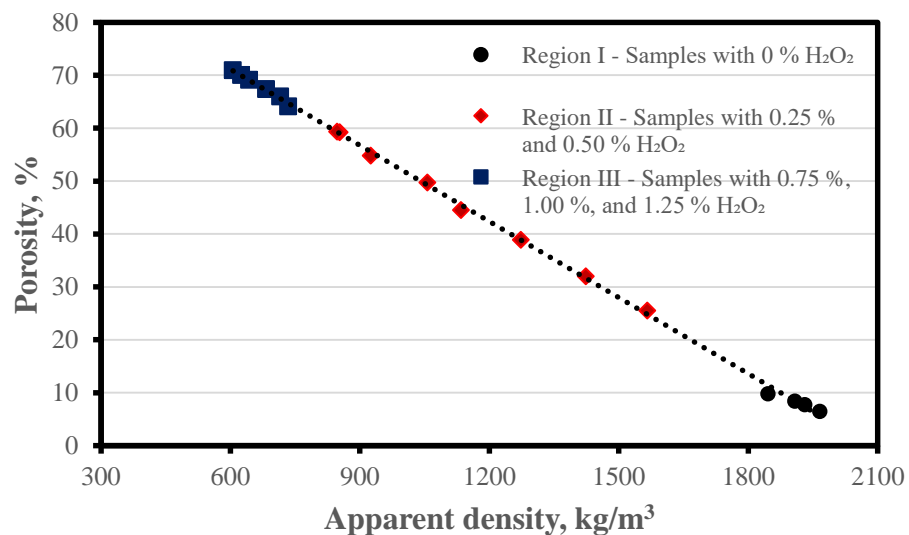


Figure 4.14 Porosity of pastes as a function of apparent density.

An inverse linear relationship can be seen between porosity and apparent density. Porosity of pastes essentially depends on the apparent density and decreases with increasing apparent density. This is because the solid content of samples decreases with increasing amount of entrained air in the samples. Three regions can be seen in the Figure 4.13: i) the region I in between porosity of 10 % and 6 % where the apparent density is between 1800 kg/m³ and 2000 kg/m³, ii) the region II in between porosity of 25 % and 60 % where the apparent density is between 1600 kg/m³ and 850 kg/m³, and iii) the region III in between porosity of 64 % and 71 % where the apparent density is between 750 kg/m³ and 600 kg/m³. These regions are also divided by increasing hydrogen peroxide content as given in the Figure 4.14.

4.6 Strength

4.6.1 Strength Development of Paste Samples

4.6.1.1 Influence of Sealed Curing

The flexural and compressive strengths of produced pastes were determined on prism samples without pre-conditioning after 28 days of curing in sealed condition at room temperature. These results are given in Table A.9 in Appendix A for pastes with different W/S and hydrogen peroxide contents.

Even though, there was no change in the mixture proportions, the apparent densities of samples produced using prism molds were different than those of samples produced cylindrical molds (see Section 4.4, on apparent density). This is most probably because of the production method followed. Mixtures show different amounts of expansion each hydrogen peroxide content and W/S. The total amount of ingredients was altered for each mixture to fill to the volume of prism molds after expansion of mixtures. Then the top surfaces of samples were cut to obtain prism test samples. There was no cut applied for the production of cylindrical samples. Since there could be some differences in the amount and size of the pores between

the top and bottom surfaces, apparent densities of prism samples were found to be different than those of cylindrical samples at identical hydrogen peroxide and water content. Attempts to produce large specimens and to cut test samples from those were not successful since samples cracked during cutting with a diamond saw, which could affect the test results.

Apparent density directly influences physical and mechanical properties of aerated concrete. Prior to performing any mechanical test on prism samples, the apparent density of each sample was measured and the average of three samples given for each mixture. Figure 4.15 shows the relationship between apparent densities of aerated pastes produced using prism molds and cylindrical molds, at identical W/S and hydrogen peroxide contents.

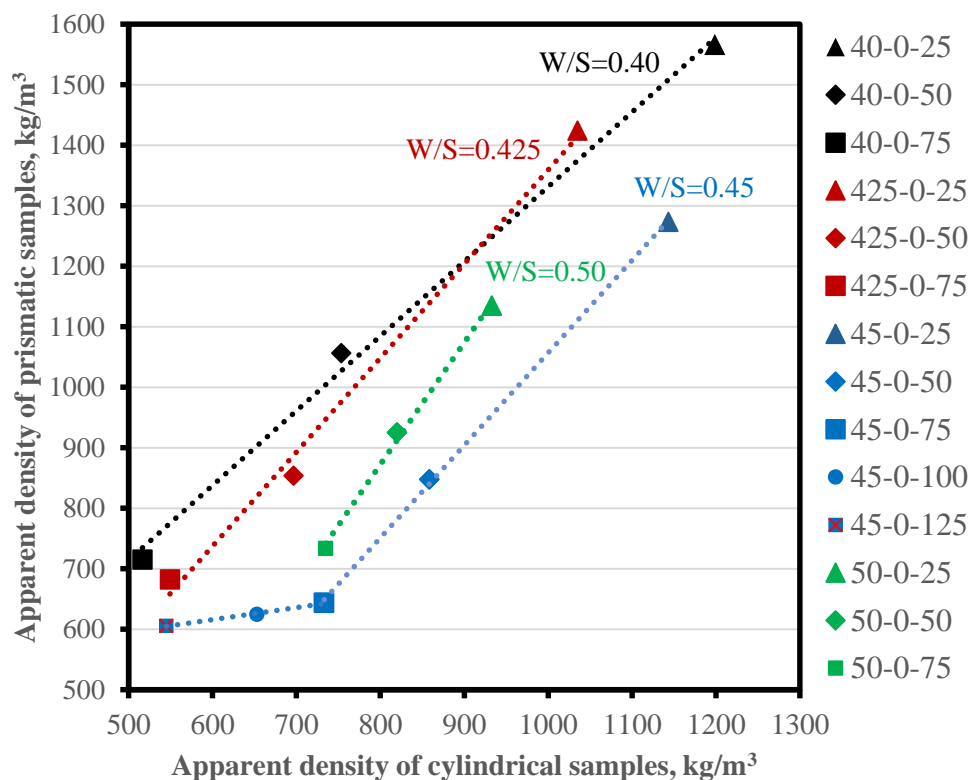


Figure 4.15 Relationship between the apparent densities of prism samples and cylindrical samples.

Apparent densities of aerated pastes produced using cylindrical molds and prism molds were in the range of 516 kg/m³ to 1199 kg/m³ and 644 kg/m³ to 1566 kg/m³, respectively. Apparent densities of prism samples were different (12 % lower to 40 % higher) than those of cylindrical samples. Prism samples with W/S=0.40 exhibited the highest differences (30-40 %) in apparent density with those of cylindrical samples at identical hydrogen peroxide contents. However, the differences decreased with the increase of water content, and yielded -12 % to 25 % for samples for W/S=0.425, 0.45 and 0.50. Figure 4.16 shows the effect of W/S on the 28-day compressive and flexural strengths of non-aerated pastes.

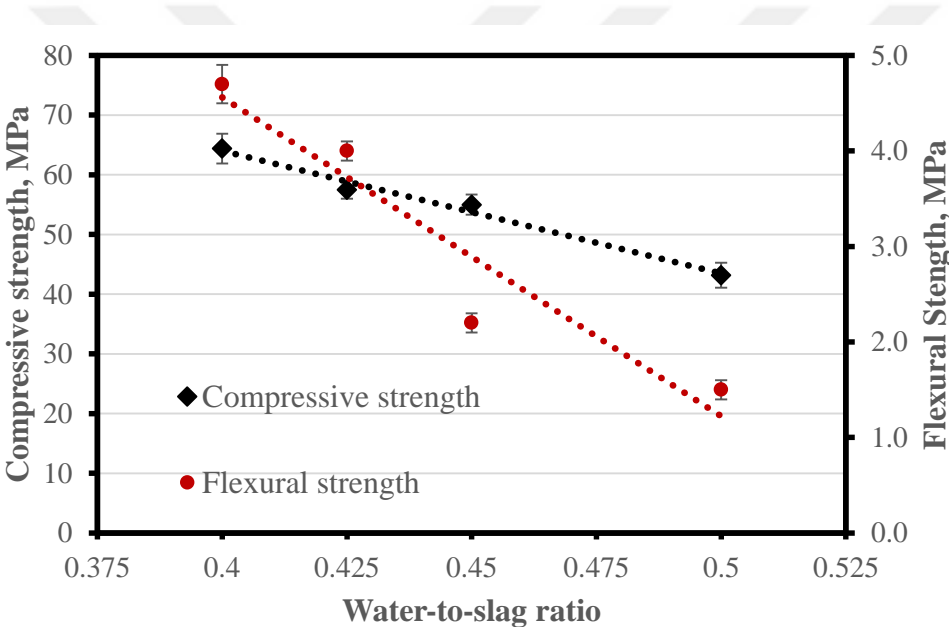


Figure 4.16 Effect of W/S ratio on the 28-day compressive and flexural strengths of sealed-cured non-aerated pastes.

An inverse linear relationship can be observed between compressive or flexural strength and W/S. As expected, the compressive and flexural strengths of samples decreased with increasing W/S, but the decrease of the latter is more dramatic. For instance, the compressive and flexural strengths of the paste with W/S=0.40 are about 50 % and 213 % higher than these of pastes with 0.50, respectively. One

explanation is that flexural strength is more sensitive to porosity and cracks in the AAS than compressive strength paste due to the increased water content. Flexural-to-compressive strength ratio of samples varied approximately between 0.03 and 0.07, decreasing with an increase in water content. Figure 4.17 shows the effect of hydrogen peroxide on the 28-day compressive strength of sealed-cured aerated pastes with different W/S.

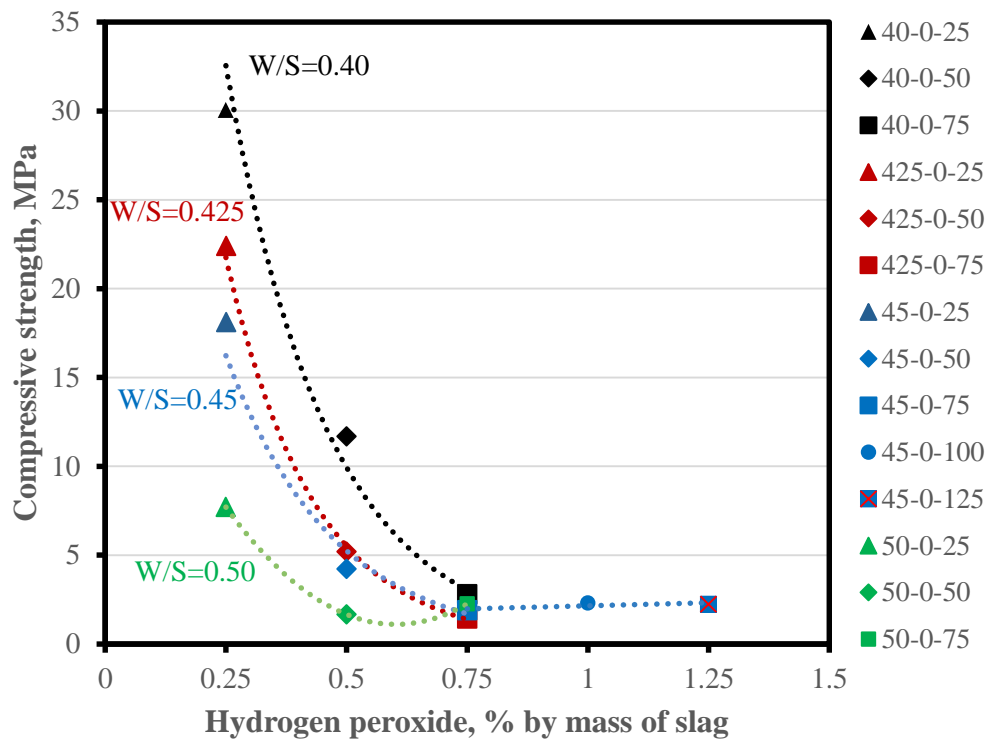


Figure 4.17 Effect of hydrogen peroxide on the 28-day compressive strength of sealed-cured aerated samples with different W/S.

Increasing hydrogen peroxide content and/or water content in the mixtures reduces the compressive strength of samples over the hydrogen peroxide range of 0.25 % to 0.75 %, this can be related to the decrease in apparent density and increase in amount and/or size of pores of the samples. 45-0-100 and 45-0-125 have slightly higher strength than 45-0-75, and 50-0-75 has higher strength than 50-0-50, despite increasing hydrogen peroxide content. The result of this behavior is not clear, but

the difference is quite small and could be judged to be within experimental uncertainty. However, changes in pore size and distribution might have also slightly increased the strength. Several researchers have reported an increase in strength with narrower pore distribution and fine pore structure (Nambiar and Ramamurthy, 2007). Figure 4.18 shows the variations of 28-day compressive strengths of sealed-cured prism samples with apparent density at different W/S and hydrogen peroxide contents.

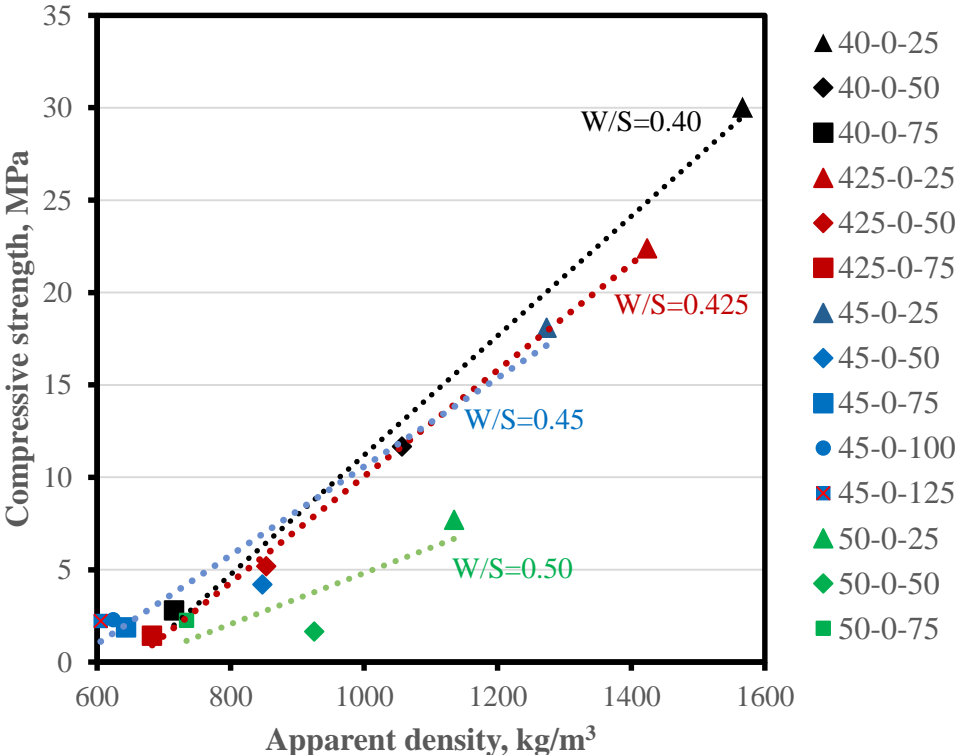


Figure 4.18 Variation of 28-day compressive strengths of sealed-cured prism samples with apparent density, at different hydrogen peroxide contents and W/S.

It can be seen clearly in Figure 4.18 that the compressive strength of aerated samples depends strongly on apparent density. There is an inverse linear relationship between them for samples with W/S=0.40, 0.425 and 0.45. However, this relation is expected to be exponential over a wider density range. The increase

of W/S to 0.50 changes the relation, the compressive strengths of 50-0-25 and 50-0-50 were found to be considerably lower than samples at the same apparent density range, even though they had narrower pore distribution and fine pore structure. For instance, apparent density of 50-0-25 is higher than 40-0-50, and apparent density of 50-0-50 is higher than 425-0-50 and 45-0-50, but 50-0-25 has quite low compressive strength than 40-0-50, and 50-0-50 has quite low compressive strength than 425-0-50 and 45-0-50. This may be a result of the high water content, since increase of water not only increases the distance between slag particles but also dilutes the alkali solution which hinders the hydration of slag (Altan and Erdoğan, 2012). On the other hand, the effect of water content reduces with decreasing apparent density beyond 800 kg/m^3 , apparent density and compressive strength of 50-0-75 and 40-0-75 are quite close. This could be because of the size and distribution of pores since 50-0-75 have narrower pore distribution and fine structure than 40-0-75. The difference in size and distribution of these samples can be seen in Section 4.8, on pore structure.

Comparing the compressive strengths of aerated samples with autoclaved aerated concrete (AAC); in the current study compressive strengths of aerated pastes varied between 1.4 MPa to 2.8 MPa in the apparent density range of 600 kg/m^3 to 750 kg/m^3 , and Aroni et al. (1996) reported the compressive strength of AAC between 3.0 MPa to 9.5 MPa in the dry density range of 600 kg/m^3 to 750 kg/m^3 . Based on this comparison, it would appear that compressive strengths of AAAS samples are significantly lower than those of ACC in the similar density range. However, these results do not completely restrict the use of aerated alkali-activated slag concrete in applications including precast reinforced cellular concrete floors, roofs, and wall units, since ACI 523 (1996) states a minimum compressive strength of 2.1 MPa for those applications. Figure 4.19 compares compressive strengths of sealed-cured aerated samples in the current study to aerated alkali-activated pastes produced using different types of gas releasing from the existing literature.

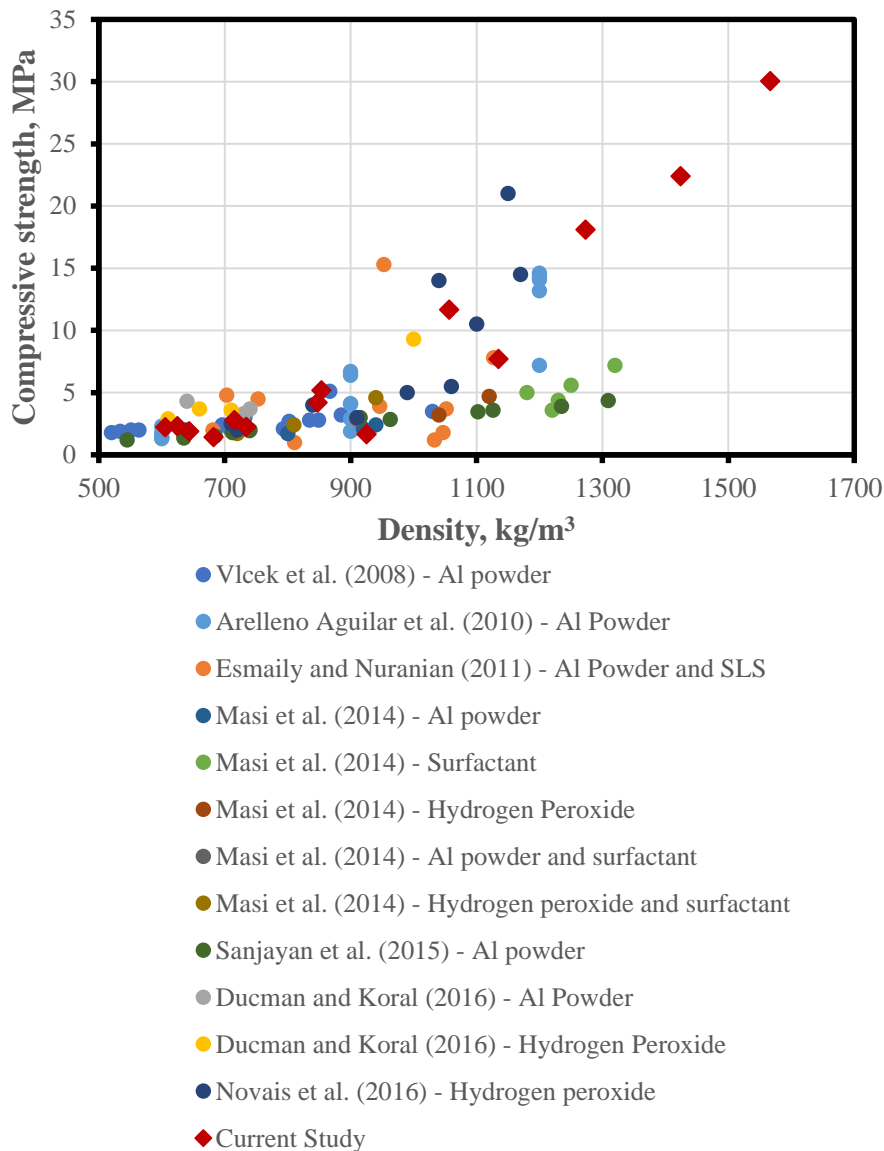


Figure 4.19 Comparison of compressive strengths of aerated pastes in the current study with aerated alkali-activated concretes produced using different types of gas-releasing agents from the existing literature.

From Figure 4.19, it would appear that compressive strength of aerated samples were in an acceptable strength range, comparable with those of aerated alkali-activated pastes in the density range of 600 kg/m³ to 1300 kg/m³.

Figure 4.20 shows the relationships between the 28-day flexural and compressive strengths of sealed-cured aerated pastes with different W/S and hydrogen peroxide contents.

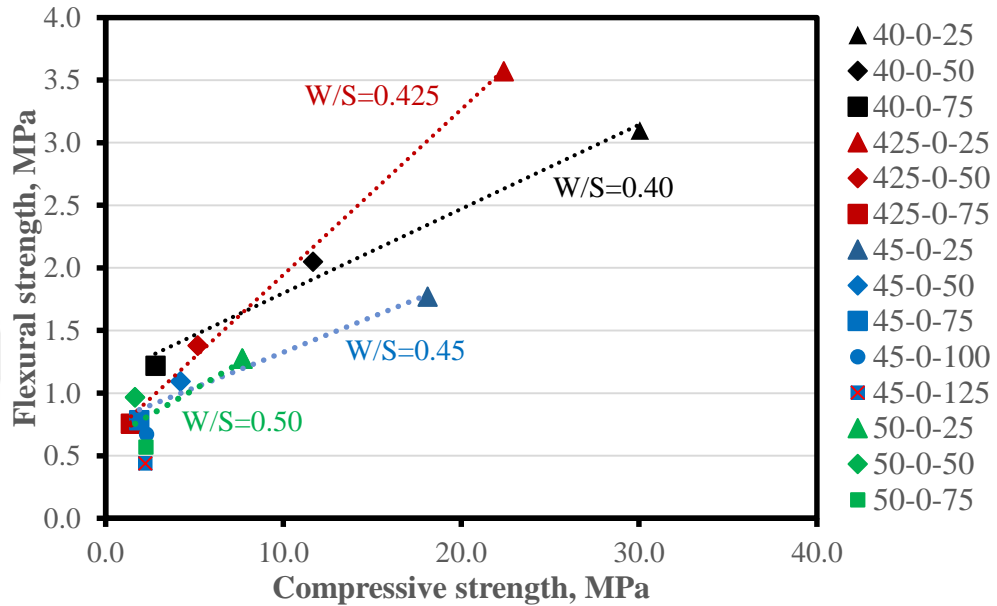


Figure 4.20 Relationships between the 28-day flexural and compressive strengths of sealed-cured aerated pastes with different hydrogen peroxide contents and W/S.

There is a strong relation between compressive and flexural strength. An increase of compressive strength yielded an increase in flexural strength of the aerated pastes, except for 45-0-100 and 45-0-125. Flexural-to-compressive strength ratios of aerated pastes are approximately between 0.10 and 0.58, and increase with decreasing apparent density. In other words, reduction in the flexural strength of aerated samples is quite low compared to the reduction in the compressive strength with increasing air voids. Yang et al. (2000) observed similar behavior for air-entrained concrete, and stated that toughness of concrete increases with the increasing air content. In addition, Hilal et al. (2016) have reported an increase in the relative ductility (Fracture Energy-Strength ratio) with decreasing apparent density. The reason for this is that large pores in paste show resistance to

propagation of cracks during flexural test resulting in an increase in the energy required for fracture (Neville and Brooks, 2010). Apparent density ratio (the ratio of density of aerated sample to density of non-aerated sample at the identical W/S) and compressive strength ratio (the ratio of compressive strength of aerated sample to compressive strength of non-aerated sample at identical W/S) were determined for aerated samples, and their relation is given in Figure 4.21 for pastes with different W/S and hydrogen peroxide contents.

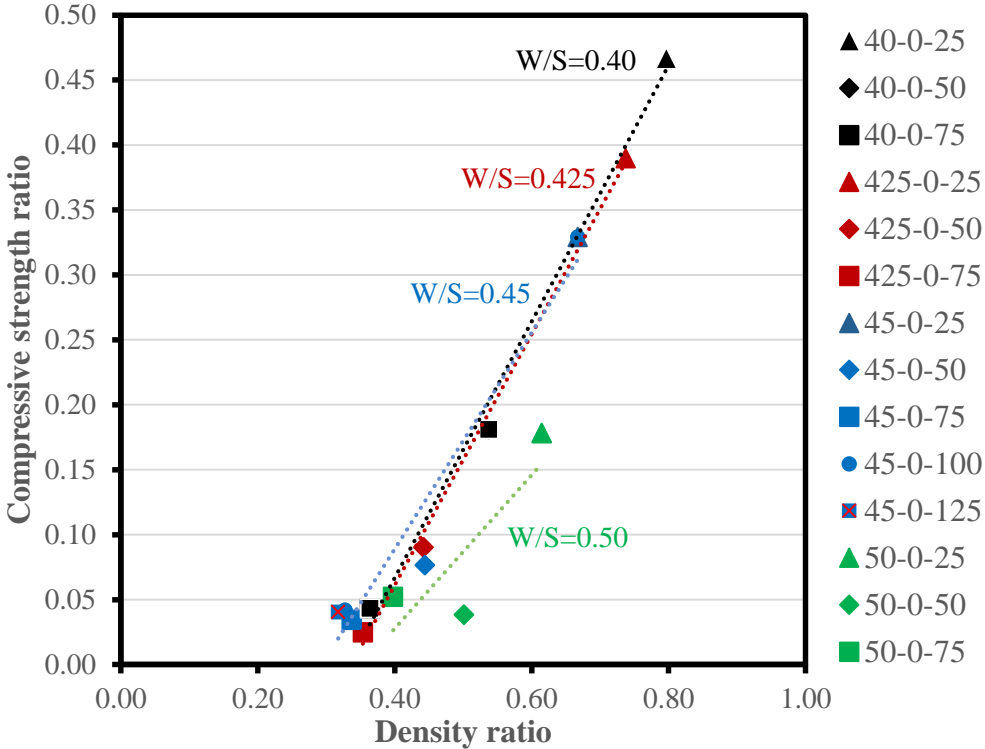


Figure 4.21 Relationships between compressive strength ratio and apparent density ratio of pastes with different W/S and hydrogen peroxide contents.

A strong relation is observed between the two, largely independent of W/S (over the W/S range of 0.40 to 0.45). Increasing W/S of samples to 0.50 yielded high deviations from the general trend. A decrease in apparent density of 20 % and 50 % yields a decrease in compressive strength of about 50 % and 90 % with respect

to compressive strength of the non-aerated samples, respectively. It is well-known that density decreases with increasing porosity resulting in a decrease in strength. In the current study, the relation between macro porosity and strength is investigated. Macro porosity of samples is the fraction of air voids to total volume. Determination of macro porosity is described in Section 3.7, on tests performed. Figure 4.22 shows the relationships between macro porosity and compressive strength of aerated pastes with different W/S and hydrogen peroxide contents.

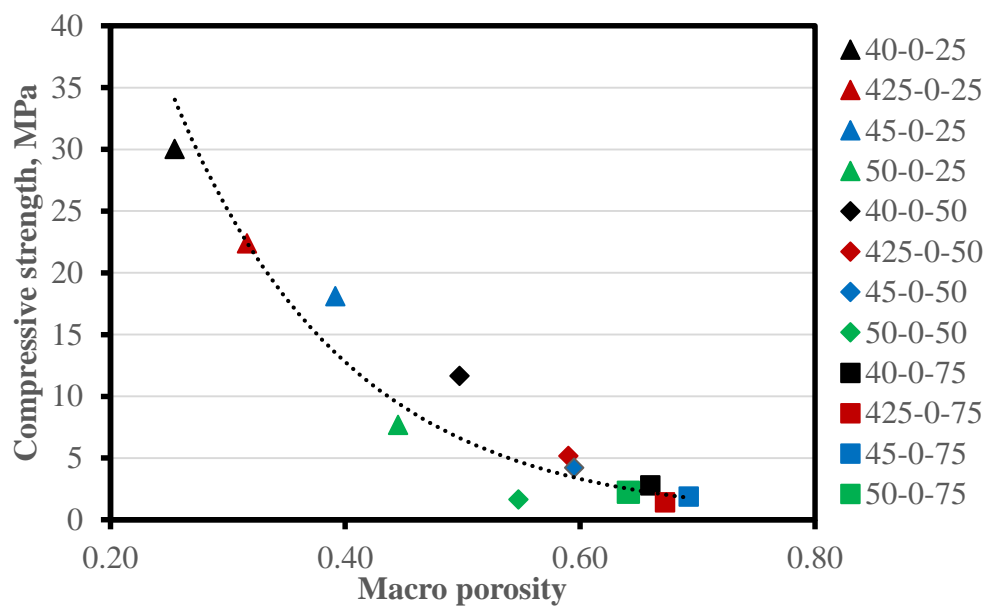


Figure 4.22 Relationship between macro porosities and compressive strengths of aerated pastes with different W/S and hydrogen peroxide contents.

There is an inverse exponential relationship between macro porosity and compressive strength of aerated samples. A similar relation has been reported for numerous materials (Mehta and Monteiro, 2006). The effect of capillary porosity on strength can be deduced from Figure 4.22 comparing the strength of 50-0-25 with 40-0-50, and the strength of 50-0-50 with 425-0-50 and 45-0-50. Even though their macro porosities are lower, the strengths of the former were found to be much less than their counterparts with lower water contents.

4.6.1.2 Strength Development of Sealed-Cured Pastes

The strength development of sealed-cured pastes was investigated on prism samples without any pre-conditioning, after 7, 14, 28 and 91-days of curing in sealed condition at room temperature. As mentioned in Section 3.5, on preparation of test samples, demolding of samples was done 3 days after casting, due to the slow strength gain. Thus, measurement of compressive strength was started at age 7 days for all samples. Tests were performed on samples with W/S=0.45 containing 0 to 1.25 % hydrogen peroxide. Figure 4.23 shows the strength development of sealed-cured pastes with W/S=0.45 and different hydrogen peroxide contents.

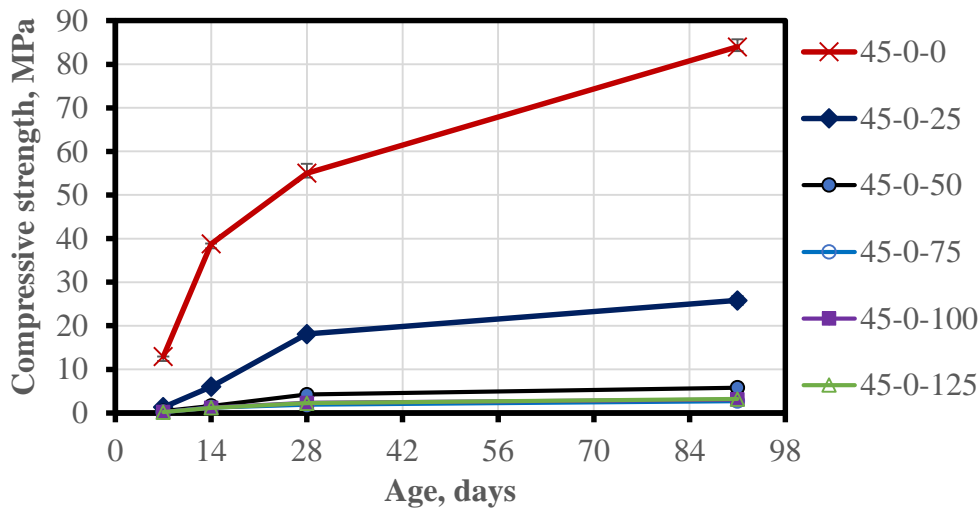


Figure 4.23 Strength development of pastes with W/S=0.45 and different hydrogen peroxide contents.

Increasing hydrogen peroxide content yielded a decrease in the rate of strength development. Non-aerated pastes (45-0-0) gained 24 % of their 28-day compressive strength in the first 7 days, but with the increase of hydrogen peroxide content strength gain at 7 days decreased considerably. The ratio of 7- to 28-day strength was between 7 % to 11 % for aerated pastes, indicating a delay in the strength gain. This could be a result of decreasing pH due to the reaction between NaOH and

hydrogen peroxide (Guo et al., 2013), and the effect of water in capillary pores. Furthermore, rate of strength development slightly decreased beyond 28 days of curing, but an increase in strength was observed for all samples. 91-day strengths of non-aerated pastes and aerated pastes were about 50 % and about 40 % higher than those of their 28-day strengths, respectively.

4.6.1.3 Influence of Ambient Curing

The flexural and compressive strength of pastes produced were determined on prism samples after 28-days of curing at ambient temperature of 21 ± 2 °C and relative humidity of 40 ± 5 %. The apparent densities of samples were measured once after demolding and again after curing. Figure 4.24 shows the compressive strength of these pastes with different W/S and hydrogen peroxide contents.

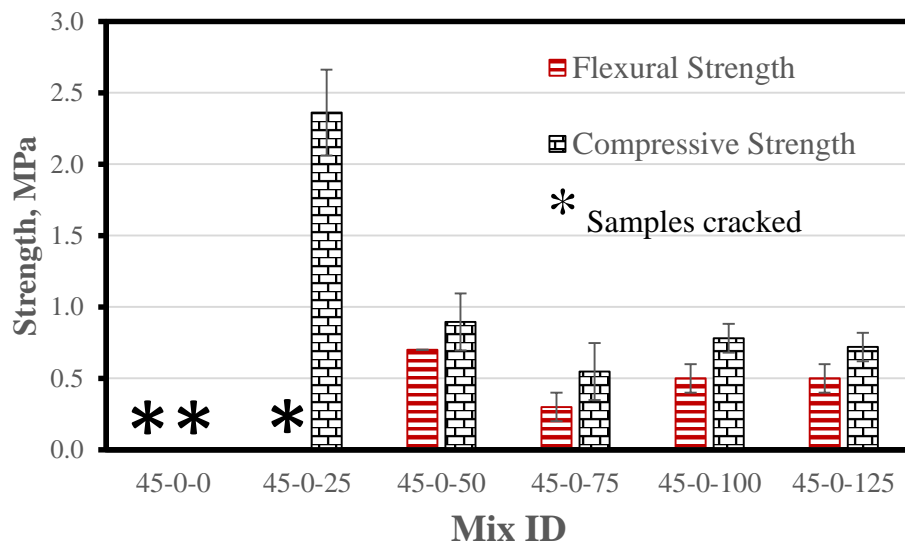


Figure 4.24 Compressive strength of ambient-cured pastes with W/S=0.45 and different hydrogen peroxide contents.

After 28 days of curing at ambient temperature, all non-aerated samples were cracked, and compressive strength tests could not be performed. This is most probably due to the drying shrinkage of samples. Samples had lost approximately

25 % of their initial masses during curing, due to the evaporation of water. Bakharev et al. (1999a) reported visible shrinkage cracks for sodium silicate-activated pastes. The decreasing trend of compressive strength with increasing hydrogen peroxide may be considered similar to that in sealed-cured samples, however compressive strengths of all samples were much lower than those of sealed-cured samples at identical hydrogen peroxide contents. For example, compressive strengths of 45-0-25 and 45-0-50 were found to be approximately 18 % and 21 % of their sealed-cured counterparts, respectively. It is obvious that ambient curing has a negative effect on strength gain. In addition to cracking, this could be a result of high leaching of alkali solution at early ages, which might have decreased the pH, hindering hydration, and strength gain of alkali-activated slag. The white deposit on the surfaces of non-aerated samples was taken, dried at 40 °C, and characterized using X-ray diffraction. Figure 4.25 shows the X-ray diffractogram of the leachate on samples. Sodium carbonate and silicon oxide were found in the samples, dictating leaching of alkali solution and formation of efflorescence.

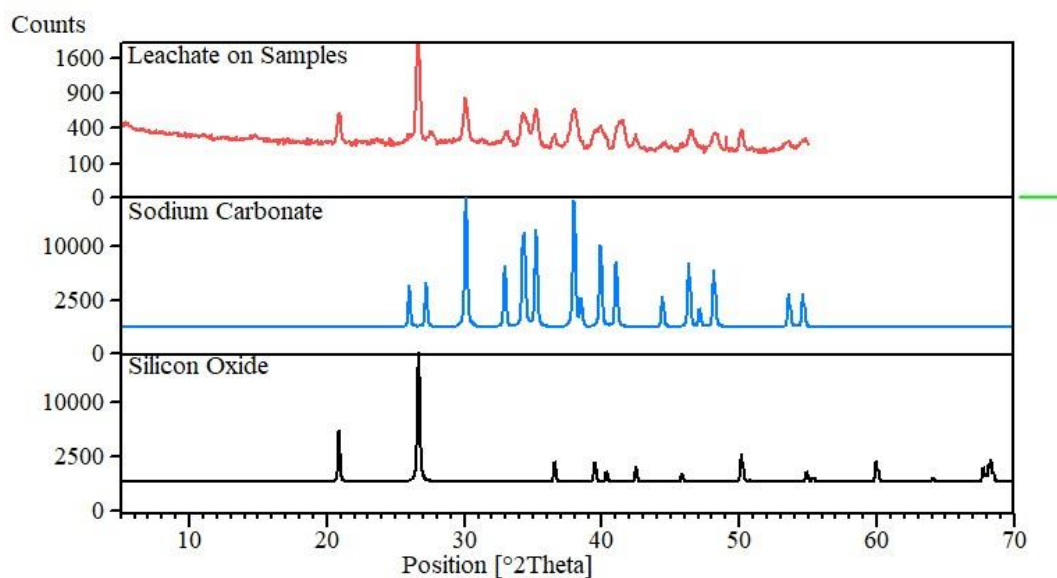


Figure 4.25 X-ray diffractogram of the leachate on samples.

During curing, images of the samples were taken regularly. Figure 4.26 shows the visual changes in the paste samples during curing.

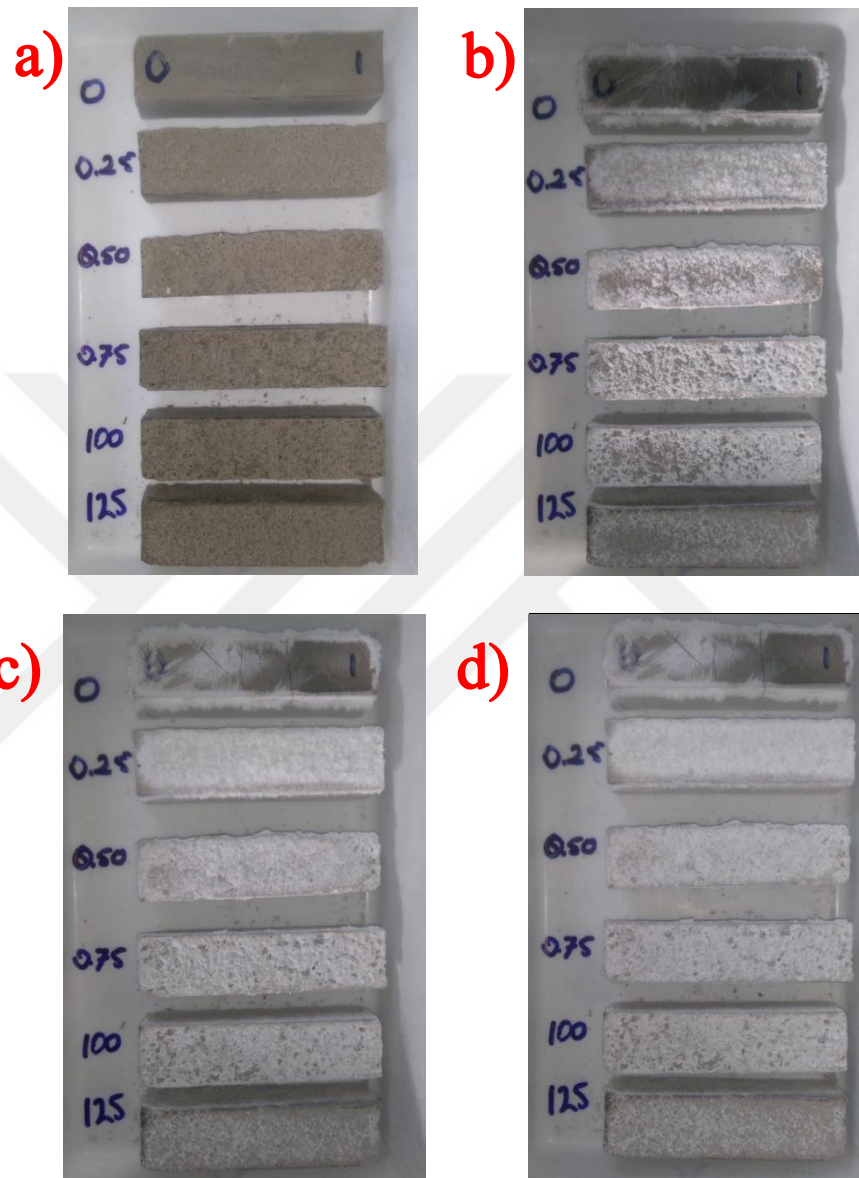


Figure 4.26 Visible changes during ambient curing for pastes with $W/S=0.45$ and different hydrogen peroxide contents: a) After demolding, b) After 2 days of curing, c) After 9 days of curing, and d) After 25 days of curing.

Efflorescence of samples occurred around the top surfaces of the samples, but there was no sodium carbonate deposit on the bottom sides. After one day of curing, formation of efflorescence was visible on all samples except 45-0-125. The severity of efflorescence of samples not only increases with increasing duration of curing time but also decreases with increasing hydrogen peroxide. Taking into account increasing hydrogen peroxide leads to a decrease in apparent density and an increase in pore size. The reduction in the efflorescence can be attributed to: i) decreasing solid content in the samples resulting in a decrease in the amount of leachable alkali solution, and ii) increasing size and amount of pores hinders leaching of alkali solution. Zhang et al. (2014) reported that higher porosity prevents rapid visible efflorescence of fly ash-based geopolymers a result of decreasing capillary transport of water, but it was found using optical microscopy that efflorescence occurred inside macropores.

4.6.1.4 Influence of Oven Curing

Compressive strength tests were performed on samples with $W/S=0.45$ in the hydrogen peroxide range of 0 to 1.25 %. Samples were cured in a humid oven for 12, 24, and 48 hours, then kept at ambient temperature for 3 days prior to testing. Apparent densities of samples were measured once after demolding and again prior to performing strength tests, however they were quite close. These results are given in Table A.12 in Appendix A. The apparent densities given are those measured prior to the performing the strength tests. Figure 4.27 shows the effect of oven curing and duration on compressive strengths of pastes with $W/S=0.45$ and different hydrogen peroxide contents.

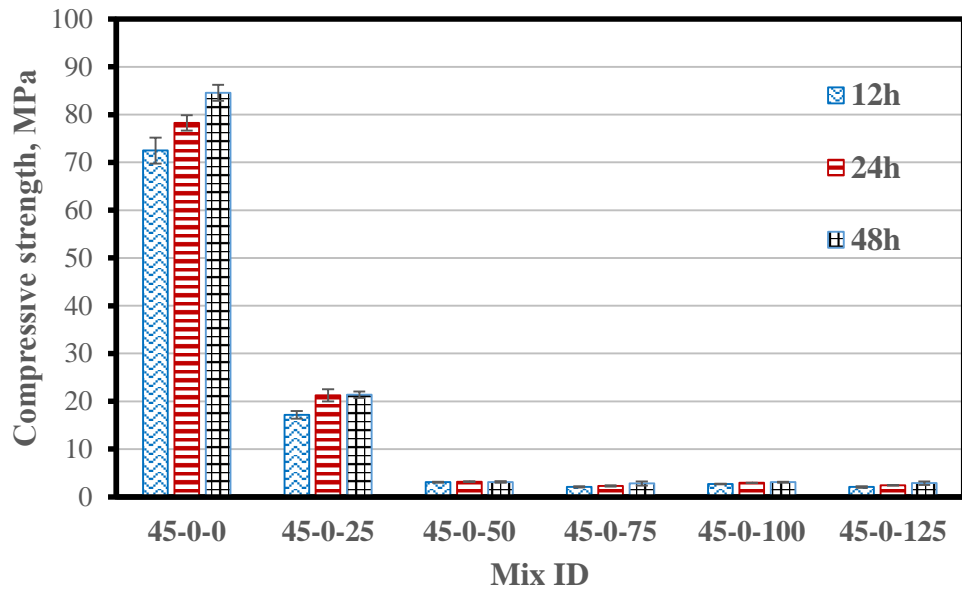


Figure 4.27 Effect of oven curing and duration on the compressive strengths of pastes with W/S=0.45 and different hydrogen peroxide contents.

Compressive strengths of oven-cured aerated pastes reached those of 28-day sealed-cured pastes after only 12 h. Besides, compressive strength of 12 h oven-cured non-aerated pastes were found to be 30 % higher than those of 28-day sealed cured pastes. It is obvious that oven curing is beneficial to the produced samples. Several researchers have reported a similar beneficial effect of high temperature curing for alkali-activated slag composites (Altan and Erdoğan, 2012; Bakharev et al., 1999b; Jimenez et al., 1999; Wang et al., 1994). On the other hand, extension of the oven curing duration slightly increased the compressive strength of samples. The compressive strengths of 45-0-0, 45-0-25, 45-0-75, 45-0-100 and 45-0-125 increased about 16 %, 24 %, 33 %, 15 % and 38 % with the increase of curing duration from 12 h to 48 h, respectively. There is no change observed for 45-0-50 with the increase of curing duration from 12 h to 48 h. In the apparent density range of 560 kg/m^3 to 700 kg/m^3 , the compressive strengths of 12 h oven-cured aerated pastes varied between 2.1 MPa to 3.1 MPa. For comparison Esmaily and Nuranian (2012) reported compressive strengths of oven-cured ($87 \text{ }^\circ\text{C}$) aerated alkali-

activated slag pastes between 2.0 MPa to 4.8 MPa in the apparent density range of 680 kg/m³ to 750 kg/m³.

4.6.2 Strength Development of Mortar Samples

4.6.2.1 Influence of Sealed Curing

The flexural and compressive strengths of mortars with a Sa/S=1 produced were determined on prism samples without pre-conditioning after 28 days of curing in sealed condition at room temperature. Figure 4.28 shows the relationship between apparent densities of aerated mortars produced using prism molds and cylindrical molds, at identical W/S and hydrogen peroxide contents.

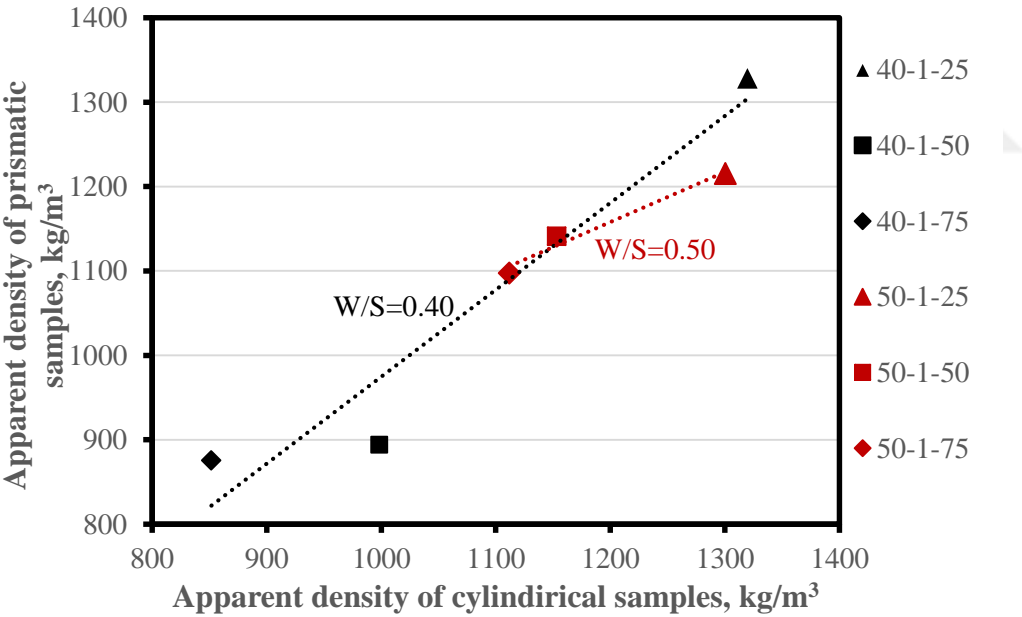


Figure 4.28 Relationship between apparent density of prism samples and cylindrical samples.

Apparent densities of prism samples were quite close to those of cylindrical samples, except 40-0-50 and 50-0-25 for which the prism sample apparent densities

were about 10 % higher than those of cylindrical samples. It can be deduced that a more uniform distribution of air bubbles is obtained with the addition of sand, similar to findings of Nambiar and Ramamurthy (2006) for aerated concrete. Figure 4.29 shows the variation of 28-day compressive strengths with apparent densities for sealed-cured mortars containing different hydrogen peroxide contents with W/S=0.40 and 0.50.

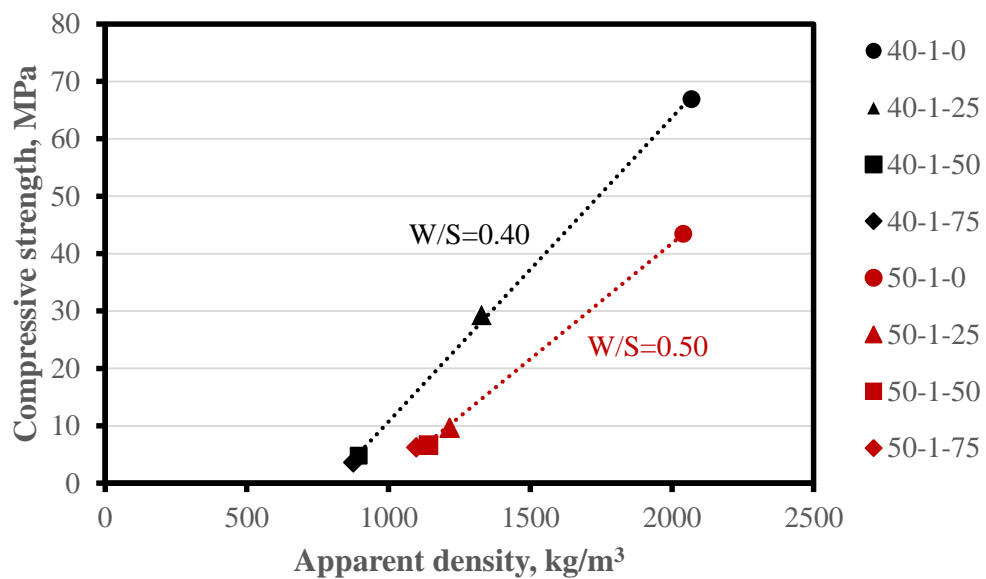


Figure 4.29 Variation of 28-day compressive strengths with apparent densities for sealed-cured mortars containing different hydrogen peroxide contents with W/S=0.40 and 0.50.

There exists a strong relation between apparent density and compressive strength of samples for each W/S, similar to the results obtained on pastes. As expected, increasing water content in mixtures yields a decrease in compressive strength. Strengths of non-aerated samples with W/S=0.40 are about 50 % higher than samples with W/S=0.50. Also, the apparent densities of 40-1-50 and 40-1-75 are quite close, but the compressive strength of the latter is 25 % lower. This could be due the increase in the pore size of the samples due to the increased hydrogen

peroxide content. For comparison, the compressive strengths of mortars and pastes with W/S=0.40 were quite close at 0.25 % hydrogen peroxide. However, the apparent densities of these samples (40-0-25 and 40-1-25) were measured as 1566 kg/m³ and 1329 kg/m³, respectively. At first glance, a sample with higher density and no sand may be expected to give higher strength, however this difference may be a result of the differences in mix preparation, and pore size and distribution. While preparing the mortars, the alkali solution and slag were mixed for one minute at the beginning, whereas for the pastes the alkali solution, water and slag were mixed almost at time same time, as a result the concentration of alkali solution decreased. Therefore, the dissolution of slag could have been less in the latter case which leads to lower strength gain. Figure 4.30 shows the relationships between 28-day flexural and compressive strengths of sealed-cured mortars with W/S=0.40 and 0.50 and different hydrogen peroxide contents.

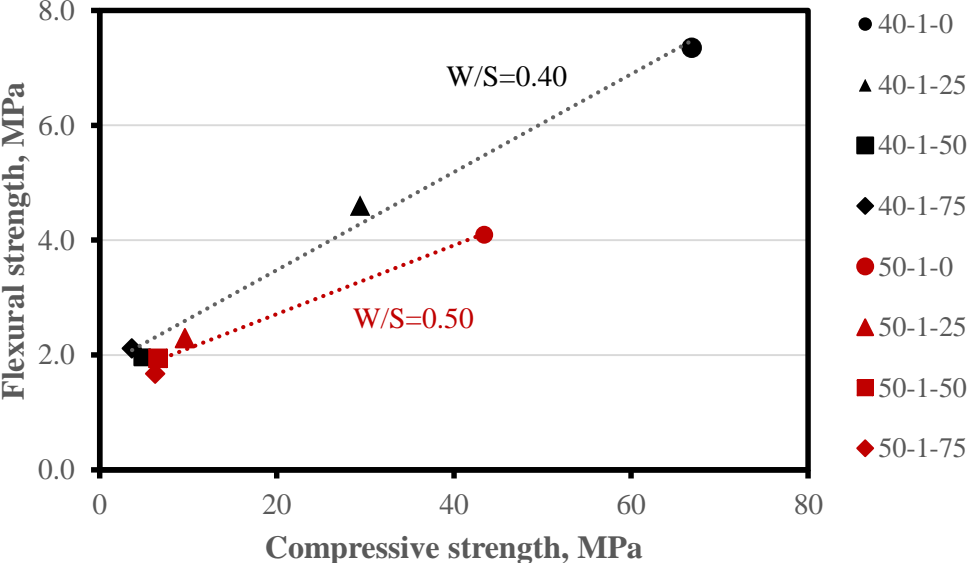


Figure 4.30 Relationship between 28-day flexural strengths and compressive strengths of sealed-cured mortars with W/S=0.40 and 0.50 and different hydrogen peroxide contents.

As expected, an increase of compressive strength leads to an increase in the flexural strength of the samples. Flexural-to-compressive strength ratios of non-aerated mortars with $W/S=0.40$ and 0.50 (40-1-0 and 50-1-0) are 0.11 and 0.09, respectively. On the other hand, flexural-to-compressive strength ratios are about 0.16 to 0.41 for aerated mortars, and increase with decreasing apparent density. As previously mentioned in Section 4.6.1, on strength development of paste samples, the reason for this could be the resistance of air pores to load during flexural strength tests. Taking the non-aerated samples as a reference for a given W/S , apparent density ratio and compressive strength ratio were determined for aerated samples and their relation is given in Figure 4.31 for aerated mortars containing different hydrogen peroxide contents with $W/S=0.40$ and 0.50 .

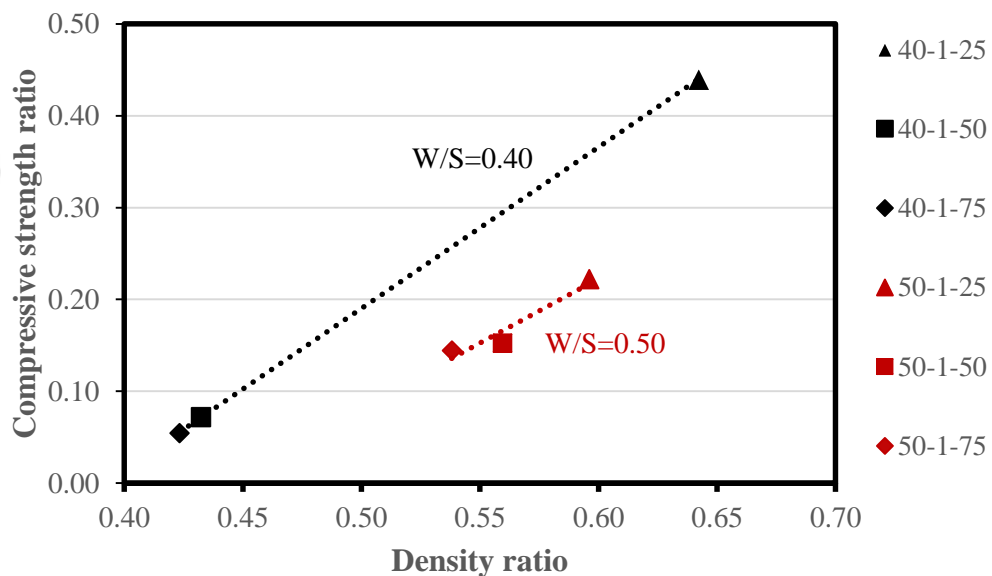


Figure 4.31 Relationship between compressive strength ratios and density ratios for aerated mortars containing different hydrogen peroxide contents with $W/S=0.40$ and 0.50 .

As expected, an increase in density ratio yielded an increase in compressive strength ratio. The range of density ratio for $W/S=0.50$ is quite narrow compared to that for

W/S=0.40. Therefore, it can be deduced that altering the hydrogen peroxide content is more effective for W/S=0.40. Furthermore, there is a large difference in compressive strength ratios of samples with W/S=0.40 and 0.50 for a given apparent density due to the large difference in water contents. It could be deduced that it is easier to achieve lower densities and high strengths using lower W/S.

4.6.2.2 Influence of Oven Curing

Compressive strength tests were performed on mortars ($S_a/S=1$) with W/S=0.40 and 0.50, and 0 to 0.75 % hydrogen peroxide. Samples were cured in a humid oven for 12, 24 and 48 hours, then kept at ambient temperature for 3 days prior to compressive strength tests. Apparent densities of samples were measured once after demolding and again prior to performing strength tests, however they were quite close. The compressive strengths and apparent densities of oven-cured mortars with W/S=0.40 and 0.50 and different hydrogen peroxide contents are given in Table A.14 in Appendix A. The indicated apparent densities listed are those measured prior to the performing strength tests. Figure 4.32 shows the effect of humid-oven curing at 80 °C and duration on compressive strengths of mortars with W/S=0.40 and different hydrogen peroxide contents.

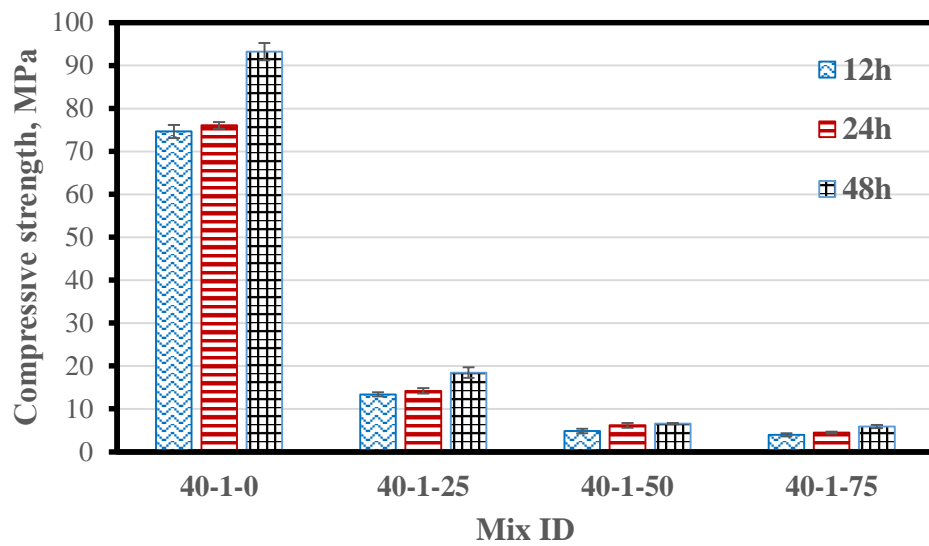


Figure 4.32 Effect of humid-oven curing at 80 °C and duration on the compressive strength of mortars (Sa/S=1) with W/S=0.40 and different hydrogen peroxide contents.

The compressive strengths of samples increase with extended curing duration from 12 h to 48 h. The compressive strengths of 40-1-0, 40-1-25, 40-1-50, and 40-1-75 increased about 25%, 37 %, 35 %, and 49 %, respectively. Compressive strength of 40-1-0 humid-oven cured for 12 h is 11 % higher than that sealed-cured for 28 days. However, compressive strength of oven-cured 40-1-25 is 54 % lower than its 28-day sealed-cured strength for 28 days. This result may be considered an experimental error since there was no such a high reduction in compressive strength of oven-cured samples compared to their sealed-cured counterparts. Compressive strengths of oven-cured 40-1-50 and 40-1-75 are slightly higher than their sealed-cured counterparts at 28 days.

Figure 4.33 shows the effect of humid-oven curing at 80 °C and duration on compressive strengths of mortars with W/S=0.50 and different hydrogen peroxide contents.

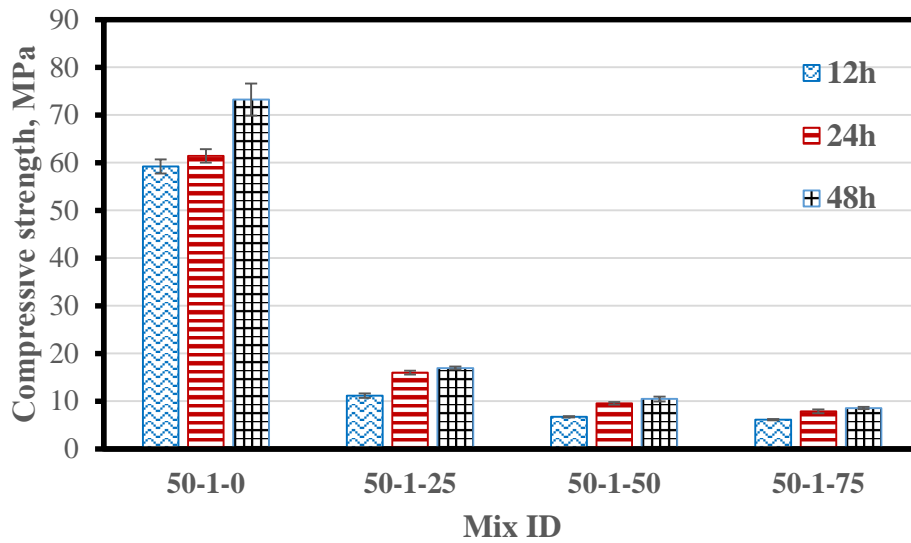


Figure 4.33 Effect of humid-oven curing at 80 °C and duration on the compressive strength of mortars (Sa/S=1) with W/S=0.50 and different hydrogen peroxide contents.

Increasing curing duration from 12 h to 48 h, the compressive strengths of 50-1-0, 50-1-25, 50-1-50 and 50-1-75 increased about 24%, 52 %, 56 % and 39 %, respectively. Compressive strengths of 50-1-0 and 50-1-25 cured for 12 h are 36 % and 16 % higher than their sealed-cured counterparts at 28 days. However, compressive strengths of oven-cured 50-1-50 and 50-1-75 are very close to their sealed-cured counterparts at 28 days. It could be concluded that humid-oven curing is more effective for samples with high water content and high apparent densities, and its effect is notable at early ages. In other words, the detrimental effect of increasing water content on compressive decreases under humid-oven curing. Therefore, highly-workable mixtures can be used to achieve higher strength using humid-oven curing at a temperature of 80 °C.

4.7 Water Absorption

4.7.1 Water Absorption of Pastes

The apparent densities, oven-dry densities and water absorption of pastes were determined on prism samples after 28 days of curing in sealed condition at room temperature. Water absorption of pastes were measured in two different ways (by volume and by weight, detailed in Section 3.7.6). These results are presented in Table A.15 in Appendix A. Increases in the W/S of non-aerated pastes did not affect the water absorption (by volume or by weight) of non-aerated samples. Since water absorption would be expected to increase with increasing water content as a result of increasing capillary porosity, this result is an indication of leaching of alkali solution from alkali-activated samples during the absorption test. For a given W/S increasing hydrogen peroxide content increases water absorption. This is expected since hydrogen peroxide content directly influences size and amount of permeable pores. Nambiar and Ramamurthy (2006) suggested expressing water absorption as a function of total volume instead of total mass to avoid misleading results. In the current study, water absorption measured by weight is slightly lower than that measured by volume for aerated pastes with apparent densities higher than 1150 kg/m³, but the difference increases with the decrease of apparent density beyond 1150 kg/m³. Figure 4.34 shows the effect of apparent density on water absorption (by volume) with different W/S and hydrogen peroxide contents.

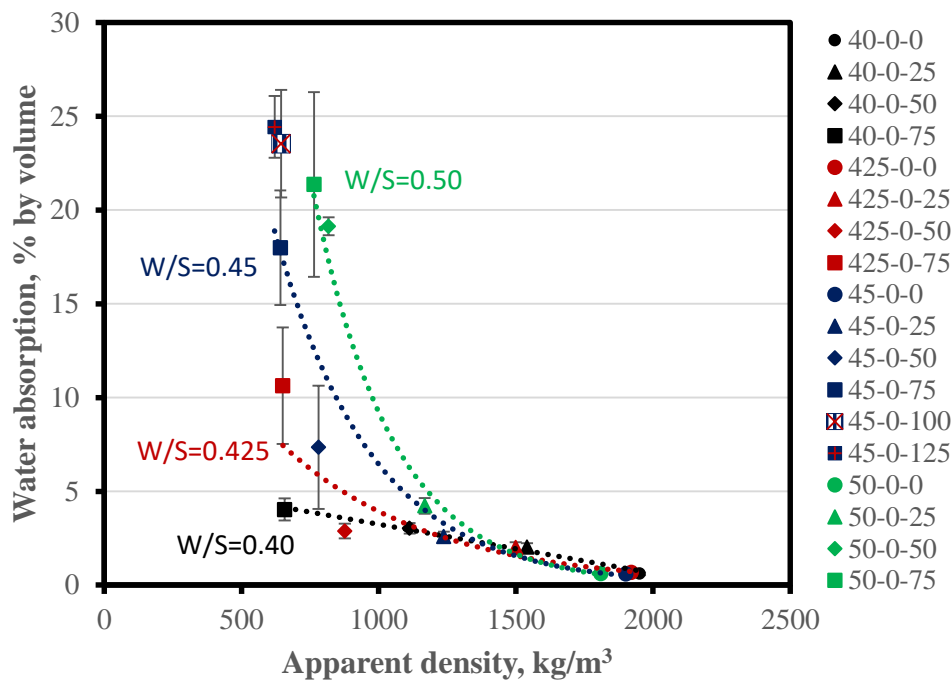


Figure 4.34 Effect of apparent density on water absorption (by volume) of pastes with different W/S and hydrogen peroxide contents.

The water absorption of aerated pastes increased dramatically with decreasing apparent density, an expected result as apparent density is a function of porosity. Similar findings were reported in the literature (Kearsley and Wainright, 2001; Novais et al., 2016). On the other hand, results conflict with the findings of Nambiar and Ramamurthy (2007), who observed a decrease in the water absorption with increasing density for aerated concrete. This is explained by the reduction in capillary pores as a result of decrease in paste content via inclusion of entrained air. Therefore, it can be concluded that increasing hydrogen peroxide content increases the capillary and permeable pores because of the reaction between NaOH and hydrogen peroxide at early ages. Furthermore, water absorption of lower apparent density samples increased considerably with increasing water content. For instance, apparent densities of 40-0-75, 425-0-75 and 45-0-75 were similar, their water absorptions (by volume) were measured as 4.0 %, and 10.6 % and 18.0 %,

respectively. This can be explained by an increase in capillary porosity due to the excess water content which not only increases the initial porosity also decreases the activating effect of the alkali solution (Shi et al., 2006), and differences in size and amount of permeable pores. By conducting water absorption test, the volume of water permeable pores was measured. However, macro porosity (the amount of air voids) of pastes are quite higher than the amount permeable pores, indicating entrained pores in the pastes are closed pores and water impermeable. Figures 4.35 and 4.36 show the effect of apparent density on water absorption (by volume and by weight) of pastes with W/S=0.45, respectively.

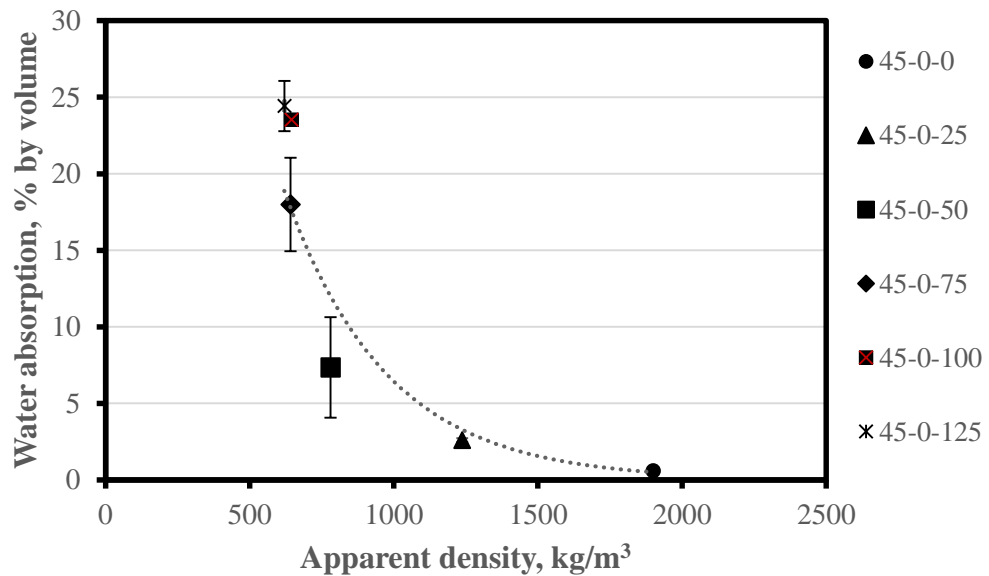


Figure 4.35 Effect of apparent density on water absorption (by volume) of pastes with W/S=0.45.

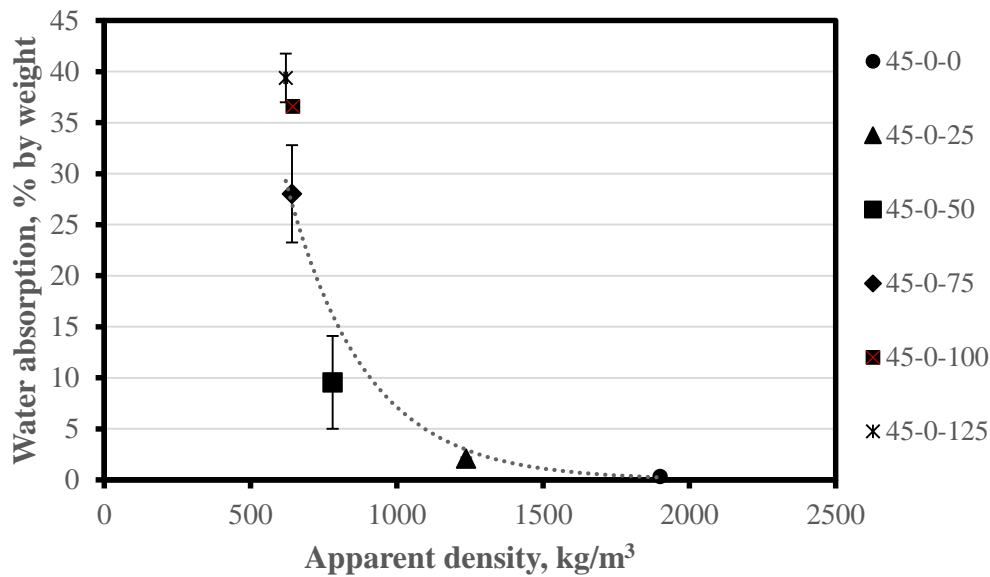


Figure 4.36 Effect of apparent density on water absorption (by weight) of pastes with W/S=0.45.

There are differences in water absorption measured by volume and by weight at identical hydrogen peroxide contents. The former results are slightly higher for 40-0-0 and 40-0-25. This is a result of higher weight per unit volume of samples. For the remaining samples weight per unit volume decreased, and consequently water absorption measured by weight yielded higher values than those measured by volume. Increasing hydrogen peroxide content beyond 0.75 % had a negligible effect on apparent densities, however water absorption increased remarkably, also suggesting an increase of capillary porosity and permeable pores due to the increase of hydrogen peroxide content. In addition, the variation in measured water absorption increased with the increase of hydrogen peroxide beyond 0.50 %. One of the reasons for this behavior is that with the increase of hydrogen peroxide content, open pores increase on the surfaces leading to variations in measurements.

4.7.2 Water Absorption of Mortars

The apparent densities, oven-dry densities and water absorption of mortars ($S_a/S=1$) with $W/S=0.40$ in the hydrogen peroxide range of 0 to 0.75 % were determined on sealed-cured prism samples at 28 days. Water absorption of pastes were measured in two different ways (by volume and by weight). These results are presented in Table A.16 in Appendix A. Incorporation of sand into the pastes increased the weight of samples per unit volume resulting in lower water absorption (by weight) for 40-0-0 and 40-1-25. The water absorption values measured by volume and by weight were quite close for 40-1-50. In addition, water absorption measured by volume for 40-1-75 was higher than that measured by weight as a result of the decrease of weight of samples per unit volume. Figures 4.37 and 4.38 show the effect of apparent density on water absorption, measured by volume and weight, for mortars with a $S_a/S=1$, respectively.

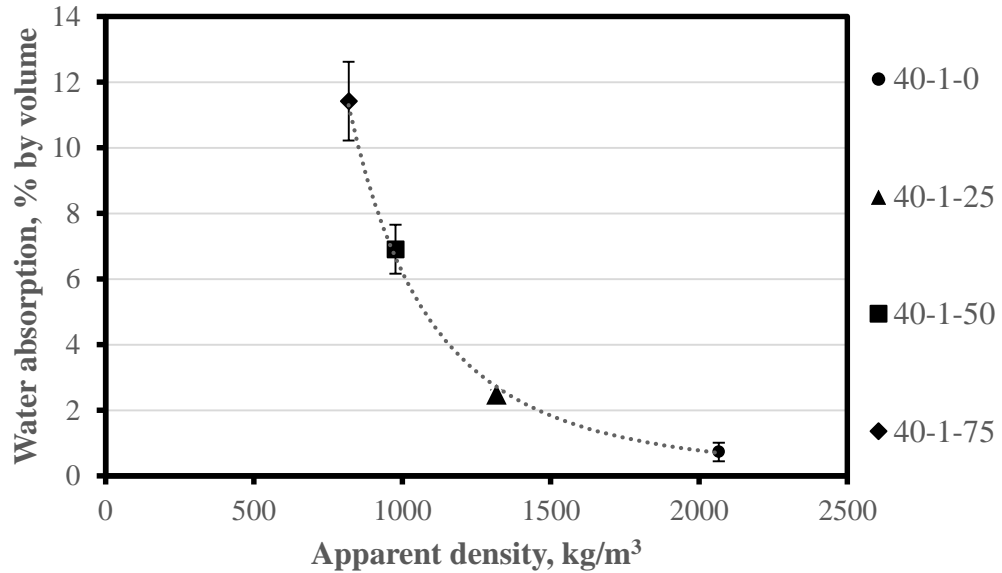


Figure 4.37 Effect of apparent density on water absorption (by volume) of mortars with $W/S=0.45$ and $S_a/S=1$.

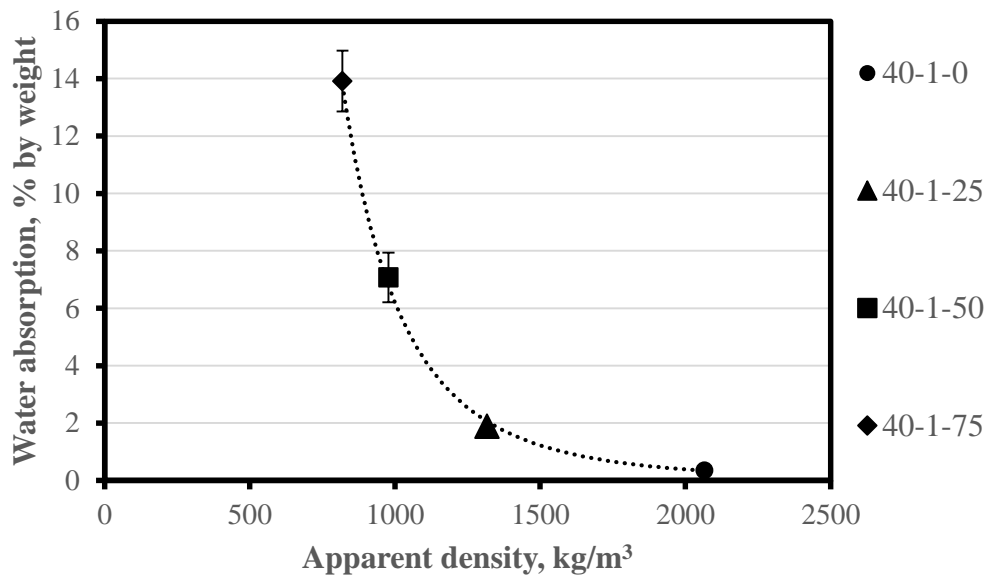


Figure 4.38 Effect of apparent density on water absorption (by weight) of mortars with W/S=0.45 and Sa/S=1.

Similar to results obtained on pastes, water absorption of mortars increased dramatically with the decrease in apparent density and increase in hydrogen peroxide content. In addition, water absorption of aerated mortars are higher than those of aerated pastes at identical W/S and hydrogen peroxide content. The main reason for this is the differences in size and amount of pores resulting differences in apparent density. Furthermore, the presence of micro cracks in the interfacial transition zone have an effect on the increase of water absorption (Mehta and Monteiro, 2006).

4.8 Pore Structure of Samples

The effects of hydrogen peroxide content and W/S of mixtures on the size and amount of pores were visually assessed using smoothed cross sections of aerated pastes, and mortars with Sa/S=1. Cylindrical samples with a diameter of 10 cm were cured for at least 14 days in sealed condition, cut in the middle with a diamond saw,

then ground with sand paper to obtain a smooth surface. Images of smoothed cross sections were captured using a flatbed scanner with an optical resolution of 2400 dpi. A distinct difference in the size, amount and distribution of pores were observed with changing W/S, Sa/S, and hydrogen peroxide content of mixtures. This difference can be seen in Figure 4.39.



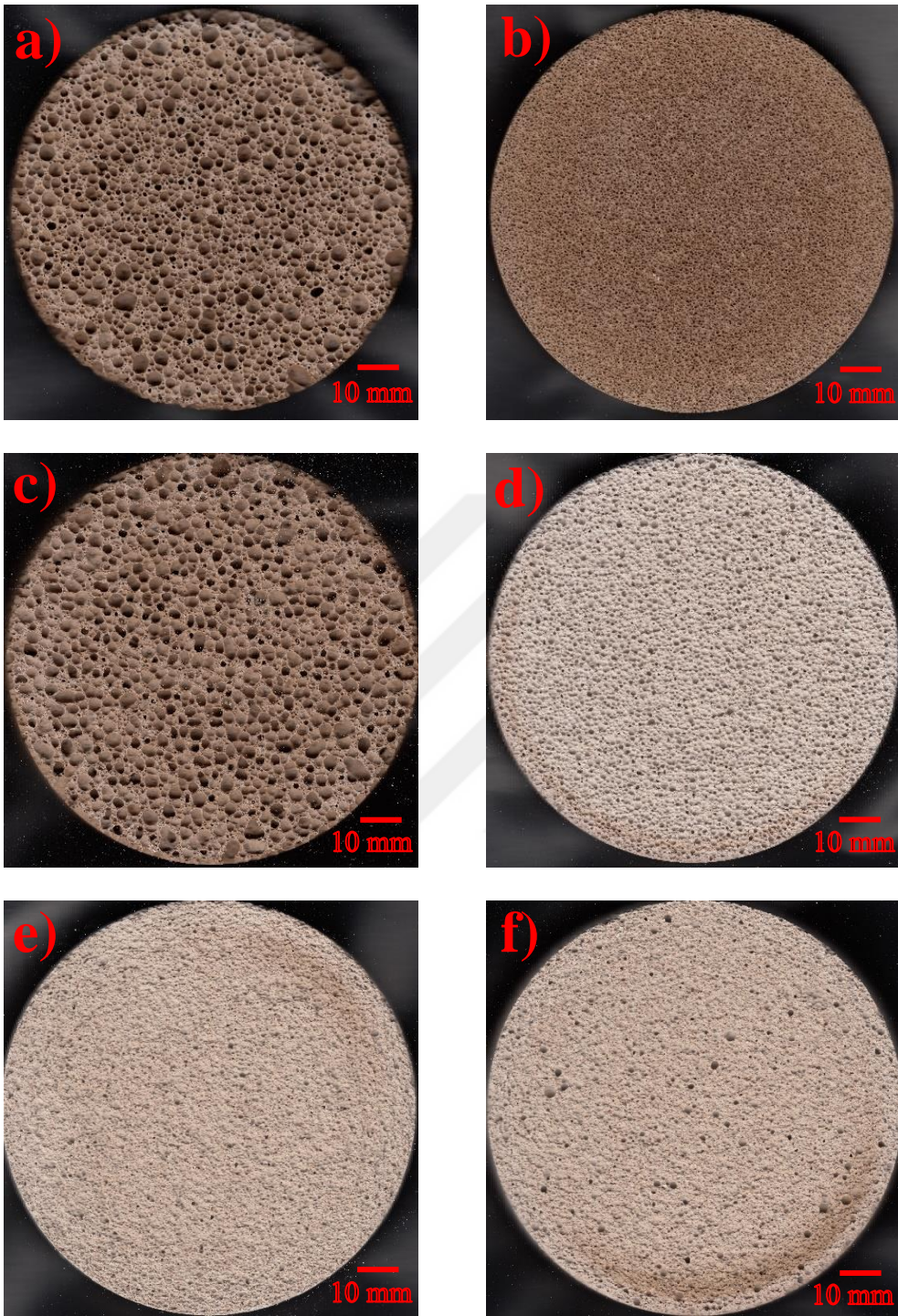


Figure 4.39 Cross sections of cylindrical samples: a) 40-0-50, b) 50-0-25, c) 375-1-50, d) 45-1-25, e) 60-2-50, and f) 50-2-25.

A square frame with a 30-mm side length was cropped from each image for clarity. The sizes of pores were measured using Image J software (Rasband, 1996) on these images. The smallest and largest observable pores in each section were determined, and were used as the boundaries of the pore size range. Tables 4.1 and 4.2 show the pore size range of aerated pastes and mortars with a W/S=0.40 and 0.50 containing hydrogen peroxide in the range of 0.25 to 0.75, respectively.

Table 4.1 Pore size range of aerated pastes.

ID	Pore Size Range (μm)
40-0-25	70 - 3000
40-0-50	95 - 4500
40-0-75	50 - 5000
50-0-25	80 - 1400
50-0-50	40 - 2100
50-0-75	75 - 2600

Table 4.2 Pore size range of aerated mortars.

ID	Pore Size Range (μm)
40-1-25	100 - 2200
40-1-50	100 - 4000
40-1-75	120 - 5000
50-1-25	100 - 1800
50-1-50	100 - 2300
50-1-75	100 - 3300

The resolution of the images obtained using the scanner did not allow the observation of features smaller than about 40 μm . The maximum size of pores in the samples increased with increasing hydrogen peroxide content for a given W/S, and decreased with increasing water content for a given hydrogen peroxide content. It is likely that there exist pores with size smaller than the ranges given in Tables 4.1 and 4.2. Figure 4.40 shows close-ups of cross sections of aerated pastes with W/S=0.40 and 0.50 containing hydrogen peroxide in the range of 0.25 % to 0.75 %.

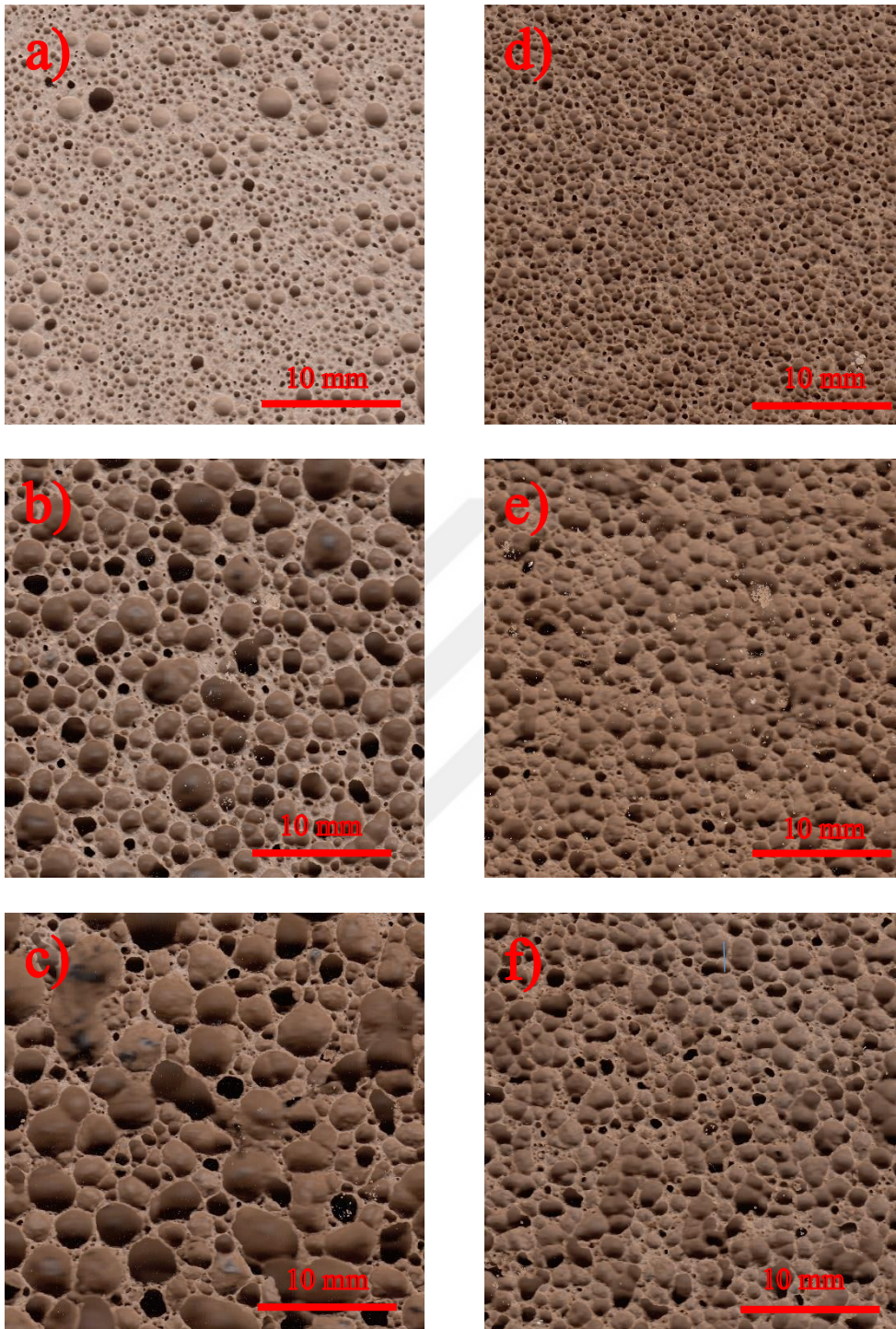


Figure 4.40 Close-ups of cross sections of aerated pastes: a) 40-0-25, b) 40-0-50, c) 40-0-75, d) 50-0-25, e) 50-0-50, and f) 50-0-75 (images are 30 mm x 30 mm).

Aerated pastes had a heterogeneous size and spatial distribution of pores. It can be observed from Figure 4.40 that increasing hydrogen peroxide increases the average size of pores, and decreases the amount of visible pores for both samples with $W/S=0.40$ (from image a to c) and samples with $W/S=0.50$ (from image d to f) resulting in a distinct reduction in the apparent density and an increase in the water absorption. The rate of reductions in the apparent densities of pastes with the incorporation of 0.50 % and 0.75 % hydrogen peroxide at $W/S=0.40$ are quite higher than those of samples with $W/S=0.50$, but not for 0.25 % hydrogen peroxide. Therefore, it can be concluded that the amount of hydrogen peroxide is low at 0.25 % for the formation of air bubbles at $W/S=0.40$. In addition, the cross-sectional shapes of pores change from circular to oval with increasing hydrogen peroxide due to the merging of air bubbles. Contrarily, increasing water content decreases the average size of pores, and increases the amount of pores for samples with 0.50 % and 0.75 % hydrogen peroxide, resulting an increase in the apparent density of samples. These results can be attributed to the reduction in the air entrapment capacity of mixtures due to the decrease in viscosity. On the other hand, the average size of pores increases with increasing water content for samples with 0.25 % hydrogen peroxide resulting in a decrease in the apparent density of samples. This is due to the high viscosity of mixtures at $W/S=0.40$ which restrict the formation of air bubbles, but viscosity reaches a sufficient level at $W/S=0.50$ which allows the formation of air bubbles. Figure 4.41 shows close-ups of cross sections of aerated mortars with $W/S=0.40$ and 0.50 containing hydrogen peroxide in the range of 0.25 % to 0.75 %.

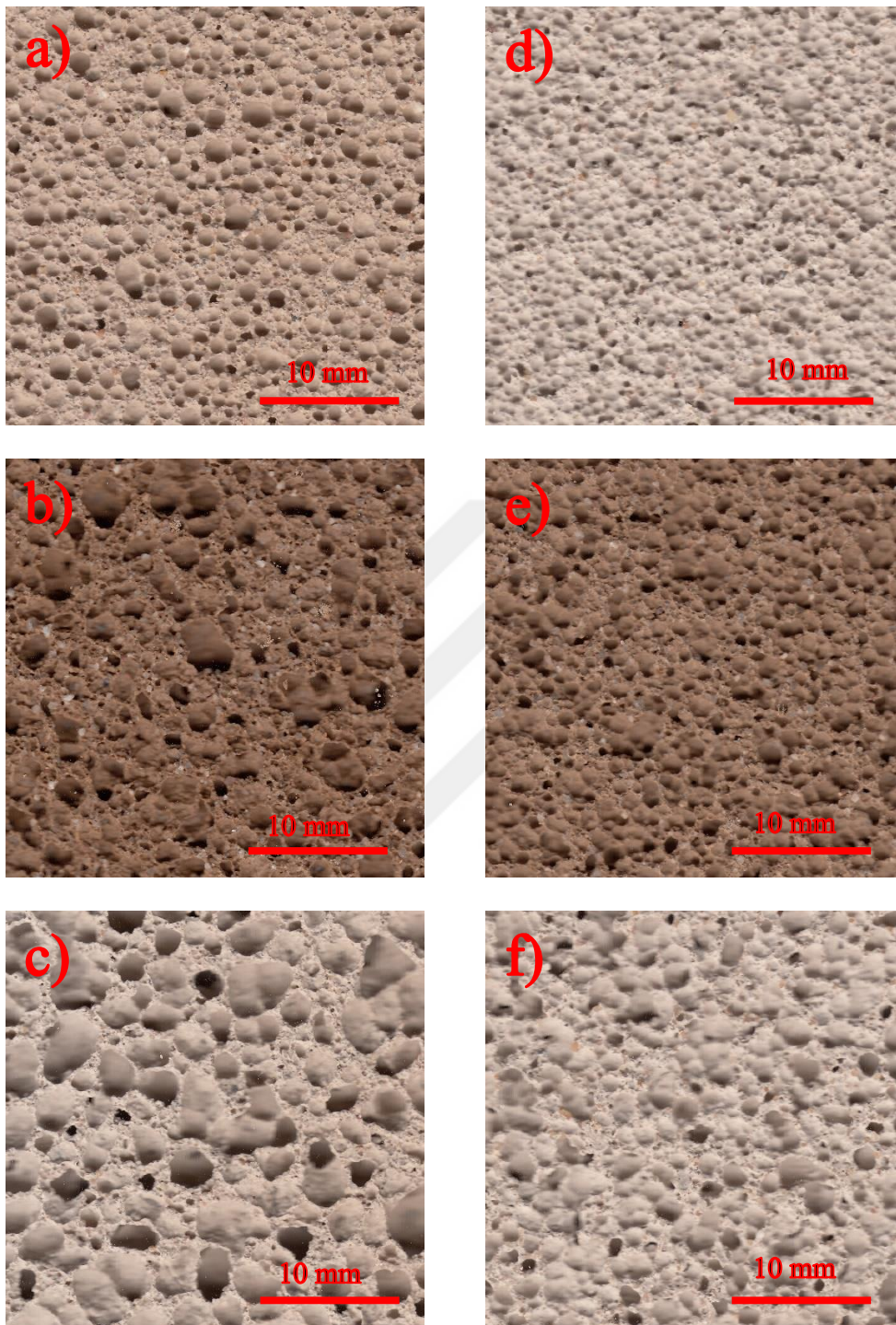


Figure 4.41 Close-ups of cross section of aerated mortars: a) 40-1-25, b) 40-1-50, c) 40-1-75, d) 50-1-25, e) 50-1-50, and f) 50-1-75 (images are 30 mm x 30 mm).

Similar to the results obtained on pastes, increasing hydrogen peroxide increases the average size of pores, and decreases the amount of pores, for samples with $W/S=0.40$ (a to c in Figure 4.41) and 0.50 (e to f in Figure 4.41) resulting in a reduction in the apparent density. Contrarily, increasing water content decreases the average pore size, and increases the amount of pores, as a result of the decrease in the viscosity of mixtures leading to a reduction in the air entrainment capacity of mixtures. The water absorption of samples with $W/S=0.40$ increase with an increase in the maximum and average size of pores. Since mortars contain sand with a distribution of different sizes, the clarities of images are lower than pastes. For comparison, the size and distribution of pores are seen to be more uniform in samples with $W/S=0.50$ than those of samples in $W/S=0.40$ at identical hydrogen peroxide contents.

4.9 SEM Analysis

Microstructures of sealed-cured pastes and mortars at age 28 days were investigated using scanning electron microscopy (SEM). Figure 4.42 illustrates SEM images of pastes with $W/S=0.45$ and different hydrogen peroxide contents.

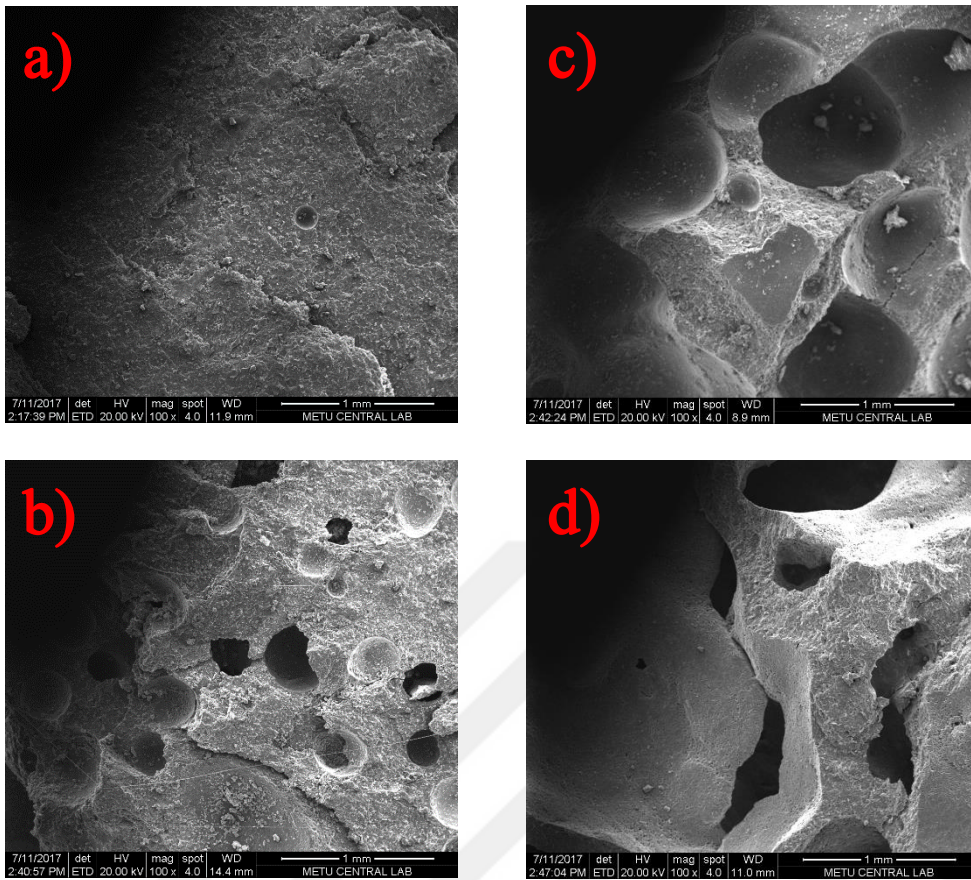


Figure 4.42 SEM images of pastes at 100x magnification: a) 45-0-0, b) 45-0-25, c) 45-0-50, and d) 45-0-100.

Comparing the microstructure of aerated pastes (Figure 4.42b, c, and d) with non-aerated paste (Figure 4.42a), it can be observed that increasing hydrogen peroxide not only increases the size of pores but also changes the shape of pores from circular to oval. In addition, uniform distribution of size of pores decreases with increasing hydrogen peroxide content due to merging of pores. Figure 4.43 compares the SEM images of pastes with $W/S=0.45$ and different hydrogen peroxide contents at a higher magnification.

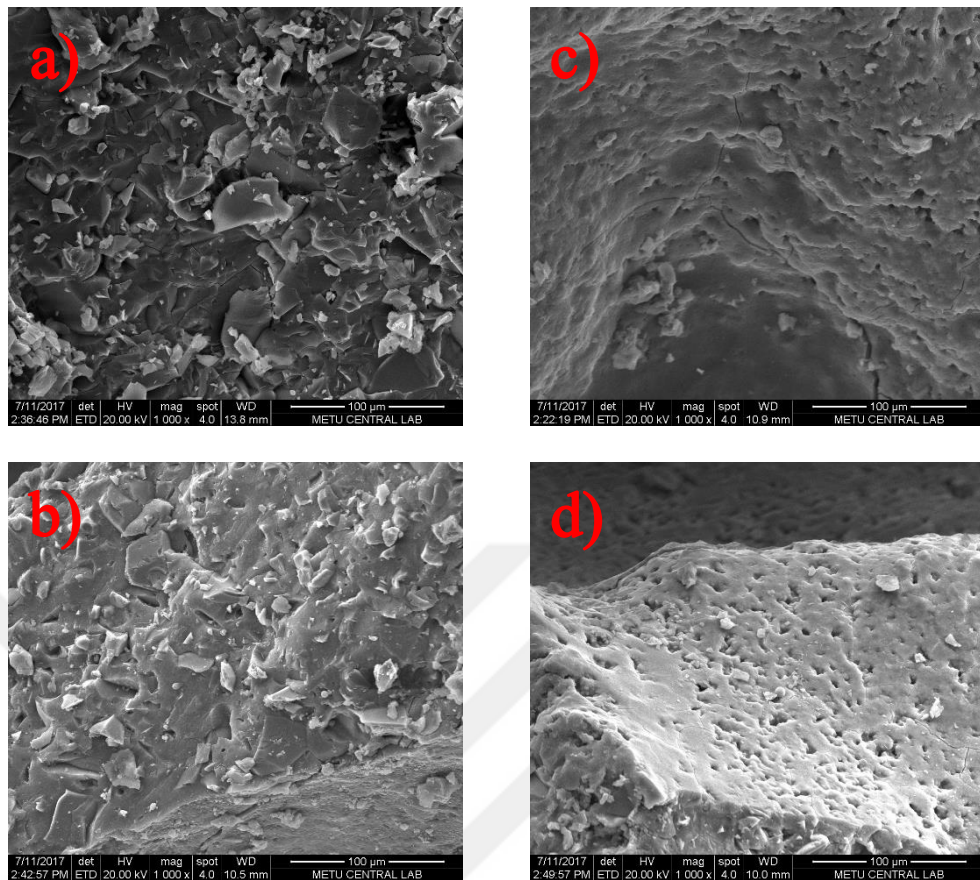


Figure 4.43 SEM images of pastes at 1000x magnification: a) 45-0-0, b) 45-0-50, c) 45-0-75, and d) 45-0-125.

The non-aerated paste has a dense structure (Figure 4.43a). With increasing hydrogen peroxide to 0.25 %, a few small pores 5-10 μm in size can be seen (Figure 4.43b). The structure of aerated paste does seem to become more porous with increasing hydrogen peroxide (Figure 4.43c and d) Pores with size larger than 10 μm can be seen. Even though these pores are bigger than 50 nm and can be classified as macropores according to Mehta and Monteiro (2006), they can be considered as macro capillary pores which have a pore size between 50 nm and 50 μm (Nambiar and Ramamurthy, 2006). Figure 4.44 shows difference in the structures of aerated samples on SEM images.

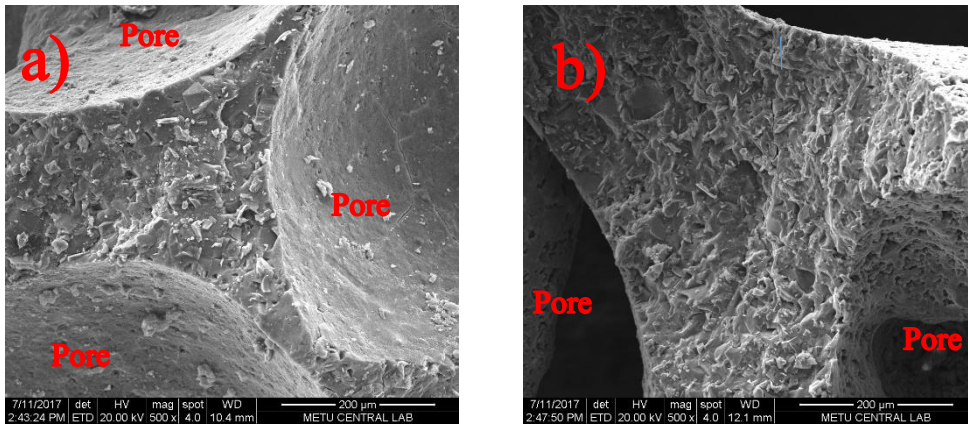


Figure 4.44 SEM images of aerated pastes at 500x magnification: a) 45-0-50 and b) 45-0-100.

It was already seen through the optical images of aerated samples that they have different structures in terms of size and amount of pores. This structure difference leads to different thickness of the paste phase around the pores. A similar situation can be seen in Figure 4.44. In addition, with increasing hydrogen peroxide the paste between the pores and on the walls of pores does seem to become more porous (Figure 4.44b). Figure 4.45 illustrates microstructure of non-aerated mortar (Figure 4.45a) and aerated mortar containing 0.75 % hydrogen peroxide (Figure 4.45b).

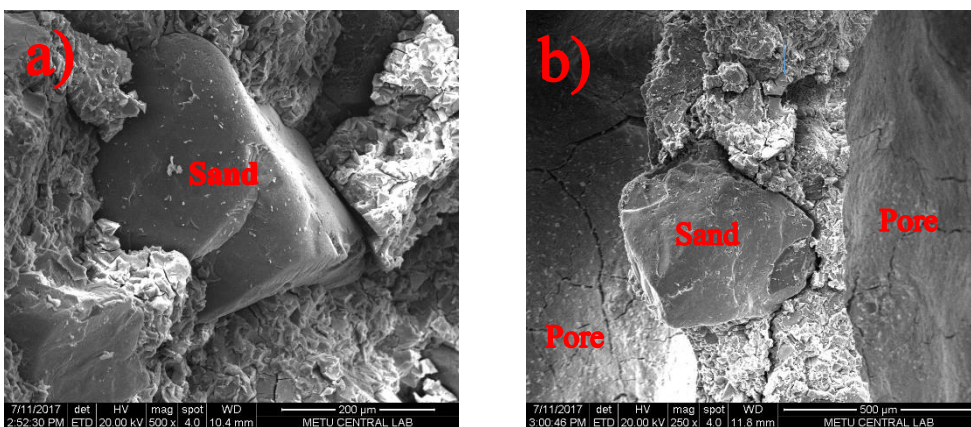


Figure 4.45 SEM images of mortars at different magnifications: a) 40-1-0 and b) 40-1-75.

Sand particles embedded within the pore walls are noticeable. Figure 4.45b also shows some cracking at the sand-paste interface and paste phase, probably due to drying in oven prior to the SEM analysis.

4.10 Thermal Conductivity of Aerated Pastes

Thermal conductivity of 16 aerated pastes were determined after oven drying cylindrical samples with a diameter of 5 cm in accordance with ASTM C1530 (2013). Test samples were cut from cylindrical samples with a diameter of 10 cm. Thermal conductivity test results are given in Table A.17 in Appendix A. The indicated dry densities are those measured on oven-dried test samples prior to testing. Figure 4.46 shows the variation of thermal conductivity with dry density for aerated pastes with different W/S and hydrogen peroxide contents.

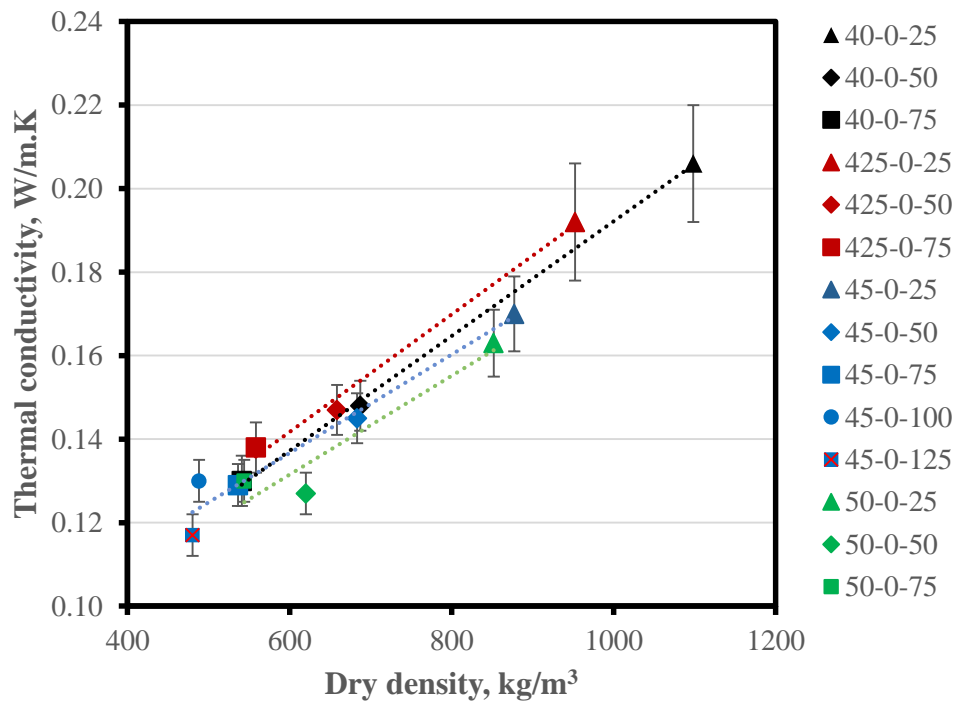


Figure 4.46 Variation of thermal conductivity with dry density for aerated pastes with different W/S and hydrogen peroxide contents.

There is a strong linear relationship between dry density and thermal conductivity of aerated pastes which is consistent with the prior literature (Narayanan and Ramamurthy, 2000). Thermal conductivity of aerated pastes decreases with decreasing density which means it decreases with increasing air content. For a given W/S, thermal conductivity of aerated pastes decreased with increasing hydrogen peroxide content, except 45-0-100 and 50-0-75. This result is expected since the amount of air voids and capillary voids increases with increasing hydrogen peroxide content. In addition, thermal conductivity of aerated pastes decreased with increasing water content, except 40-0-75 and 50-0-75, for a given hydrogen peroxide content. Thermal conductivity of cementitious materials decreases with increasing W/S (Liu et al., 2015). It can be observed that thermal conductivity of 45-0-100 and 45-0-125 are quite different (0.130 W/m.K and 0.117 W/m.K) even though their densities are quite close (488 kg/m^3 and 480 kg/m^3). On the other hand, densities and thermal conductivities of 40-0-75 and 50-0-75 are quite close (541 kg/m^3 and 540 kg/m^3 , and 0.130 W/m.K). These results may be due to differences in shape, size, and distribution of pores in the samples. The macro pores of 45-0-100 are bigger and more oval than those in 45-0-125 which might have increased its thermal conductivity. The images of aerated pastes can be seen in Appendix B. Figure 4.47 compares the thermal conductivities of aerated pastes in the current study to thermal conductivities of autoclaved aerated concretes and aerated alkali-activated slag concretes.

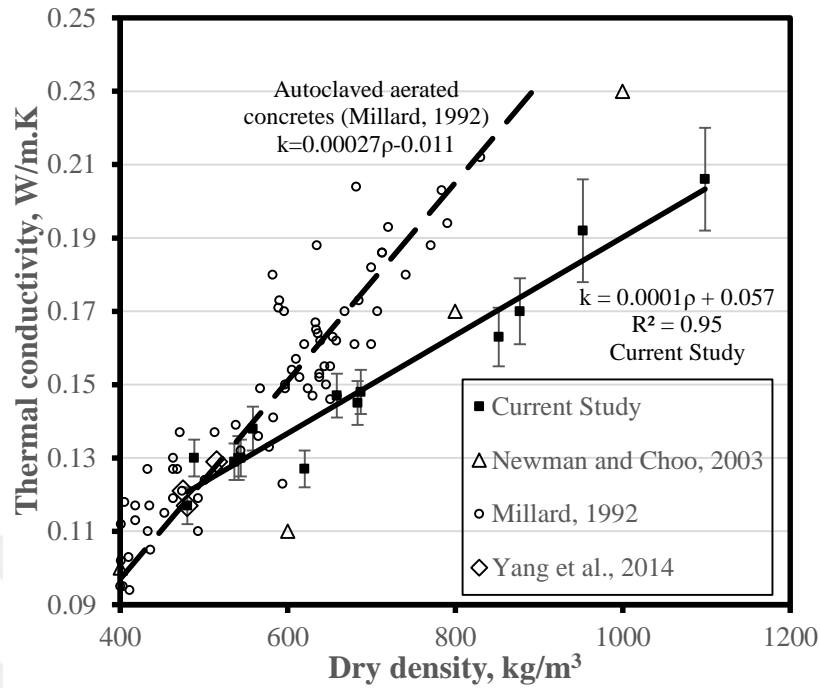


Figure 4.47 Comparison of thermal conductivities of aerated pastes to some of aerated concretes in literature.

The relationship between dry density and thermal conductivity of aerated pastes could be approximated ($R^2=0.95$) using Eq. 4.2.

$$k = 0.0001 \cdot \rho + 0.057 \quad \text{Eq. 4.2}$$

where k is thermal conductivity (W/m.K) and ρ is dry density (kg/m^3). Millard (1992) obtained the relationship between dry density and thermal conductivity of autoclaved aerated concrete (AAC) using data from AAC samples (also given in Figure 4.47) as;

$$k = 0.00027 \cdot \rho - 0.011 \quad \text{Eq. 4.3}$$

It is noteworthy that there is a difference in the thermal conductivity measurement techniques between AAC (Millard, 1992) and aerated alkali-activated slag (AAAS) pastes in the current study. Thermal conductivity measurements were made using a guarded hot plate apparatus (absolute method) for AAC and a heat flow apparatus (comparative method) in the current study. A difference of about 2.0 % is expected between their results since thermal conductivity of reference samples used for the calibration of heat flow apparatus are determined using a guarded hot plate apparatus (ASTM C177, 2013). The thermal conductivities of AAC and AAAS pastes are found to be close in the density range of about 450 kg/m³ and 600 kg/m³. In this range, thermal conductivities of samples essentially are dominated by density. However, the difference increases with increasing density beyond 600 kg/m³. Beyond this density, the effect of other parameters such as microstructure of samples, size, amount, and distribution of macro pores, and thermal conductivity of constituent materials might have been greater resulting in lower thermal conductivities for AAAS pastes. On the other hand, the thermal conductivity of AAAS pastes in this density range appear more similar to the thermal conductivity of aerated concretes reported by Newman and Choo (2003). Yang et al. (2014) reported thermal conductivities 0.117 W/m.K, 0.121 W/m.K and 0.129 W/m.K for aerated alkali-activated slag concrete with densities of 480 kg/m³, 475 kg/m³, and 515 kg/m³, respectively. Thermal conductivities of aerated alkali activated slag concretes are quite close to those of aerated pastes in this study, indicating the significance of microstructure since different materials do not show similar thermal conductivities at similar densities. A manufacturer of AAC in Turkey reported the thermal conductivity of their products as 0.09 W/m.K, 0.110 W/m.K, and 0.150 W/m.K for dry densities of 350 kg/m³, 400 kg/m³, and 600 kg/m³, respectively (AKG, 2017). Thermal conductivity of AAC is quite higher than those of aerated pastes in the density range of 600 kg/m³, but it appears more similar for densities lower than 600 kg/m³.

CHAPTER 5

CONCLUSIONS AND RECOMMENDATIONS

5.1 Concluding Remarks

In the current study, alkali-activated slag based lightweight composites with or without addition of sand were produced using hydrogen peroxide, and their physical, thermal, and mechanical properties were investigated, under different curing regimes. The following conclusions were drawn from the findings of the study:

- Flowability of mixtures increased with increasing water content. No significant effect of hydrogen peroxide was observed on the flowability of mixtures in the hydrogen peroxide range of 0.25 % to 1.25 %. However, flowability of mixtures decreased beyond a hydrogen peroxide content of 1.50 %, due to the high decomposition rate of hydrogen peroxide.
- The expansion of alkali-activated mixtures essentially depends on their water and hydrogen peroxide contents. Hydrogen peroxide content influences the amount and rate of formation of air bubbles. Water content directly influences several parameters such as the rate of decomposition of hydrogen peroxide, the viscosity, setting time, pH of the fresh mixture, and heat of hydration. Viscosity of the mixture affects the growth, size and amount of air bubbles in the fresh mixture. Changes in pH and temperature of the fresh paste affect the decomposition rate of hydrogen peroxide, and

setting time controls the duration of expansion. Efficient expansion directly depends on the interrelationship of these parameters. Consequently, a properly designed mixture should have a long-enough setting period to allow expansion, sufficient pH and heat of hydration to provide the conditions necessary for the effective decomposition of hydrogen peroxide, contain sufficient hydrogen peroxide required for oxygen production, and have a low-enough viscosity that will not make the formation of air bubbles difficult, but high-enough to allow the growth of air bubbles and to keep the formed air bubbles from escaping.

- Incorporation of sand into the pastes reduces the amount of expansion observed for a given W/S and hydrogen peroxide, due to the increase in viscosity and increase in the unit weight, leading to an increase in the apparent density of samples.
- For a given mixture composition, apparent density of aerated samples is a function of the expansion amount. Therefore, parameters such as water, hydrogen peroxide, and sand contents, which affect the expansion of mixtures directly, influence the apparent density of aerated samples. Generally, there is an inverse relationship between apparent density and hydrogen peroxide content, but this relation can change when using a high amount of hydrogen peroxide and with the incorporation of sand, for some mixtures. Apparent density usually increases with increasing water content due to the reduction in the air entrapment capacity of fresh mixtures, but hydrogen peroxide and water contents of mixtures are of a great importance. Because, large variations in water content alter significantly decomposition of hydrogen peroxide and viscosity, setting times, pH and the heat evaluation of pastes, thus the size, amount, and distribution of air bubbles vary resulting different amounts of expansions and apparent densities. Apparent density of aerated samples increases with the increase of sand

content, for a given mixture composition, due to the high specific gravity of sand.

- The use of hydrogen peroxide in the range of 0.25 % -0.75 % (by mass of slag) was sufficient to produce lightweight composites.
- It is possible to produce aerated alkali-activated slag pastes and mortars with a broad apparent density range by altering mixture compositions. In the current study, the apparent densities of aerated alkali-activated slag pastes, mortars with a Sa/S=1, and mortars with a Sa/S=2 were in the ranges of 516 kg/m³ to 1199 kg/m³, 890 kg/m³ to 1235 kg/m³, and 1417 kg/m³ to 1603 kg/m³, respectively.
- Apparent densities of aerated pastes produced using prism molds were different (-10 % - 40 %) than those of samples produced using cylindrical molds, for a given mixture composition. The difference decreased with the addition of sand due to the uniform distribution of air bubbles.
- Apparent density is the most influential property on compressive strength for a given age, curing type, and water content.
- Compressive strengths of sealed-cured aerated samples produced using alkali-activated slag pastes and mortars with a Sa/S=1 were in the range of 0.6 MPa to 30.0 MPa and 3.6 MPa to 29.4 MPa, respectively.
- Ambient curing has a detrimental effect on the strength development of alkali-activated slag pastes, due to the leaching of alkali solution which forms efflorescence. The severity of efflorescence decreased with increasing hydrogen peroxide content and decreasing apparent density.

- Humid-oven curing is more effective for strength development than curing in a sealed condition at room temperature. Extending the oven-curing time from 12 h to 48 h increased the compressive strength of samples.
- Leaching of the alkali activating solution during the water absorption test yielded misleading results. Water absorption increases with decreasing apparent density and increasing porosity. For a given apparent density, increase of water content yields higher water absorption. In addition, water absorption increases with increasing average pore size of samples.
- Water absorption measured by weight is slightly lower than that measured by volume for aerated pastes with apparent densities higher than 1150 kg/m³, but the difference increases for lower apparent densities. Expressing water absorption as a percentage of volume is more appropriate at low densities.
- Aerated samples had a heterogeneous size and distribution of pores. The average pore size of aerated pastes and mortars increase with increasing hydrogen peroxide and decrease with increasing water content.
- Aerated pastes showed lower thermal conductivities than those of AAC in the literature. They varied from 0.117 W/m.K to 0.206 W/m.K in the dry density range of 480 kg/m³ and 1098 kg/m³.
- It was demonstrated that aerated pastes and mortars based on alkali-activated slag can be produced at room and elevated temperatures using hydrogen peroxide as a gas-releasing agent. This could lead to the consumption of GGBFS in higher amounts, and the use of hydrogen peroxide which is a relatively benign environmentally friendly gas-releasing

agent compared to various others. Thus, low-CO₂ and low-energy composites can be produced for insulation and semi-structural purposes.

5.2 Recommendations for Future Work

- In the current study, sand was used as an aggregate. Lightweight aggregates such as perlite, vermiculite, pumice etc. could be considered for the production of lower-density composites.
- Samples cured at ambient temperature exhibited severe efflorescence. Research has to be carried out on the reduction of efflorescence.
- In the current study, the desired viscosity is supplied with increasing water content. The influence of water-reducing admixtures and viscosity modifiers could be studied to enhance the viscosity and achieve high strength.
- The durability of samples to different environmental conditions could be investigated.



REFERENCES

- Abdollahnejad, Z., Miraldo, S., Pacheco-Torgal, F., Aguiar, J. B. (2017). Cost-efficient one-part alkali-activated mortars with low global warming potential for floor heating systems applications. *European Journal of Environmental and Civil Engineering*, 21(4), 412-429.
- Abdollahnejad, Z., Pacheco-Torgal, F., Félix, T., Tahri, W., Barroso Aguiar, J. (2015). Mix design, properties and cost analysis of fly ash-based geopolymer foam. *Construction and Building Materials*, 80, 18–30.
- ACI 116. (2005). *Cement and concrete terminology*, ACI Committee 116 Report, ACI 116R-00, American Concrete Institute, Farmington Hills, MI.
- ACI 213. (2003). *Guide for structural lightweight aggregate concrete*, ACI Committee 213 Report, ACI 213R-03. American Concrete Institute, Farmington Hills, MI.
- ACI 233. (2003). *Slag cement in concrete and mortar*. ACI Committee 233 Report, ACI 233R-03, American Concrete Institute, Farmington Hills, MI.
- ACI 523. (1996). *Guide for precast cellular concrete floor, roof, and wall units*, ACI Committee 523.2R Report, ACI 523R-96. American Concrete Institute, Farmington Hills, MI.
- Adolph, G., Pohl, T. (1935). Process for the manufacture of masses and articles having a porous cellular structure. *U.S. Patent No. 2,024,791*. Washington, DC: U.S. Patent and Trademark Office.

- AKG. (2017). Product catalog in Turkish. Retrieved 16 September 2017 from <http://www.akg-gazbeton.com/Pdf/kapsamli-turkce-subat-2017.pdf>.
- Al Bakri Abdullah, M. M., Hussin, K., Bnhussain, M., Ismail, K. N., Yahya, Z., Razak, R. A. (2012). Fly ash-based geopolymer lightweight concrete using foaming agent. *International Journal of Molecular Sciences*, 13(6), 7186–7198.
- Al-Otaibi, S. (2002). *Performance of alkali-activated slag concrete*. Ph.D. Thesis, University of Sheffield, Sheffield.
- Allahverdi, A., Kani, N. E., Hossain A. M. K., Lachemi, M. (2013). *Methods to control efflorescence in alkali-activated cement-based materials*. Pacheco-Torgal, F., Labrincha, J., Leonelli, C., Palomo, A., Chindaprasit, P. (Eds.). Handbook of alkali-activated cements, mortars and concretes. Elsevier.
- Altan, E., Erdoğan, S. T. (2012). Alkali activation of a slag at ambient and elevated temperatures. *Cement and Concrete Composites*, 34(2), 131–139.
- Arellano Aguilar, R., Burciaga Díaz, O., Escalante García, J. I. (2010). Lightweight concretes of activated metakaolin-fly ash binders, with blast furnace slag aggregates. *Construction and Building Materials*, 24(7), 1166–1175.
- Aroni, S., De Groot, G. J., Robinson, M. J., Svanholm, G., Wittman, F. H. (Eds.). (1993). *Autoclaved aerated concrete: properties, testing, and design: RILEM recommended practice*. London and New York: Taylor and Francis Group.
- ASTM C109. (2016). *Standard Test Method for Compressive Strength of Hydraulic Cement Mortars (Using 2-in. or [50-mm] Cube Specimens)*. ASTM International, West Conshohocken, PA.

ASTM C177. (2013). *Standard Test Method for Steady-State Heat Flux Measurements and Thermal Transmission Properties by Means of the Guarded-Hot-Plate Apparatus*. ASTM International, West Conshohocken, PA.

ASTM C188. (2016). *Standard Test Methods for Density of Hydraulic Cement*. ASTM International, West Conshohocken, PA.

ASTM C191. (2013). *Standard Test Methods for Time of Setting of Hydraulic Cement by Vicat Needle*. ASTM International, West Conshohocken, PA.

ASTM C230. (2014). *Standard Specification for Flow Table for Use in Tests of Hydraulic Cement*. ASTM International, West Conshohocken, PA.

ASTM C348. (2014). *Standard Test Method for Flexural Strength of Hydraulic-Cement Mortars*. ASTM International, West Conshohocken, PA.

ASTM C495. (2012). *Standard Test Method for Compressive Strength of Lightweight Insulation Concrete*. ASTM International, West Conshohocken, PA.

ASTM C513. (2011). *Standard Test Method for Obtaining and Testing Specimens of Hardened Lightweight Insulating Concrete for Compressive Strength*. ASTM International, West Conshohocken, PA.

ASTM C518. (2017). *Standard Test Method for Steady-State Thermal Transmission Properties by Means of the Heat Flow Meter Apparatus*. ASTM International, West Conshohocken, PA.

ASTM C642. (2013). *Standard Test Method for Density, Absorption, and Voids in Hardened Concrete*. ASTM International, West Conshohocken, PA.

- ASTM C778. (2017). *Standard Specification for Standard Sand*. ASTM International, West Conshohocken, PA.
- ASTM C796. (2012). *Standard Test Method for Foaming Agents for Use in Producing Cellular Concrete Using Preformed Foam*. ASTM International, West Conshohocken, PA.
- ASTM C1044. (2016). *Standard Practice for Using a Guarded-Hot-Plate Apparatus or Thin-Heater Apparatus in the Single-Sided Mode*. ASTM International, West Conshohocken, PA.
- ASTM C1113. (2013). *Standard Test Method for Thermal Conductivity of Refractories by Hot Wire (Platinum Resistance Thermometer Technique)*. ASTM International, West Conshohocken, PA.
- ASTM C1114. (2013). *Standard Test Method for Steady-State Thermal Transmission Properties by Means of the Thin-Heater Apparatus*. ASTM International, West Conshohocken, PA.
- ASTM E1530. (2016). *Standard Test Method for Evaluating the Resistance to Thermal Transmission of Materials by the Guarded Heat Flow Meter Technique*. ASTM International, West Conshohocken, PA.
- Atiş, C. D., Bilim, C., Çelik, Ö., Karahan, O. (2009). Influence of activator on the strength and drying shrinkage of alkali-activated slag mortar. *Construction and Building Materials*, 23(1), 548–555.
- Aydın, S., Baradan, B. (2012). Mechanical and microstructural properties of heat cured alkali-activated slag mortars. *Materials & Design*, 35, 374–383.
- Aylsworth, J. W., Dyer, F. L. (1914). Porous artificial stone and its production. *U.S. Patent No. 1,087,098*. Washington, DC: U.S. Patent and Trademark Office.

- Bakharev, T., Sanjayan, J. G., Cheng, Y.-B. (1999a). Alkali activation of Australian slag cements. *Cement and Concrete Research*, 29(1), 113–120.
- Bakharev, T., Sanjayan, J. G., Cheng, Y.-B. (1999b). Effect of elevated temperature curing on properties of alkali-activated slag concrete. *Cement and Concrete Research*, 29(10), 1619–1625.
- Bean, D. L., Malone, P. G. (1997). Alkali-activated glassy silicate foamed concrete. *U.S. Patent No. 5,605,570*. Washington, DC: U.S. Patent and Trademark Office.
- Bell, J. L., Kriven, W. M. (2009). *Preparation of ceramic foams from metakaolin-based geopolymer gels*. H.T. Lin, K. Koumoto, W.M. Kriven, E. Garcia, I.E. Reimanis, D.P. Norton (Eds.), *Developments in strategic materials*, Ceram Eng Sci Proc, John Wiley & Sons Inc., New Jersey, pp. 97–112.
- Bergman, T. L., Dewit, D. P., Lavine, A. S., Incropera, F. P. (2011). *Fundamentals of heat and mass transfer*. New Jersey: John Wiley & Sons.
- Brady, K.C., Watts, G. R. A. and Jones, M. R. (2001). *Specification for foamed concrete*. Quality Services, Civil Engineering, Highways Agency. Application Guide 39. TRL Ltd.
- Brough, A. R., Holloway, M., Sykes, J., Atkinson, A. (2000). Sodium silicate-based alkali-activated slag mortars: Part II. The retarding effect of additions of sodium chloride or malic acid. *Cement and Concrete Research*, 30(9), 1375-1379.
- Brough, A., Atkinson, A. (2002). Sodium silicate-based, alkali-activated slag mortars: Part I. Strength, hydration and microstructure. *Cement and Concrete Research*, 32(6), 865–879.

- Buck, W. and Rudtsch S. (2006). *Thermal Properties*. Springer Handbook of Materials Measurement Methods, H. Czichos, T. Saito, and L. Smith, Editors. Springer Berlin Heidelberg.
- Carslaw, H. S. Jaeger, J. C. (1959). *Conduction of Heat in Solids*, Oxford: Clarendon Press.
- CEMBUREAU. (2015). *CEMBUREAU Activity Report*. Retrieved from https://cembureau.eu/media/1503/2015activityreport_cembureau.pdf
- Chang, J. (2003). A study on the setting characteristics of sodium silicate-activated slag pastes. *Cement and Concrete Research*, 33(7), 1005–1011.
- Chassevent, L. (1937). Hydraulicity of slags. *Comptes Rendires*. 205, 670–672.
- Chi, M. (2012). Effects of dosage of alkali-activated solution and curing conditions on the properties and durability of alkali-activated slag concrete. *Construction and Building Materials*, 35, 240-245.
- Collins, F. G., Sanjayan, J. G. (1999a). Workability and mechanical properties of alkali activated slag concrete. *Cement and Concrete Research*, 29(3), 455–458.
- Collins, F., Sanjayan, J. (1999b). Effects of ultra-fine materials on workability and strength of concrete containing alkali-activated slag as the binder. *Cement and Concrete Research*, 29(3), 459-462.
- Collins, F., Sanjayan, J. (2001). Microcracking and strength development of alkali activated slag concrete. *Cement and Concrete Composites*, 23(4–5), 345–352.

- Davidovits, J. (1981). Synthetic mineral polymer compound of the silicoaluminates family and preparation process. *U.S. Patent No. 4,472,199*. Washington, DC: U.S. Patent and Trademark Office.
- Davis, J. R. (1993). *ASM Specialty Handbook: Aluminum and aluminum alloys*. Materials Park, Ohio. ASM international.
- Dow, C., Glasser, F. P. (2003). Calcium carbonate efflorescence on Portland cement and building materials. *Cement and Concrete Research*, 33(1), 147-154.
- Ducman, V., Korat, L. (2016). Characterization of geopolymer fly-ash based foams obtained with the addition of Al powder or H₂O₂ as foaming agents. *Materials Characterization*, 113, 207–213.
- Duxson, P., Provis, J. L., Lukey, G. C., van Deventer, J. S. J. (2007). The role of inorganic polymer technology in the development of “green concrete.” *Cement and Concrete Research*, 37(12), 1590–1597.
- Erdoğan T. Y. (1997). *Admixtures for concrete*. Ankara, Turkey: METU Press.
- Erdoğan, S. T. (2014a). Are geopolymers environmentally friendly?. *Cement and Concrete World*, 19(107), 50–62.
- Erdoğan, S. T. (2014b). Properties of ground perlite geopolymer mortars. *Journal of Materials in Civil Engineering*, 27(7), 04014210-10.
- Escalante-García, J. I., Fuentes, A. F., Gorokhovskiy, A., Fraire-Luna, P. E. and Mendoza-Suarez, G. (2003). Hydration products and reactivity of blast furnace slag activated by various alkalis. *Journal of the American Ceramic Society*, 86: 2148–2153.

- Esmaily, H., Nuranian, H. (2012). Non-autoclaved high strength cellular concrete from alkali activated slag. *Construction and Building Materials*, 26(1), 200–206.
- Exerowa, D., Kruglyakov, P. M. (1997). *Foam and foam films, theory, experiment, application*. Amsterdam. Elsevier.
- Feret, R. (1939). Slags for the manufacture of cement, *Rev. Mater. Constr. Trav. Publications*, 22, 1-145.
- Fernández-Jiménez, A., Puertas, F. (2001). Setting of alkali-activated slag cement. Influence of activator nature. *Advances in Cement Research*, 13(3), 115-121.
- Fernández-Jiménez, A., Palomo, J. G., Puertas, F. (1999). Alkali-activated slag mortars: Mechanical strength behaviour. *Cement and Concrete Research*, 29(8), 1313-1321.
- Fernández-Jiménez, A., Puertas, F. (2003). Effect of activator mix on the hydration and strength behaviour of alkali-activated slag cements. *Advances in Cement Research*, 15(3), 129-136.
- Flynn, D. R. (1999). *Response of high performance concrete to fire conditions: review of thermal property data and measurement techniques*. National Institute of Standards and Technology. Gaithersburg, MD, USA.
- Fouad, F. H. (2006). *Cellular concrete*. In F. J. Lamond, H. J. Pielert (Eds.). STP169D-EB Significance of Tests and Properties of Concrete and Concrete-Making Materials. ASTM International. West Conshohocken, PA.
- Francl, J., Kingery, W. D. (1954). Thermal conductivity: IX, experimental investigation of effect of porosity on thermal conductivity. *Journal of the American Ceramic Society*, 37(2), 99-107.

- Franco, A. (2007). An apparatus for the routine measurement of thermal conductivity of materials for building application based on a transient hot-wire method. *Applied Thermal Engineering*, 27 (14–15), 2495-2504.
- Ghanta, M., Subramaniam, B. (2017). *Development of a sustainable and economically viable process for making ethylene oxide: A case study*. In M. Abraham, *Encyclopedia of Sustainable Technologies*. Elsevier.
- Glukhovsky, V.D. (1959). *Gruntosilikaty (Soil Silicates)*. Gosstroyizdat, Kiev.
- Glukhovsky, V.D. (1994). Ancient, modern and future concretes. In: Krivenko, P.V. (ed.). *Proceedings of the First International Conference on Alkaline Cements and Concretes*, Kiev, Ukraine, vol. 1, pp. 1–9. VIPOL Stock Company.
- Glukhovsky, V. D., Rostovkaya, G. S. and Rumyna, G. V. (1980). High strength slag-alkali cement. *7th International Congress on the Chemistry of Cements*, Paris, France, III, V-164–168.
- Goor, G. (1992). *Hydrogen peroxide: manufacture and industrial use for production of organic chemicals*. In Strukul, G. (Ed.). *Catalytic oxidations with hydrogen peroxide as oxidant (Vol. 9)*. Springer Science & Business Media.
- Goor, G., Glenneberg, J., Jacobi, S. (2000). *Hydrogen Peroxide*. In Ullmann's Encyclopedia of Industrial Chemistry. Wiley-VCH Verlag GmbH & Co. KGaA.
- Guo, T. X., Zhao, Y., Ma, S. C., Liu, S. T. (2013). Decomposition characteristics of hydrogen peroxide in sodium hydroxide solution. In *Advanced Materials Research*, 610, 359-362, Trans Tech Publications.

- Gustafsson, S. E., Karawacki, E., Khan, M. N. (1979). Transient hot-strip method for simultaneously measuring thermal conductivity and thermal diffusivity of solids and fluids. *Journal of Physics D: Applied Physics*, 12(9), 1411.
- Habert, G., d'Espinose de Lacaillerie, J. B., Roussel, N. (2011). An environmental evaluation of geopolymer based concrete production: reviewing current research trends. *Journal of Cleaner Production*, 19(11), 1229–1238.
- Haha, M. B., Lothenbach, B., Le Saout, G., Winnefeld, F. (2011). Influence of slag chemistry on the hydration of alkali-activated blast furnace slag — Part I: Effect of MgO. *Cement and Concrete Research*, 41(9), 955–963.
- Haha, M. B., Lothenbach, B., Le Saout, G., Winnefeld, F. (2012). Influence of slag chemistry on the hydration of alkali-activated blast furnace slag — Part II: Effect of Al₂O₃. *Cement and Concrete Research*, 42(1), 74–83.
- Hao, H., Geng, Y., Hang, W. (2016). GHG emissions from primary aluminum production in China: regional disparity and policy implications. *Applied Energy*, 166, 264-272.
- Hilal, A. A., Thom, N. H., Dawson, A. R. (2016). Failure mechanism of foamed concrete made with/without additives and lightweight aggregate. *Journal of Advanced Concrete Technology*, 14(9), 511-520.
- Hlaváček, P., Šmilauer, V., Škvára, F., Kopecký, L., Šulc, R. (2015). Inorganic foams made from alkali-activated fly ash: Mechanical, chemical and physical properties. *Journal of the European Ceramic Society*, 35(2), 703-709.
- ISO 22007-2. (2008). *Plastics - Determination of thermal conductivity and thermal diffusivity - Part 2: Transient plane heat source (hot disk) method*. International Organization for Standardization, Geneva, Switzerland.

- Jiang, W. (1997). *Alkali activated cementitious materials: Mechanism, microstructure and properties*. Ph.D. Thesis, The Pennsylvania State University, Pennsylvania.
- Jones, M. R., McCarthy, M. J., McCarthy, A. (2003). Moving fly ash utilization in concrete forward: a UK perspective. In *Proceedings of the 2003 international ash utilization symposium, center for applied energy research*. University of Kentucky.
- Juenger, M. C. G., Winnefeld, F., Provis, J. L., Ideker, J. H. (2011). Advances in alternative cementitious binders. *Cement and Concrete Research*, 41(12), 1232–1243.
- Just, A., Middendorf, B. (2009). Microstructure of high-strength foam concrete. *Materials Characterization*, 60(7), 741–748.
- Kani, E. N., Allahverdi, A., Provis, J. L. (2012). Efflorescence control in geopolymer binders based on natural pozzolan. *Cement and Concrete Composites*, 34(1), 25-33.
- Kearsley, E. P., Wainwright, P. J. (2001). Porosity and permeability of foamed concrete. *Cement and Concrete Research*, 31(5), 805-812.
- Kingery, W. D., McQuarrie, M. C. (1954). Thermal conductivity: I, concepts of measurement and factors affecting thermal conductivity of ceramic materials. *Journal of the American Ceramic Society*, 37(2), 67-72.
- Kovtun, M., Kearsley, E. P., Shekhovtsova, J. (2015). Dry powder alkali-activated slag cements. *Advances in Cement Research*, 27(8), 447-456.

- Krivenko, P. V. (1994). Alkaline cements. In: Krivenko, P.V. (ed.). *Proceedings of the First International Conference on Alkaline Cements and Concretes*, Kiev, Ukraine, vol. 1, pp. 11–129. VIPOL Stock Company.
- Krivenko, P. V. (2010). Status and prospects of research and application of alkali-activated materials. In *Advances in Science and Technology*, Vol. 69, pp. 1-10). Trans Tech Publications.
- Kühl, H. (1908). Slag cement and process of making the same. *U.S. Patent No. 900,939*. Washington, DC: U.S. Patent and Trademark Office.
- Li, Z. (2011). *Advanced concrete technology*. Hoboken, New Jersey: John Wiley & Sons, Inc.
- Li, C., Sun, H., Li, L. (2010). A review: The comparison between alkali-activated slag (Si+Ca) and metakaolin (Si+Al) cements. *Cement and Concrete Research*, 40(9), 1341–1349.
- Liu, K., Wang, Z., Jin, C., Wang, F., Lu, X. (2015). An experimental study on thermal conductivity of iron ore sand cement mortar. *Construction and Building Materials*, 101, 932-941.
- Masi, G., Rickard, W. D. A., Vickers, L., Bignozzi, M. C., Van Riessen, A. (2014). A comparison between different foaming methods for the synthesis of light weight geopolymers. *Ceramics International*, 40(9 Part A), 13891–13902.
- Mehta, P. K., Monteiro, P. J. M. (2006). *Concrete: Microstructure, properties, and materials*. New York. McGraw-Hill Education.
- Millard. R. W. (1992). *The thermal performance of European autoclaved aerated concrete*. In Wittmann. F. H. (ed). *Advances in Autoclaved Aerated Concrete*. A. A. Balkema. 83-88.

- Nambiar, E. K. K., Ramamurthy, K. (2006). Influence of filler type on the properties of foam concrete. *Cement and Concrete Composites*, 28(5), 475–480.
- Nambiar, E. K. K., Ramamurthy, K. (2007). Sorption characteristics of foam concrete. *Cement and Concrete Research*, 37(9), 1341–1347.
- Narayanan, N., Ramamurthy, K. (2000). Structure and properties of aerated concrete: A review. *Cement and Concrete Composites*, 22(5), 321–329.
- Neville, A. M. (1995). *Properties of concrete* (4th ed.). London. Pearson Prentice Hall.
- Neville, A. M., Brooks, J. J. (2010). *Concrete technology*. London. Pearson Prentice Hall.
- Newman, J., Choo, B. S. (2003). *Advanced concrete technology 3: Processes*. Butterworth-Heinemann: Elsevier.
- Novais, R. M., Ascensão, G., Buruberry, L. H., Senff, L., Labrincha, J. A. (2016). Influence of blowing agent on the fresh-and hardened-state properties of lightweight geopolymers. *Materials & Design*, 108, 551-559.
- Othuman, M. A., Wang, Y. C. (2011). Elevated-temperature thermal properties of lightweight-foamed concrete. *Construction and Building Materials*, 25(2), 705-716.
- Öner, M. (2000). A study of intergrinding and separate grinding of blast furnace slag cement. *Cement and Concrete Research*, 30(3), 473-480.
- Pacheco-Torgal, F., Labrincha, J., Leonelli, C., Palomo, A., Chindaprasit, P. (Eds.). (2014). *Handbook of alkali-activated cements, mortars and concretes*. Amsterdam. Woodhead Publishing, Elsevier.

- Provis, J. L., Van Deventer. J. (2014). *Alkali activated materials: State-of-the-art report, RILEM TC 224-AAM*. Dordrecht: Springer Netherlands.
- Puertas, F., Fernández-Jiménez, A., Blanco-Varela, M. T. (2004). Pore solution in alkali-activated slag cement pastes. Relation to the composition and structure of calcium silicate hydrate. *Cement and Concrete Research*, 34(1), 139–148.
- Puertas, F., Martínez-Ramírez, S., Alonso, S., Vázquez, T. (2000). Alkali-activated fly ash/slag cements. Strength behavior and hydration products. *Cement and Concrete Research*, 30(10), 1625–1632.
- Qureshi, M. N. Ghosh, S. (2013). Workability and setting time of alkali activated blast furnace slag paste. *Advances in Civil Engineering Materials*, 2 (1), 62-77.
- Ramamurthy, K., Kunhanandan Nambiar, E. K., Indu Siva Ranjani, G. (2009). A classification of studies on properties of foam concrete. *Cement and Concrete Composites*, 31(6), 388–396.
- Ramamurthy, K., Narayanan, N. (2000). Factors influencing the density and compressive strength of aerated concrete. *Magazine of Concrete Research*, 52(3), 163–168.
- Rasband, W.S. (1997). ImageJ, U. S. National Institutes of Health, Bethesda, Maryland, USA, <https://imagej.nih.gov/ij/>
- Rashad, A. M., Bai, Y., Basheer, P. A. M., Milestone, N. B., Collier, N. C. (2013). Hydration and properties of sodium sulfate activated slag. *Cement and Concrete Composites*, 37, 20-29.

- Ravikumar, D., Neithalath, N. (2012). Effects of activator characteristics on the reaction product formation in slag binders activated using alkali silicate powder and NaOH. *Cement and Concrete Composites*, 34(7), 809–818.
- Regourd, M., (1980). Structure and Behavior of Slag Portland Cement Hydrates, *Proceedings of 7th International Congress on the Chemistry of Cements*, Vol.I, 2/11 - 2/26, Paris, 1980.
- Richard, T., Dobogai, J., Gerhardt, T., Young, W. (1975). Cellular concrete-A potential load-bearing insulation for cryogenic applications?. *IEEE Transactions on Magnetics*, 11(2), 500-503.
- Rudnai, G. (1963). *Lightweight Concretes*. Budapest. Akademi Kiado.
- Purdon, A.O. (1940). The action of alkalis on blast furnace slag. *Journal of the Society of Chemical Industry*. 59, 191-202.
- Sanjayan, J. G., Nazari, A., Chen, L., Nguyen, G. H. (2015). Physical and mechanical properties of lightweight aerated geopolymer. *Construction and Building Materials*, 79, 236–244
- Schumb, W. C., Satterfield, C. N., Wentworth, R. L. (1955). *Hydrogen Peroxide*. New York, NY: Reinhold Publishing Corporation.
- Scrivener, K. L., Kirkpatrick, R. J. (2008). Innovation in use and research on cementitious material. *Cement and Concrete Research*, 38(2), 128-136.
- Shi, C. (1996). Strength, pore structure and permeability of alkali-activated slag mortars. *Cement and Concrete Research*, 26(12), 1789–1799.
- Shi, C., Day, R. L. (1996). Selectivity of alkaline activators for the activation of slags. *Cement, Concrete and Aggregates*, 18(1), 8-14.

- Shi, C., Krivenko, P. V., Roy, D. (2006). *Alkali-Activated Cements and Concretes*. London: Taylor and Francis.
- Short, A., Kinniburgh, W. (1963). *Lightweight Concrete*. London: C.R. Books Limited.
- Škvára, F., Šmilauer, V., Hlaváček, P., Kopecký, L., Cílová, Z. (2012). A weak alkali bond in (N, K)-A-S-H gels: Evidence from leaching and modeling. *Ceramics - Silikaty*, 56(4), 374–382.
- Straub, C., Quercia, G., Florea, M. V. A., Brouwers, H. J. H. (2014). Slump flow of Autoclaved Aerated Concrete slurries. *International Conference on Non-Traditional Cement and Concrete*, Brno, Czech Republic.
- USGS. (2015). USGS minerals yearbook, aluminum. Retrieved 16 September 2017 from <https://minerals.usgs.gov/minerals/pubs/commodity/aluminum/myb1-2015-alumi.pdf>
- Taylor, H. W., (1997). *Cement chemistry* (2nd Ed.). London: Thomas Telford.
- Temuujin, J., van Riessen, A. (2009). Effect of fly ash preliminary calcination on the properties of geopolymer. *Journal of Hazardous Materials*, 164(2–3), 634–639.
- Tokyay, M. (2016). *Cement and concrete mineral admixtures*. Boca Raton: CRC Press, Taylor & Francis Group.
- Torres-Carrasco, M., Rodríguez-Puertas, C., del Mar Alonso, M., Puertas, F. (2015). Alkali activated slag cements using waste glass as alternative activators. *Rheological behaviour. Boletín de la Sociedad Española de Cerámica y Vidrio*, 54(2), 45-57.

- Touloukian, Y. S., Powell, R. W., Ho, C. Y., Klemens, P. G. (1970). *Thermophysical Properties of Matter-The TPRC Data Series. Volume 2. Thermal Conductivity-Nonmetallic Solids*. Thermophysical and Electronic Properties Information Analysis Center, Lafayette IN.
- Valore Jr, R. C. (1961). Foam and gas concrete. *In BRI Conference on Structural Foams*. Publication Volume 892. National Academy of Sciences – National Research Council, Washington, DC.
- Vaou, V., Papias, D. (2010). Thermal insulating foamy geopolymers from perlite. *Minerals Engineering*, 23(14), 1146–1151.
- Vlcek J, Tomková V, Babková P, Vavro M. (2009). Alkali-activated composites based on slags from iron and steel metallurgy. *Metalurgija*, 48(4), 223–7.
- Wang, S. D., Scrivener, K. L., Pratt, P. L. (1994). Factors affecting the strength of alkali-activated slag. *Cement and Concrete Research*, 24(6), 1033-1043.
- Wang, S. D., Scrivener, K. L. (1995). Hydration products of alkali activated slag cement. *Cement and Concrete Research*, 25(3), 561–571.
- Wang, W. C., Wang, H. Y., Lo, M. H. (2015). The fresh and engineering properties of alkali activated slag as a function of fly ash replacement and alkali concentration. *Construction and Building Materials*, 84, 224-229.
- Wei, S., Yiqiang, C., Yunsheng, Z., Jones, M. R. (2013). Characterization and simulation of microstructure and thermal properties of foamed concrete. *Construction and Building materials*, 47, 1278-1291.
- Yang, K. H., Lee, K. H., Song, J. K., Gong, M. H. (2014). Properties and sustainability of alkali-activated slag foamed concrete. *Journal of Cleaner Production*, 68, 226–233.

- Yang, Q., Zhu, P., Wu, X., Huang, S. (2000). Properties of concrete with a new type of saponin air-entraining agent. *Cement and Concrete Research*, 30(8), 1313-1317.
- Yao, X., Yang, T., Zhang, Z. (2016). Compressive strength development and shrinkage of alkali-activated fly ash–slag blends associated with efflorescence. *Materials and Structures*, 49(7), 2907-2918.
- Zhang, Z., Provis, J. L., Reid, A., Wang, H. (2014). Fly ash-based geopolymers: The relationship between composition, pore structure and efflorescence. *Cement and Concrete Research*, 64, 30–41.
- Živica, V. (2007). Effects of type and dosage of alkaline activator and temperature on the properties of alkali-activated slag mixtures. *Construction and Building Materials*, 21(7), 1463-1469.

APPENDIX A

TEST RESULTS

Table A.1 Initial and final setting times of non-aerated pastes.

Water-to-Slag Ratio	Initial Setting Time (min)	Final Setting Time (min)
0.40	51	165
0.425	56	190
0.45	86	270
0.50	165	415

Table A.2 Effect of W/S on flow of non-aerated pastes.

W/S	0.40	0.425	0.45	0.50	0.55	0.60
Flow, %	190	210	220	240	260	285

Table A.3 Effect of W/S on flow of non-aerated mortars with Sa/S=1.

W/S	0.40	0.45	0.50
Flow, %	155	190	220

Table A.4 Apparent densities of pastes with different W/S and hydrogen peroxide contents.

		Water-to-Slag Ratio			
		0.40	0.425	0.45	0.50
Hydrogen Peroxide, % by mass of slag	0	1932 ± 31	1908 ± 30	1890 ± 15	1863 ± 20
	0.25	1199 ± 24	1035 ± 32	1143 ± 27	933 ± 21
	0.50	753 ± 24	697 ± 29	858 ± 24	820 ± 15
	0.75	516 ± 36	549 ± 34	733 ± 19	735 ± 16
	1.00	1	2	653 ± 26	681 ± 33
	1.50	1	516 ± 19	540 ± 23	679 ± 18

¹ Could not be prepared, ²Was not performed, Apparent Density: ± 1 kg/m³

Table A.5 Apparent densities of mortars (Sa/S=1) with different W/S and hydrogen peroxide contents.

		Water-to-Slag Ratio				
		0.35	0.375	0.40	0.45	0.50
Hydrogen Peroxide, % by mass of slag	0	2069 ± 8	2058 ± 13	2070 ± 38	2045 ± 30	2035 ± 30
	0.25	1235 ± 27	1341 ± 25	1320 ± 10	1273 ± 16	1300 ± 17
	0.50	1106 ± 22	1126 ± 72	998 ± 14	1005 ± 23	1153 ± 90
	0.75	732 ± 29	746 ± 29	852 ± 25	985 ± 18	1112 ± 7
	1.00	920 ± 34	954 ± 59	983 ± 14	994 ± 19	1150 ± 13
	1.50	893 ± 2	868 ± 12	890 ± 6	1016 ± 39	1135 ± 40

Apparent Density : ± 1 kg/m³

Table A.6 Apparent densities of mortars (Sa/S=2) with different W/S and hydrogen peroxide contents.

		Water-to-Slag Ratio			
		0.50	0.55	0.60	0.65
Hydrogen Peroxide, % by mass of slag	0	2072 ± 23	2062 ± 63	2078 ± 33	2110 ± 50
	0.25	1483 ± 14	1548 ± 19	1603 ± 22	1603 ± 11
	0.50	1501 ± 27	1519 ± 14	1520 ± 11	1521 ± 4
	0.75	1455 ± 15	1476 ± 7	1517 ± 40	1538 ± 17
	1.00	1471 ± 18	1462 ± 4	1504 ± 3	1522 ± 12
	2.25	¹	1428 ± 5	1417 ± 26	1421 ± 53

¹ Could not be prepared, Apparent Density: ± 1 kg/m³

Table A.7 The calculated apparent densities (kg/m³) of the paste phases of mortars (Sa/S=1) and pastes with different W/S and hydrogen peroxide contents.

		Water-to-Slag Ratio					
		0.40		0.45		0.50	
		Paste	Paste in mortar	Paste	Paste in mortar	Paste	Paste in mortar
Hydrogen peroxide, % by mass of slag	0.25	1199	933	1143	957	933	990
	0.5	753	708	858	721	820	856
	0.75	516	589	733	703	735	819
	1.00	N/A	695	653	711	68	853
	1.50	N/A	620	540	730	679	839

N/A: Not available

Table A.8 Apparent density, powder density, and porosity of pastes with different W/S and hydrogen peroxide contents.

ID	W/S	H₂O₂¹ (%)	Apparent Density (kg/m³)	Powder Density (kg/m³)	Porosity (%)
40-0-0	0.40	0	1966 ± 7	2102	6.5
40-0-25	0.40	0.25	1566 ± 20		25.5
40-0-50	0.40	0.50	1057 ± 11		49.7
40-0-75	0.40	0.75	715 ± 24		66.0
425-0-0	0.425	0	1931 ± 20	2093	7.7
425-0-25	0.425	0.25	1424 ± 29		32.0
425-0-50	0.425	0.50	854 ± 12		59.2
425-0-75	0.425	0.75	682 ± 7		67.4
45-0-0	0.45	0	1908 ± 19	2083	8.4
45-0-25	0.45	0.25	1273 ± 32		38.9
45-0-50	0.45	0.50	848 ± 29		59.3
45-0-75	0.45	0.75	644 ± 12		69.1
45-0-100	0.45	1.00	625 ± 7		70.0
45-0-125	0.45	1.25	606 ± 15		70.9
50-0-0	0.50	0	1846 ± 24	2045	9.7
50-0-25	0.50	0.25	1135 ± 24		44.5
50-0-50	0.50	0.50	925 ± 7		54.8
50-0-75	0.50	0.75	734 ± 23		64.1

¹By mass of slag, Apparent Density: ± 1 kg/m³

Table A.9 Apparent density, flexural strength, and compressive strength of pastes with different W/S and hydrogen peroxide contents.

Mix No	W/S	H ₂ O ₂ ¹ (%)	Apparent Density (kg/m ³)	Flexural Strength (MPa)	Compressive Strength (MPa)
1	0.40	0	1966 ± 7	4.7 ± 0.2	64.4 ± 2.5
2	0.40	0.25	1566 ± 20	3.1 ± 0.2	30.0 ± 1.2
3	0.40	0.50	1057 ± 11	2.1 ± 0.3	11.7 ± 0.8
4	0.40	0.75	715 ± 24	1.2 ± 0.1	2.8 ± 0.4
5	0.425	0	1931 ± 20	4.0 ± 0.1	57.5 ± 1.5
6	0.425	0.25	1424 ± 29	3.6 ± 0.1	22.4 ± 1.3
7	0.425	0.50	854 ± 12	1.4 ± 0	5.2 ± 0.4
8	0.425	0.75	682 ± 7	0.8 ± 0.1	1.4 ± 0.1
9	0.45	0	1908 ± 19	2.2 ± 0.1	55.0 ± 1.7
10	0.45	0.25	1273 ± 32	1.8 ± 0.2	18.1 ± 1.0
11	0.45	0.50	848 ± 29	1.1 ± 0	4.2 ± 0.4
12	0.45	0.75	644 ± 12	0.8 ± 0	1.9 ± 0.2
13	0.45	1	625 ± 7	0.7 ± 0.1	2.3 ± 0.2
14	0.45	1.25	606 ± 15	0.4 ± 0	2.2 ± 0.1
15	0.50	0	1846 ± 24	1.5 ± 0.1	43.2 ± 2.1
16	0.50	0.25	1135 ± 24	1.3 ± 0.1	7.7 ± 0.7
17	0.50	0.50	925 ± 7	1.0 ± 0.1	1.7 ± 0.3
18	0.50	0.75	734 ± 23	0.6 ± 0	2.3 ± 0.1

¹By mass of slag, Density: ± 1 kg/m³, Strength: ± 0.1 MPa

Table A.10 Compressive strength development of sealed-cured pastes with W/S=0.45 and different hydrogen peroxide contents.

ID	Curing Duration											
	7 Days		14 Days		28 Days		91 Days					
	Apparent Density (kg/m ³)	Compressive Strength (MPa)	Apparent Density (kg/m ³)	Compressive Strength (MPa)	Apparent Density (kg/m ³)	Compressive Strength (MPa)	Apparent Density (kg/m ³)	Compressive Strength (MPa)				
45-0-0	1897 ± 18	13.0 ± 0.1	1920 ± 25	39.0 ± 2.2	1908 ± 19	55.0 ± 1.7	1932 ± 11	84.2 ± 2.5				
45-0-25	1321 ± 11	1.3 ± 0.2	1305 ± 18	6.0 ± 0.5	1273 ± 32	18.1 ± 1.0	1333 ± 24	25.8 ± 0.8				
45-0-50	869 ± 21	0.4 ± 0.1	857 ± 19	1.6 ± 0.1	848 ± 29	4.2 ± 0.4	890 ± 15	5.8 ± 0.5				
45-0-75	665 ± 17	0.2 ± 0	660 ± 26	1.2 ± 0.1	644 ± 12	1.9 ± 0.2	680 ± 23	2.7 ± 0.2				
45-0-100	646 ± 23	0.2 ± 0	620 ± 13	1.2 ± 0.1	625 ± 7	2.3 ± 0.2	618 ± 17	3.1 ± 0.3				
45-0-125	619 ± 17	0.2 ± 0	601 ± 22	1.2 ± 0.1	606 ± 15	2.2 ± 0.1	620 ± 13	3.2 ± 0.1				

Apparent Density: ± 1 kg/m³ Compressive Strength: ± 0.1 MPa

Table A.11 Compressive strengths of ambient-cured pastes with W/S=0.45 and different hydrogen peroxide contents.

ID	Apparent Density (kg/m ³)		28-day Flexural Strength (MPa)	28-day Compressive Strength (MPa)
	After demolding	After Curing		
45-0-0	1910 ± 28	N/A ¹	N/A ¹	N/A ¹
45-0-25	1181 ± 18	919 ± 12	N/A ¹	2.4 ± 0.3
45-0-50	831 ± 34	654 ± 30	0.7 ± 0.1	0.9 ± 0.2
45-0-75	661 ± 31	519 ± 24	0.3 ± 0.1	0.5 ± 0.2
45-0-100	642 ± 25	501 ± 19	0.5 ± 0.1	0.8 ± 0.1
45-0-125	626 ± 17	489 ± 13	0.5 ± 0.1	0.7 ± 0.1

¹Samples cracked, Apparent density: ± 1 kg/m³, Strength: ± 0.1 MPa

Table A.12 Compressive strengths of oven-cured pastes with W/S=0.45 and different hydrogen peroxide contents.

ID	Curing Duration					
	12 h		24 h		48 h	
	Apparent Density (kg/m ³)	Comp. Strength (MPa)	Apparent Density (kg/m ³)	Comp. Strength (MPa)	Apparent Density (kg/m ³)	Comp. Strength (MPa)
45-0-0	1894 ± 12	72.5 ± 2.7	1943 ± 35	78.3 ± 1.6	1884 ± 21	84.6 ± 1.7
45-0-25	1276 ± 23	17.2 ± 0.8	1314 ± 13	21.3 ± 1.3	1339 ± 18	21.4 ± 0.7
45-0-50	705 ± 19	3.1 ± 0.1	766 ± 28	3.2 ± 0.1	718 ± 13	3.1 ± 0.2
45-0-75	621 ± 11	2.1 ± 0.1	623 ± 19	2.3 ± 0.1	626 ± 17	2.8 ± 0.4
45-0-100	620 ± 22	2.7 ± 0.1	602 ± 17	2.9 ± 0.1	603 ± 15	3.1 ± 0.1
45-0-125	567 ± 24	2.1 ± 0.2	566 ± 11	2.4 ± 0.1	567 ± 19	2.9 ± 0.4

Apparent density: ± 1 kg/m³ Compressive strength: ± 0.1 MPa

Table A.13 Effect of W/S and hydrogen peroxide content on the apparent density, flexural strength, and compressive strength of mortars (Sa/S=1).

ID	H ₂ O ₂ ¹ (%)	Apparent Density (kg/m ³)	Flexural Strength (MPa)	Compressive Strength (MPa)
40-1-0	0	2069 ± 9	7.3 ± 0.3	66.9 ± 3.0
40-1-25	0.25	1329 ± 16	4.6 ± 0.1	29.4 ± 1.3
40-1-50	0.50	894 ± 22	2.0 ± 0.3	4.8 ± 0.3
40-1-75	0.75	876 ± 15	2.1 ± 0.3	3.6 ± 0.1
50-1-0	0	2039 ± 10	4.1 ± 0.1	43.4 ± 2.9
50-1-25	0.25	1215 ± 11	2.3 ± 0.2	9.6 ± 0.5
50-1-50	0.50	1141 ± 13	1.9 ± 0.1	6.6 ± 0.6
50-1-75	0.75	1097 ± 10	1.7 ± 0.1	6.3 ± 0.6

¹By mass of slag, Density: ± 1 kg/m³, Strength: ± 0.1 MPa

Table A.14 Effect of oven curing on flexural and compressive strengths of mortars (Sa/S=1) with W/S=0.40 and 0.50, and different hydrogen peroxide contents.

ID	Curing Duration					
	12 h		24 h		48 h	
	Apparent Density (kg/m ³)	Comp. Strength (MPa)	Apparent Density (kg/m ³)	Comp. Strength (MPa)	Apparent Density (kg/m ³)	Comp. Strength (MPa)
40-1-0	2194 ± 21	74.6 ± 1.5	2125 ± 39	76.1 ± 0.8	2210 ± 16	93.3 ± 2.0
40-1-25	1275 ± 32	13.4 ± 0.5	1277 ± 23	14.2 ± 0.6	1301 ± 27	18.4 ± 1.2
40-1-50	892 ± 19	4.9 ± 0.5	889 ± 26	6.2 ± 0.6	897 ± 16	6.6 ± 0.2
40-1-75	891 ± 17	4.0 ± 0.4	895 ± 23	4.5 ± 0.2	878 ± 22	5.9 ± 0.4
50-1-0	2121 ± 26	59.2 ± 1.5	2128 ± 33	61.4 ± 1.4	2153 ± 19	73.2 ± 3.4
50-1-25	1261 ± 15	11.1 ± 0.4	1279 ± 19	16.0 ± 0.4	1285 ± 23	16.9 ± 0.3
50-1-50	1047 ± 32	6.7 ± 0.1	1068 ± 25	9.5 ± 0.2	1102 ± 16	10.5 ± 0.5
50-1-75	1075 ± 27	6.1 ± 0.1	1069 ± 22	7.9 ± 0.4	1104 ± 11	8.5 ± 0.2

Apparent density: ± 1 kg/m³ Compressive Strength: ± 0.1 MPa

Table A.15 Water absorption, apparent density, and oven-dry density of pastes with different W/S and hydrogen peroxide contents.

ID	W/S	H ₂ O ₂ ¹ (%)	Apparent Density (kg/m ³)	Oven Dry Density (kg/m ³)	Absorption by volume (%)	Absorption by weight (%)
40-0-0	0.40	0	1952 ± 31	1856 ± 4	0.6 ± 0.1	0.3 ± 0
40-0-25	0.40	0.25	1541 ± 24	1268 ± 20	2.0 ± 0.2	1.3 ± 0.2
40-0-50	0.40	0.50	1113 ± 15	947 ± 9	3.0 ± 0.3	2.7 ± 0.3
40-0-75	0.40	0.75	657 ± 7	585 ± 13	4.0 ± 0.6	6.1 ± 1.0
425-0-0	0.425	0	1921 ± 31	1837 ± 17	0.7 ± 0.2	0.4 ± 0.1
425-0-25	0.425	0.25	1500 ± 24	1266 ± 8	2.0 ± 0.3	1.3 ± 0.2
425-0-50	0.425	0.50	877 ± 18	751 ± 29	2.9 ± 0.4	3.3 ± 0.5
425-0-75	0.425	0.75	650 ± 28	565 ± 21	10.6 ± 3.1	16.4 ± 4.6
45-0-0	0.45	0	1901 ± 7	1771 ± 42	0.6 ± 0.1	0.3 ± 0
45-0-25	0.45	0.25	1237 ± 13	998 ± 14	2.6 ± 0.2	2.1 ± 0.2
45-0-50	0.45	0.50	781 ± 37	645 ± 31	7.4 ± 3.3	9.6 ± 4.5
45-0-75	0.45	0.75	642 ± 5	544 ± 2	18.0 ± 3.1	28 ± 4.8
45-0-100	0.45	1.00	645 ± 20	527 ± 16	23.5 ± 2.9	36.6 ± 5.0
45-0-125	0.45	1.25	621 ± 24	503 ± 16	24.4 ± 1.6	39.4 ± 2.4
50-0-0	0.50	0	1810 ± 51	1739 ± 12	0.6 ± 0.1	0.3 ± 0.1
50-0-25	0.50	0.25	1168 ± 36	956 ± 37	4.2 ± 0.4	3.6 ± 0.5
50-0-50	0.50	0.50	818 ± 26	647 ± 30	19.1 ± 0.5	23.4 ± 0.5
50-0-75	0.50	0.75	764 ± 25	620 ± 41	21.4 ± 4.9	28.1 ± 7.1

¹By mass of slag, Apparent Density: ± 1 kg/m³, Absorption: ± 0.1 %

Table A.16 Water absorption, apparent density, and oven-dry density of mortars (Sa/S=1) with different W/S and hydrogen peroxide contents.

ID	Apparent Density (kg/m³)	Oven-dry Density (kg/m³)	Absorption by volume (%)	Absorption by weight (%)
40-1-0	2067 ± 6	1908 ± 5	0.73 ± 0.28	0.35 ± 0.14
40-1-25	1317 ± 23	1197 ± 15	2.5 ± 0.14	1.90 ± 0.10
40-1-50	977 ± 21	888 ± 31	6.9 ± 0.75	7.08 ± 0.86
40-1-75	819 ± 25	751 ± 27	11.42 ± 1.20	13.92 ± 1.06

¹By mass of slag, Density: ± 1 kg/m³, Absorption: ± 0.1 %

Table A.17 Thermal conductivity of aerated pastes.

ID	W/S	H₂O₂¹ (%)	Dry Density (kg/m³)	Thermal Conductivity (W/m.K)
40-0-25	0.40	0.25	1098	0.206 ± 0.014
40-0-50	0.40	0.50	687	0.148 ± 0.006
40-0-75	0.40	0.75	541	0.130 ± 0.006
425-0-25	0.425	0.25	952	0.192 ± 0.014
425-0-50	0.425	0.50	659	0.147 ± 0.006
425-0-75	0.425	0.75	558	0.138 ± 0.006
45-0-25	0.45	0.25	877	0.170 ± 0.009
45-0-50	0.45	0.50	683	0.145 ± 0.006
45-0-75	0.45	0.75	536	0.129 ± 0.005
45-0-100	0.45	1.00	488	0.130 ± 0.005
45-0-125	0.45	1.25	480	0.117 ± 0.005
50-0-25	0.50	0.25	852	0.163 ± 0.008
50-0-50	0.50	0.50	620	0.127 ± 0.005
50-0-75	0.50	0.75	544	0.130 ± 0.005

¹By mass of slag, ± 0.001 W/m.K (calculated uncertainty)

APPENDIX B

AERATED PASTE SAMPLES USED FOR THE THERMAL CONDUCTIVITY MEASUREMENTS

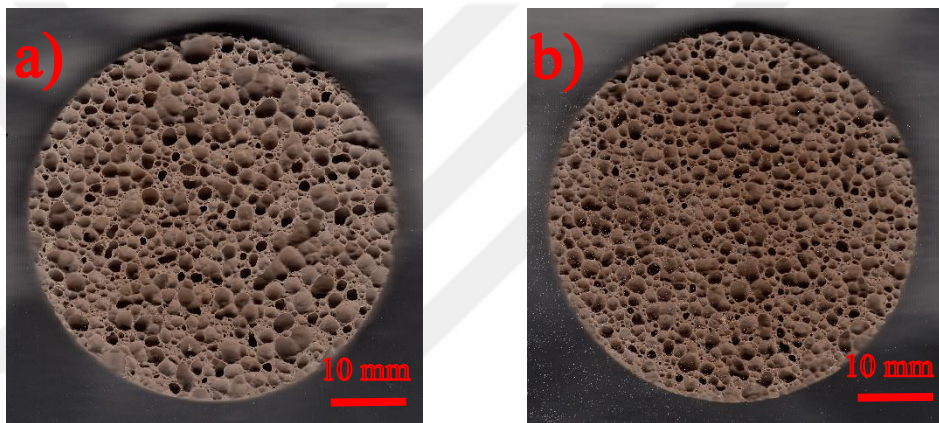


Figure B.1 Aerated Pastes: a) 45-0-100 and b) 45-0-125.

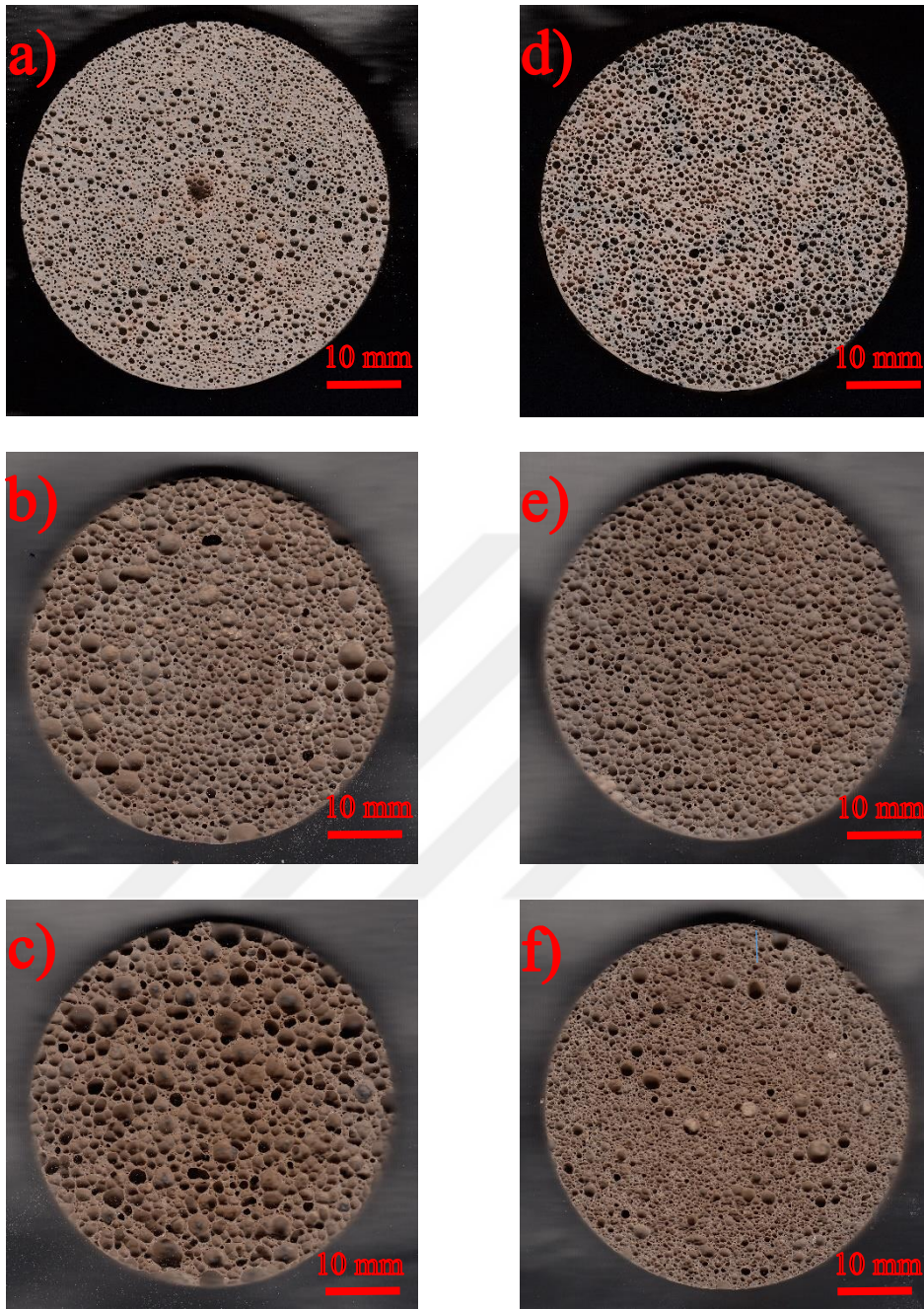


Figure B.2 Aerated pastes: a) 40-0-25, b) 40-0-50, c) 40-0-75, d) 425-0-25, e) 25-0-50, and f) 425-0-75.

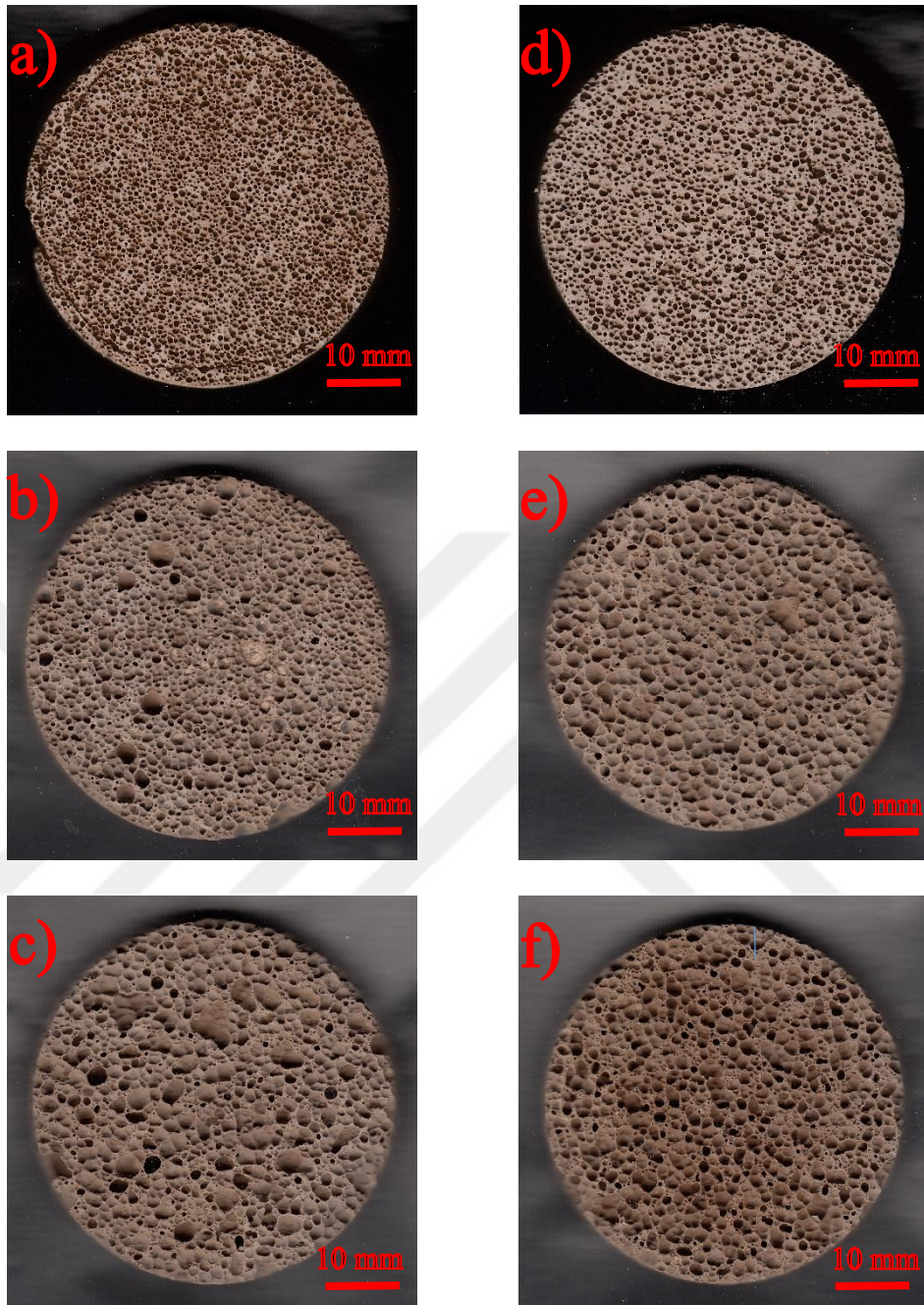


Figure B.3 Aerated pastes: a) 45-0-25, b) 45-0-50, c) 45-0-75, d) 50-0-25, e) 50-0-50, and f) 50-0-75.



CURRICULUM VITAE

PERSONAL INFORMATION

Surname, Name : Şahin Murat

Nationality : Turkish (TC)

Date of Birth : 21.08.1982

Marital Status : Single

EDUCATION

MS	Department of Civil Engineering Bozok University	2011
BS	Department of Civil Engineering Niğde University	2005
High School	Yozgat Anadolu High School	2000

WORK EXPERIENCE

2011-present	Department of Civil Engineering Middle East Technical University	Research Assistant
2009-2011	Department of Civil Engineering Bozok University	Research Assistant

PUBLICATIONS

- Şahin, M., Mahyar, M., Erdoğan, S. T. (2016). Mutual activation of blast furnace slag and a high-calcium fly ash rich in free lime and sulfates. *Construction and Building Materials*, 126, 466-475.
- Şahin, M., Erdoğan, S. T. (2016). Thermal conductivity and durability of ground perlite insulation blocks. *12th International Congress on Advances in Civil Engineering*. Istanbul, Turkey.
- Şahin, M., Mahyar, M., Erdoğan, S. T. (2015) Afşin Elbistan uçucu külü ve yüksek fırın cürufu içeren çimentosuz bağlayıcılar hazırlanması. *9. Ulusal Beton Kongresi*. Antalya, Türkiye.